RDU 1403114

DEVELOPMENT OF WELDED STIFFENER PLATES USING DISSIMILAR AND SIMILAR METAL JOINING TECHNIQUE

MAHADZIR BIN ISHAK

RESEARCH VOTE NO:
RDU1403114

Faculty of Mechanical Engineering
Universiti Malaysia Pahang

2017

ABSTRACT

DEVELOPMENT OF WELDED STIFFENER PLATES USING SIMILAR AND DISSIMILAR METAL JOINING TECHNIQUE

(keywords; stiffened plates, dissimilar, AA7075, AA2024, FSW, RSM, FEM)

The advantage of reinforcing a plate by stiffeners lies in a rise of strength and stability with minimum increase of weight to the overall structures. Consequently, rational design and parametric studies of the response of stiffened plates have long been a major concern of researchers. Over the past years, a vast number of papers have been published at the theoretical and experimental level, reporting studies of the influence of various loading and boundary conditions, different locations and sizes of stiffeners, assembling techniques and fabrication methods, and materials used in manufacturing. This work was carried out on dissimilar metal joining of the hard-to-weld aluminum alloys, which has become an important application in the modern industries. The study aims on producing defects-free welds of high strength AA7075-T6 and AA2024-T351 aluminum alloys by the friction stir welding (FSW), which has been proposed as an alternative welding method. The experimental setup was developed through introducing proper design of welding tool and backing/clamping system, considering the process variables (welding speeds, tool tilt angle, clamping force, dwell sequence and relative materials position and orientation). Different pin tool profiles (cylindrical and tapered, smooth and threaded, flatted and non-flatted) were investigated in conjunction with varying levels of machine variables through the central composite design method.

The purpose of this work is to outline the research studies that have been conducted on stiffened plates in general. Developed theoretical and numerical methods, finite element analyses and experimental investigations have been explored in this survey with a brief summary of some results obtained by the researchers. The dissimilar AA7075-AA2024 weld strength of about 400 MPa, which represents an efficiency of 89% was recorded when the softer AA2024 alloy was fixed on the advancing side at 900 rpm of spindle speed, 100 mm/min of traverse rate, 3° of tilting angle and moderate clamping pressure of 3 kN. The results clarified that the effect of backing and clamping materials on the weld strength is changed related to the applied welding speed. Moreover, a considerable difference in process temperature was noticed between the advancing and retreating sides of the weld. The outcomes of the present study provided advanced knowledge for the future work in dissimilar metal joining.

Key researchers **:** Mahadzir bin Ishak
Siti Rabiatull Aisha binti Idris
Luqman Hakim bin Ahmad Shah
Mohd Ruzaimi bin Mat Rejab

E-mail : *mahadzir@ump.edu.my*
Tel. No. : 09 424 6235

Vote No. : RDU1403114

ABSTRAK

Kelebihan mengukuhkan plat oleh pengukuh terletak pada peningkatan kekuatan dan kestabilan dengan kenaikan minimum berat kepada struktur keseluruhan. Oleh itu, reka bentuk rasional dan kajian parametrik mengenai tindak balas plat tegar telah menjadi kebimbangan utama penyelidik. Sejak beberapa tahun kebelakangan ini, sejumlah besar kertas telah diterbitkan di peringkat teoretikal dan eksperimen, pelaporan kajian tentang pengaruh pelbagai syarat pemuatan dan sempadan, lokasi dan saiz yang berbeza dari pengejar, teknik pemasangan dan kaedah fabrikasi, dan bahan yang digunakan dalam pembuatan . Kajian ini dilakukan pada pelbagai logam yang digunakan bagi menyambung bahagian aloi aluminium yang sukar dikimpal tetapi kini menjadi aplikasi penting dalam industri moden. Kajian ini bertujuan untuk menghasilkan kimpalan bebas-kecacatan yang mempunyai kekuatan AA7075-T6 dan aloi aluminium AA2024-T351 yang berkuasa. Tinggi dengan menggunakan cara geseran kacau kimpalan (FSW) yang telah dicadangkan sebagai kaedah kimpalan alternatif. Prosedur percubaan telah dibangunkan dengan memperkenalkan reka bentuk alat kimpalan dan sistem sokongan/penjepit yang betul dengan memnggunakan pemboleh ubah proses (kelajuan kimpalan, sudut kecondongan alat, daya pengapit, urutan dan kedudukan bahan relatif dan orientasi). Ciri-Ciri alat pin yang berbeza (silinder dan tirus, licin dan diulirkan, rata dan tidak rata) disiasat bersama dengan pelbagai peringkat pembolehubah mesin melalui kaedah reka bentuk komposit berpusat

Tujuan kerja ini adalah untuk menggariskan kajian penyelidikan yang telah dijalankan pada plat yang tegar pada umumnya. Kaedah teoretikal dan berangka yang dibangunkan, analisis unsur terhingga dan penyiasatan eksperimen telah diterokai dalam tinjauan ini dengan ringkasan ringkas beberapa keputusan yang diperoleh oleh penyelidik. Kekuatan kimpalan AA7075-AA2024 kira-kira 400 MPa yang mewakili kecekapan sebanyak 89% dicatatkan apabila aloi AA2024 yang lebih lembut telah ditetapkan pada bahagian hadapan dengan kelajuan gelendong 900 rpm, 100 mm / min kadar traverse, 3° sudut miring dan tekanan pengapit sederhana 3 kN. Hasilnya menjelaskan bahawa kesan sokongan dan bahan penjepit pada kekuatan kimpal berubah dengan kelajuan kimpalan yang digunakan. Lebih-lebih lagi, perbezaan dalam suhu proses telah diperhatikan antara sisi pemanjangan dan pengembalian kimpalan. Hasil kajian ini mengandungi pengetahuan terkini yang boleh digunakan dalam kajian masa depan dengan menggunakan gabungan logam yang berbeza.

TABLE OF CONTENTS

LIST OF TABLES

LIST OF FIGURES

LIST OF ADDITIONAL RELATED PUBLICATIONS

CHAPTER 1

INTRODUCTION

1.1 INTRODUCTION

This chapter introduces the background related to the dissimilar welding between aluminium (Al) which consists of different element compositions. Dissimilar metal welding is the joining of two separate metals which would not ordinarily weld together as they have differing chemical and mechanical qualities, and are from different alloy systems. If the core properties of two metals are different but they share the same name, they are still dissimilar in nature. Finally, the main objectives and scopes of the project will be presented.

1.2 BACKGROUND

Stiffened plates are the main components of various engineering structures, such as aircraft fuselage and wings, aerospace composite structures, ship hulls, vehicles, as well as in many other civil engineering and offshore platforms. Stiffeners are often added to the plate to enhance its strength and stability and to provide a means of slowing down or arresting the growth of cracks with minimum increase of weight to the overall structures. Several shapes and types of stiffeners may be used like bulb, flat, I, L, T, U, Z, trapezoidal, triangular, or other open and closed shapes. Joining dissimilar metals has benefits for many different industries, such as the construction, automotive and electronics industry, whereby there is often a necessity to weld together different parts and components to save on material costs or to use the best possible metals always for the perfect product [1].

Recently, the design of vehicles in modern manufacturing emphasizes on lessening weight to improve fuel economy and to increase the carrying capability; therefore, the thin plate stiffened structures have become widespread. To study the strength of these structures under applied load conditions, as well as extreme and accidental loads, it is important to have knowledge about the behaviour of their structural elements. However, a comprehensive understanding to all aspects of the behaviour is still not realized, due to its complexity and many influencing parameters

involved. Although a number of welding techniques, such as laser and gas metal arc plug welding have been developed so far to deal with different types of materials [2], friction stir welding (FSW), the green technology, has become one of the most operative and economic joining techniques due to its ability to connect a wide range of ferrous and even nonferrous materials such as steel [3], titanium [4], aluminum [5], magnesium [6] and some of polymers and plastic [7].

Dissimilar welding of the heat-treatable and hard-to-weld 7xxx, 6xxx and 2xxx aluminum alloys has become more efficient by using this joining process [8]. These alloys are widely used in the automotive, aerospace, aircraft, pipelines, storage tanks, marine frames, and transportation industries due to their high strength-to-weight ratio, good machinability and high resistance to corrosion [9, 10]. However, these materials cannot be welded by the traditional fusion methods, since they are highly affected by the elevated temperature required for material melting [11]. For this reason, mechanical fastener assembly was the traditional technique used in the fabrication of the aircraft stiffened panels, which are produced from the aluminum highly alloyed series [12]. Among aluminum alloys, AA7075-T6 represents the strongest alloy whose tensile strength is about double of the widely used AA6061-T6 alloy. The advanced AA2024-T351 aircraft aluminum alloy is different from AA2024-T3 due to the unlike processing procedure. It has a lower tensile and yield strength and more pronounced plasticity than AA2024-T3 and deforms more homogeneously than the AA7075-T6 alloy [13, 14]. FSW of this developed alloy results in an average static strength of about 85% of the base material and a very high fatigue strength [15]. Consequently, joining this developed alloy to the higher strength AA7075-T6 alloy could enhance the mechanical properties of the produced construction.

The melting points of materials would not be exceeded during the FSW process, and the welding occurs in a solid-state due to the relatively lower heat energy input [16]. Accordingly, this advanced technology has been introduced as an alternative joining method to riveting in the automotive and transportation industries. It has become a very impressive way to reduce the manufacturing cost and time by eliminating the requisite for expensive non-standard materials [12]. The static strength and fatigue properties of joints produced by this novel technology are higher in comparison with the mechanical fastening and traditional fusion welding methods [17]. Materials of thickness ranging from less than 1 mm to about 75 mm could be joined by the FSW [18] in various

configurations including square butt, edge butt, T-butt, lap, multiple lap, T-lap and fillet joints [19].

1.3 PROBLEM STATEMENT

The heat treatable aluminum 2xxx, 6xxx, and 7xxx series are crack sensitive and categorized as unweldable or difficult to weld by the conventional fusion welding method [15] . The relatively new FSW technique permits to join such these materials in a solid state and produce high-integrity joints. However, the assembly of dissimilar aluminum alloys differing in mechanical, thermal and chemical properties still a challenge [1]. Furthermore, there is limited studies regarding the joining of highest strength AA7075 alloy with aluminum AA6061 and AA2024 by the FSW. These advanced lightweight aluminum alloys are widely used in transportation industries to improve fuel economy while maintaining and improving safety and performance (Mishra et al., 2014).

Joint formulation by the FSW is considered as a complex procedure due to the interaction between the processing parameters, and the difficulty increases when the connected materials are dissimilar. The success of weld depends on the thermal conditions under which the process is carried out [20]. Unlike other hot working technologies, the heat flux in the FSW is primarily generated during the process by the friction (at the interface between the welding tool and the workpieces) and the deformation process, so it is very hard to control its amount. This heat must keep the maximum temperature in the workpieces high enough to sufficiently soft the abutting materials for the pin to stir, but low enough to prevent the melting of these materials [21].

Too cold welding results in a non-bonding and volumetric or void formation and too hot welding results in an excessive material flow, which lead to material expulsion such as flash formation, collapse of the nugget within the mixing stir zone (SZ), reduction of the weld hardness, especially at the heat affected zone (HAZ) and hence degradation of the mechanical properties of the joint [22]. A successful weld with high strength and smooth surface finish could be then achieved by a careful selection of the welding parameters such as tool design, spindle speed, traverse rate and tool tilt angle. The tool should be designed to give the desired material flow and heat generation based on the workpiece materials and dimensions, welding speeds, joint configuration and user's own experiences and preferences [23] . Periodic use of the welding tool results in

a permanent deformation in its profile and dimensions due to the mechanical and other types of wear, especially in the initial heating stage during the plunge and dwell periods of the process [24]. This change in tool design affects the way of material mixing at the nugget zone and results in a weak and unstable joint.

The clamping force and construction can impact the weld quality and process variables. The use of improper clamping system causes in a non-uniform temperature distribution in addition to the ability of spreading or lifting of the [25]. Thermal boundary conditions that are present at the workpieces are also affect the temperature distribution and hence the strength of the joint for a given set of welding parameters. The rate of heat flux through the top, sides and bottom of workpieces mostly depends on the thermal diffusivity of backing plate and fixtures, as was pointed out in literature [26]. Furthermore, it was reported that the temperature are higher on the advancing side when welding similar materials [27]. Consequently, location of the welding materials in dissimilar FSW leads to severe temperature asymmetry.

This asymmetry in temperature between the advancing and retreating sides could significantly affect the joint quality and mechanical properties, which mainly depends on the properties of base materials and welding parameters [28]. It is hence thought necessary to understand the influence of process variables in conjunction with varying levels of the thermal conductivity of backing/clamping materials and materials position. In the previous studies, the effect of thermal boundary conditions has not received as much attention as the other process parameters, especially in case of welding dissimilar materials. Accordingly, the present work aims on providing an effective design of welding tool and backing clamping/system to produce quality joints of dissimilar aluminum alloys using the friction stir welding.

1.4 OBJECTIVES

The core objectives of the study are:

i. to design a welding tool for efficient joining of dissimilar aluminum alloys by the FSW.
ii. to identify the optimal spindle speed, traverse rate, clamping force and initial heating stage or dwell sequence for the FSW of high-strength AA7075-T6 and AA2024-T351 aluminum alloys.

iii. to access the temperature distribution during the FSW of dissimilar aluminum alloys by developing a new design of composite backing/clamping system.

iv. to investigate the influence of pin tool flute radius on the material flow of dissimilar aluminum alloys.

1.5 SCOPE OF STUDY

This work aims to produce high quality weld of dissimilar aluminum alloys. Accordingly, the tests are experimentally conducted to identify the optimal tool design, process parameters (tool rotation speed; tool traverse rate; tool tilt angle; relative materials position; clamping force; dwell sequence) and thermal boundary conditions. In this regard, the following points are noted down to clarify the scope of the study:

i. FSW technique is used to join the welding coupons with butt configuration.

ii. The welding joints were prepared from dissimilar aluminum alloys of the same metal family (AA7075-T6, AA2024-T351 and AA6061-T6). The latter alloy, which is relatively inexpensive material was joined to the AA7075-T6 alloy during the identification of the optimal tool design using the design of experiment and statistical analysis in order to reduce the total cost.Conduct a new technique of gas metal arc lap plug welding method to join dissimilar A7075-T651 and AZ31B alloys using ER308L-Si stainless steel and ER5356 aluminum filler wires.

iii. Pin tool profile is considered with concave shoulder design, and all tools were made of AISI H13 steel.

iv. The weldments are naturally aged before the mechanical and metallurgical tests without any post-weld heat treatment

v. The workpieces are subjected to equal vertical and lateral clamping forces.

vi. AISI 304 stainless steel and aluminum 6061-T6 are used to fabricate the backing/clamping systems.

vii. Temperature distributions during the welding process are measured experimentally at the mid-plane of the workpieces along the transverse centerline using high quality thermocouple wires.

1.6 REFERENCE

[1]. Kumar, N., Mishra, R. S., & Yuan, W. (2015). Friction stir welding of dissimilar alloys and materials: A volume in the friction stir welding and processing book series: Butterworth-Heinemann.

[2]. Islam, M. R., Ishak, M., Shah, L. H., Idris, S. R. A., & Meriç, C. (2016). Dissimilar welding of A7075-T651 and AZ31B alloys by gas metal arc plug welding method. *The International Journal of Advanced Manufacturing Technology*, *88*(9-12), 2773-2783.

[3]. El-Batahgy, A.-M., Miura, T., Ueji, R., & Fujii, H. (2016). Investigation into feasibility of FSW process for welding 1600MPa quenched and tempered steel. *Materials Science and Engineering: A*, *651*, 904-913.

[4]. Fu, M. J., Li, X. H., Han, X. Q., & Xu, H. Y. (2016). *Research on Work Hardening Type Superplastic Deformation Behavior of FSW Titanium Alloy*. Paper presented at the Materials Science Forum.

[5]. Salih, O. S., Ou, H., Sun, W., & McCartney, D. G. (2015). A review of friction stir welding of aluminium matrix composites. *Materials & Design*, *86*, 61-71.

[6]. Pasha, M. A., Reddy, P. R., Laxminarayana, P., & Khan, I. A. (2016). The Effects of SiC Particle Addition as Reinforcement in the weld Zone during Friction Stir Welding of Magnesium Alloy AZ31B. *IRA-International Journal of Technology & Engineering (ISSN 2455-4480)*, *3*(3)

[7]. Eslami, S., Tavares, P. J., & Moreira, P. M. G. P. (2016). Friction stir welding tooling for polymers: review and prospects. *The International Journal of Advanced Manufacturing Technology*.

[8]. N., Mishra, R. S., & Yuan, W. (2015). *Friction stir welding of dissimilar alloys and materials: A volume in the friction stir welding and processing book series*: Butterworth-Heinemann.

[9]. Ishak, M., Noordin, N., Razali, A., Shah, L., & Romlay, F. (2015). Effect of filler on weld metal structure of AA6061 aluminum alloy by tungsten inert gas welding. *International Journal of Automotive & Mechanical Engineering*, *11*.

[10]. Moghadam, D. G., Farhangdoost, K., & Nejad, R. M. (2016). Microstructure and Residual Stress Distributions Under the Influence of Welding Speed in Friction Stir Welded 2024 Aluminum Alloy. *Metallurgical and Materials Transactions B-Process Metallurgy and Materials Processing Science*, *47*(3), 2048-2062.

[11]. Bertoncello, J. C. B., Manhabosco, S. M., & Dick, L. F. P. (2015). Corrosion study of the friction stir lap joint of AA7050-T76511 on AA2024-T3 using the scanning vibrating electrode technique. *Corrosion Science*, *94*, 359-367.

[12]. Murphy, A., Ekmekyapar, T., Özakça, M., Poston, K., Moore, G., & Elliott, M. (2014). Buckling/post-buckling strength of friction stir welded aircraft stiffened panels. *Proceedings of the Institution of Mechanical Engineers, Part G: Journal of Aerospace Engineering 228*(2), 178-192.

[13]. Đurđević, A., Živojinović, D., Grbović, A., Sedmak, A., Rakin, M., Dascau, H., & Kirin, S. (2015). Numerical simulation of fatigue crack propagation in friction stir welded joint made of Al 2024-T351 alloy. *Engineering Failure Analysis 58, Part 2*, 477-484.

[14]. Wang, W., Li, T. Q., Wang, K. S., Cai, J., & Qiao, K. (2016). Effect of Travel Speed on the Stress Corrosion Behavior of Friction Stir Welded 2024-T4 Aluminum Alloy. *Journal of Materials Engineering and Performance*, *25*(5), 1820-1828. Dursun, T., & Soutis, C. (2014). Recent developments in advanced aircraft aluminium alloys. *Materials & Design*, *56*, 862-871.

[15]. Caseiro, J. F., Valente, R. A. F., Andrade-Campos, A., & Yoon, J. W. (2013). On the elasto-plastic buckling of Integrally Stiffened Panels (ISP) joined by Friction Stir Welding (FSW): Numerical simulation and optimization algorithms. *International Journal of Mechanical Sciences 76*, 49-59.

[16]. Shao, Q., He, Y., Zhang, T., & Wu, L. (2014). Numerical analysis of static performance comparison of friction stir welded versus riveted 2024-T3 aluminum alloy stiffened panels. *Chinese Journal of Mechanical Engineering*, *27*(4), 761-767.

[17]. Thomas, W., & Nicholas, E. (1997). Friction stir welding for the transportation industries. *Materials & Design*, *18*(4), 269-273.

[18]. Mishra, R. S., & Mahoney, M. W. (2007). *Friction stir welding and processing*: ASM International.

[19]. Schmidt, H. N. B. (2010). 10 - Modelling thermal properties in friction stir welding. In D. Lohwasser & Z. Chen (Eds.), *Friction Stir Welding* (pp. 277-313): Woodhead Publishing.

[20]. Tang, W., Guo, X., McClure, J., Murr, L., & Nunes, A. (1998). Heat input and temperature distribution in friction stir welding. *Journal of Materials Processing and Manufacturing Science 7*, 163-172.

[21]. Zettler, R., Vugrin, T., & schmÜcker, M. (2010). 9 - Effects and defects of friction stir welds. In D. Lohwasser & Z. Chen (Eds.), *Friction Stir Welding* (pp. 245-276): Woodhead Publishing.
[22]. Mishra, R. S., Mahoney, M. W., Sato, Y., & Hovanski, Y. (2015). *Friction Stir Welding and Processing VIII*: Wiley.
[23]. Miles, M. P., Ridges, C. S., Hovanski, Y., Peterson, J., Santella, M. L., & Steel, R. (2013). Impact of tool wear on joint strength in friction stir spot welding of DP 980 steel. *Science and Technology of Welding and Joining 16*(7), 642-647.
[24]. Richter-Trummer, V., Suzano, E., Beltrão, M., Roos, A., dos Santos, J. F., & de Castro, P. M. S. T. (2012). Influence of the FSW clamping force on the final distortion and residual stress field. *Materials Science and Engineering: A, 538*(0), 81-88.
[25]. Upadhyay, P., & Reynolds, A. (2014). Effect of backing plate thermal property on friction stir welding of 25-mm-thick AA6061. *Metallurgical and Materials Transactions A, 45*(4), 2091-2100.
[26]. Nandan, R., Debroy, T., & Bhadeshia, H. (2008). Recent advances in friction-stir welding – Process, weldment structure and properties. *Progress in Materials Science 53*(6), 980-1023.
[27]. Guo, J. F., Chen, H. C., Sun, C. N., Bi, G., Sun, Z., & Wei, J. (2014). Friction stir welding of dissimilar materials between AA6061 and AA7075 Al alloys effects of process parameters. *Materials & Design, 56*, 185-192

CHAPTER2

TECHNICAL PAPER #1

Title:- A simplified design of clamping system and fixtures for friction stir welding of aluminium alloys (Journal of Mechanical Engineering and Science (2015) 1628-1639 doi: 10.15282/jmes.9.2015.10.0158 – Scopus Indexed)

2.1 ABSTRACT

Sound friction stir welds could be attained by using an active design of backing/clamping system with a proper selection of the welding parameters. This work presented a simplified design of fixtures and backing plates to be used for friction stir welding of aluminum alloys. The test-rig was constructed to prevent dispersal or lifting of the specimens throughout the joining process and to ensure uniform distribution of temperature along the plates. The workpieces were subjected to uniform lateral and vertical pressures by means of bolts and nuts. Compound backing plates and pressure bars with additional side plates were included to increase the heat sink. Several coupons of dissimilar aluminum alloys AA7075 and AA6061 were joined to inspect the validity of this design. The tests showed promising results with defects-free welds, good strength and smooth surface finish without geometric imperfection and gap creation between the welded specimens. Efficiency of the joint reached its maximum value of about 82% with respect to the ultimate strength of the AA6061 alloy at 1100 rpm rotation speed and 300 mm/min feed. These results encourage using and improving the present design for future studies of friction stir welding.

2.2 INTRODUCTION

In fiction stir welding (FSW), backing plates and fixtures are quite significant factors [1-
3]. It is important that the workpieces should not spread or be lifted during the process; therefore, welding fixtures must be designed with features that are enable to achieve this objective. The quality of welding is dependent on the manufacturing precision of the clamping system and the welding table [4]. Moreover, the impact of clamping process on
the joint performance should be recognized so that the required constant quality could be
ensured. The method of clamping and its effects on machine processes are well understood. Besides that, clamping claws is an easy and less costly system, however, it leads to varying temperature distributions which could be improved through the use of pressure bars [5-7].

Advanced research have indicated that continuous clamping approaches could lead to a more consistent FSW quality along the joint's length [8]. Essential forces are required in FSW that should be supported by the fixtures, leading to a significant rise in total process costs. Thus, appropriate knowledge regarding the required forces would result in the chances of optimization of clamping system with respect to cost and efficiency [9]. At the time of designing new optimized clamping systems for particular applications, there is a need for essential information about the actual forces required so that the parts to be joined in place are held correctly. Little information is available in the literature regarding the impact of clamping systems on the
mechanical behavior of the welded joints. Clamping force with simplified clamping conditions for the purpose of fusion and laser welding were studied by a number of researchers [10-16].

Through the investigations, it was observed that increasing the restraining force results in improvement of the welded joints. In FSW, Christner and Sylva [17] recorded that the formation of gap between specimens up to 36% of the plate thickness does not affect the joint strength. In a similar work, Leonard and Lockyer [18] noted that a gap presence up to 33% of the workpiece thickness could be tolerated without
the existence of weld flaws. On the other hand, Richter and his group of researchers [19]

observed that lesser distortion and a more consistent residual stresses distribution through
the thickness can be achieved by applying higher clamping forces. It was demonstrated that the possibility of defects could also be minimized by preventing any creation of gaps
between the two butt plates, as shown in Fig. 2.1.

Fig. 2.1. Gap between specimens at the start of the FSW process based on the condition of clamping [19]. (a) without lateral pressure, (b) with lateral pressure.

During the FSW process of higher-temperature alloys, such as steel and titanium, it was found that cooling of the welding tool and anvil is essential to avoid movement of the thermal energy into the machine's spindle. A good design of fixture can lead to dissipating heat away from the workpiece, and hence improving the weld quality and performance [20]. On contrary, cooling is not required for the FSW of lower-temperature
aluminum and magnesium alloys. Such alloys are commonly friction stir welded with ambient air-cooled anvil and welding tool [8]. However, material mixing and mechanical
properties of the joint can be significantly improved by the use of compound backing plates with different thermal diffusivity [16, 21-25]. This paper aims to accomplish and equip a simplified design of clamping system and fixtures to be used as a FSW test-rig.

The validity of this design is verified experimentally by welding some pairs of AA7075–AA6061 aluminum alloys and investigating the mechanical properties and microstructure of joints. These two alloys are widely used in the automotive, aircraft, aerospace, marines,and transportation industries [26-29]. Aluminum 7075, along with the traditional welding techniques, is relatively a high strength material that can be used for highly stressed structural parts [30]. The widely available AA6061-T6 has a good workability, high resistance to corrosion, and excellent joining characteristics [31]. For instance, the FSWof these dissimilar alloys fully utilizes both materials [32, 33].

Although the FSW ofsimilar and dissimilar materials has been used in many research studies [34-39], limitedinterest was found in literature regarding these two series of aluminum alloys [40-44]. Inall of these articles, weld temperature, process parameters and the placement of materialson the advancing side (AS) and retreating side (RS) were examined without any referringto the clamping system and fixtures. High and low speeds, in several conditions wereapplied. Using Taguchi method, parametric optimization was achieved by Shah et al. [43] to evaluate the tensile strength of joint under several welding speeds and tool tilt angle.

Maximum tensile strength of 219.6 MPa was observed at 1000 rpm and 110 mm/minwelding speeds and 3º of tilt angle. Furthermore, Guo et al. [40] reported that high traverse speed can be used to join these two alloys when the softer alloy was placed on the AS, inwhich joint efficiency reached 79% with respect to the tensile strength of the AA6061 base material. In another study, Sathari et al. [44] noticed the same behavior when theAA6061 was placed on the AS. They found that the maximum joint strength of 207 MPa was resulted by this configuration. In the work of Cole et al. [42], the AA6061 alloy was also placed on the AS and the welding tool was shifted toward the AA7075 to improve the joint strength. Other than that, the same material position was made by İpekoğlu andÇam [41] to investigate the behavior of AA7075-AA6061 friction stir weldments under different temper conditions and post-weld heat treatment. Consequently, nine pairs of toolrotation and welding speeds were selected in the present work to examine the ability ofthe self-designed backing/clamping system of producing sound welds with high tensile strength.

2.3 EXPERIMENTAL SET UP

2.3.1 Test-Rig Characterization

Fig. 2.2 shows a photo of the simplified FSW testing structure. Length of the backing plates and fixtures is selected to be suitable for the available milling machine table, while

the width can be enlarged depending on the dimensions of the welded coupons. The vertical clamping forces are applied by means of pressure bars, bolts, and nuts to ensure uniform pressure and temperature distribution throughout the welded plates [5].

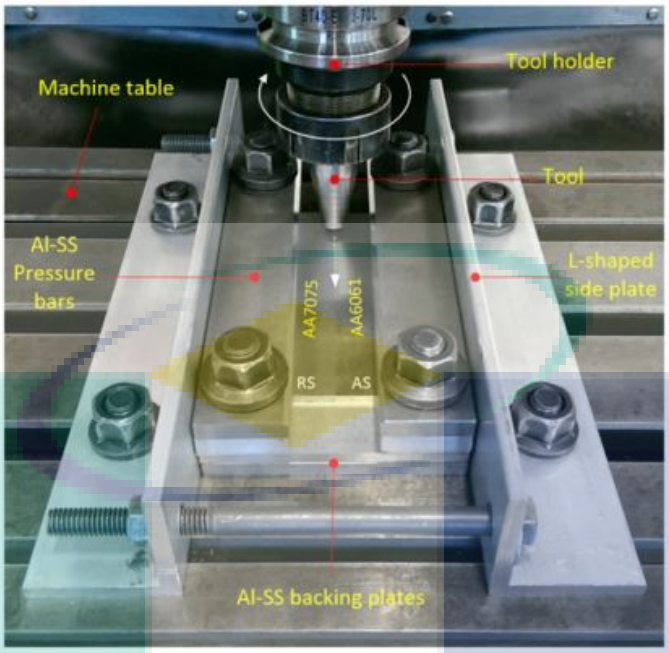

Fig. 2.2. The assembly of the FSW test-rig on the machine's table.

The lateral restraints consist of two L-shaped aluminum plates and two end-screwed bolts. This enables to increase the heat sink [21] and to apply uniform side pressure on the specimens [19]. This side pressure is applied by an easy and economical way, using nuts at the end of the two horizontal bolts. The horizontal plane containing the two specimens is free of bolts and their holes, which aims to avoid any change in the heat sink during the process. The design facilitates to use multi-layers of backing plates and pressure bars. Aluminum and stainless steel (Al-SS) compound system is used to increase the cooling rate and hence improving the joint strength [21, 22]. Width of the backing plates is slightly less than the total width of the workpiece in order to apply the lateral pressure directly on the workpiece by means of the two L-shaped side plates. This low cost test-rig can be easily handled and it allows controlling the position of the welding tool on the specimens. It is specially designed for butt-joint FSW researches.

2.3.2 Experimental Procedure

To indicate the effectiveness of the simplified design, dissimilar aluminum AA6061-T6 and AA7075-T6 rolled sheets with dimensions of 125×50×3 mm were joined in butt configuration by FSW technique. The chemical compositions and physical properties of these two alloys are listed in Tables 2.1 and 2.2 respectively. The edges of specimens were ground by an auto-grinding machine and cleaned with acetone and at the same time, a vertical milling machine was used for the FSW process.

Table 2.1. Chemical composition (wt. %) of the base materials [45].

Material	Cu	Mg	Zn	Mn	Si	Fe	Cr	Ti	Al
7075-T6	1.2-2	2.1-2.9	5.1-6.1	Max 0.3	Max 0.4	Max 0.5	0.18-0.28	Max 0.2	87.1-91.4
6061-T6	0.15-0.4	0.8-1.2	Max 0.25	Max 0.15	0.4-0.8	Max 0.7	0.04-0.35	Max 0.15	95.8-98.6

Table 2.2. Mechanical properties of the base materials.

Material	Yield Strength (MPa)	Tensile Strength (MPa)	Vickers Hardness	Elongation (%)
7075-T6	1.2-2	2.1-2.9	5.1-6.1	Max 0.3
6061-T6	0.15-0.4	0.8-1.2	Max 0.25	Max 0.15

Welding line was parallel to the rolling direction of the two sheets. The AA6061 was placed on the AS. A tool made of H13 steel was used to produce the welding joints [8, 46]. The shoulder diameter is 12 mm having an 8º concave. The pin was tapered with
10º from 4.2 mm diameter on the base alongside a length of 2.7 mm. Left-hand threads and single flat were added to the core of the probe to improved the local deformation and
material flow [8, 47, 48]. Three distinct tool rotational speed levels of 1000, 1100 and 1200 rpm with three travel velocities of 250, 300 and 350 mm/min were utilized, as shown
in Table 2.3.

Table 2.3. Welding parameters.

Specimen	Rotation speed (rpm)	Welding speed (mm/min)
A1	1000	250
A2	1000	300
A3	1000	350
B1	1100	250
B2	1100	300
B3	1100	350
C1	1200	250
C2	1200	300
C3	1200	350

The tool tilt angle stayed constant at 3º for all cases

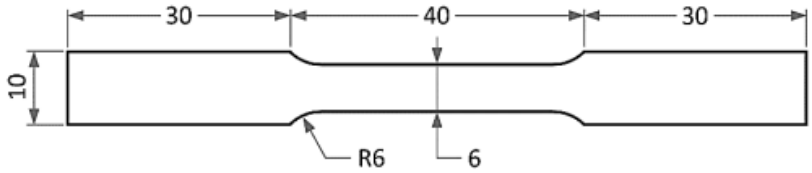

Fig. 2.3. Geometry and dimensions of the tensile specimen in millimeters according to the ASTM E8-11 standard.

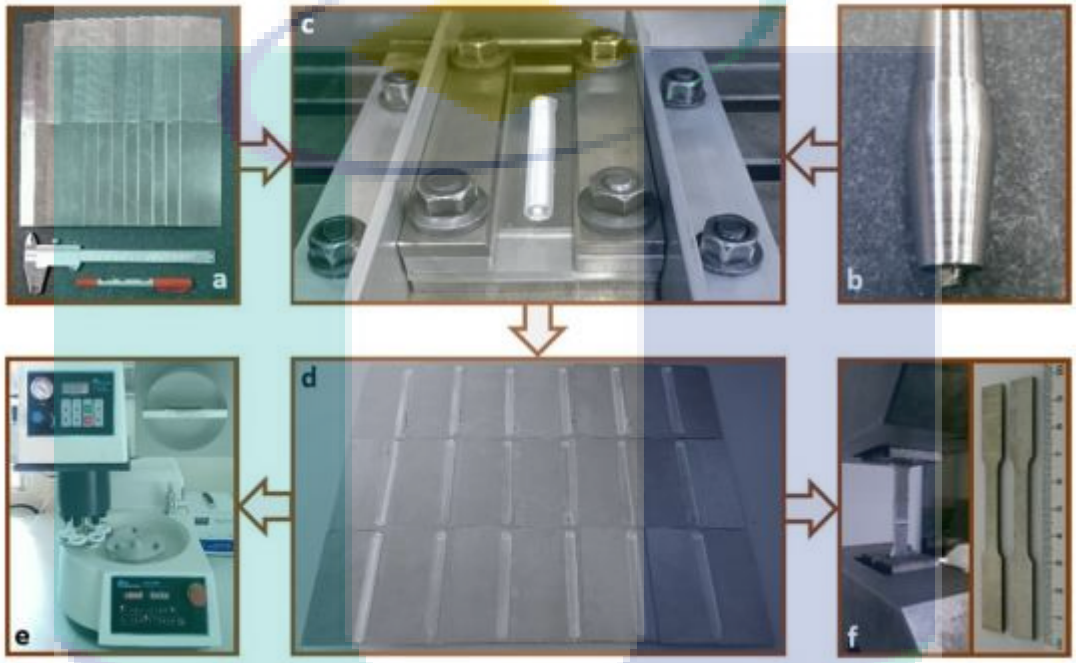

Fig. 2.4. The key stages of the experiment: (a) preparation of the specimens, (b) welding tool, (c) clamping and FSW, (d) welded coupons, (e) grinding and polishing the metallographic specimens, and (f) tensile testing.

The tool tilt angle stayed constant at 3º from the normal of the workpiece further from the direction of travel. These welding parameters were selected according to

a number of preliminary tests based on the literature findings. The rotating tool pin was gradually inserted between the two sheets until the shoulder could penetrate to about 0.2 mm inside the workpiece. This generates a frictional heat that is needed to soften the materials around the tool probe. Subsequently, stirring started at a consistent speed along the centerline between the two alloys. After natural aging of about one month since welding, transverse tensile specimens for the welded and base materials are prepared as per the American Society for Testing of Materials (ASTM E8-11) standard. Fig. 2.3 presents the geometry and dimensions of these specimens. Tensile tests have been done at room temperature with a speed of 1 mm/min using a 50 kN universal

testing machine with bluehill 3 software. Finally, three tensile specimens for each joint were tested, and then the average values of the ultimate tensile strength were noted down.

Standard metallographic technique was followed to prepare the metallographic specimens. After complete grinding and polishing using automatic and manual devices, the specimens were etched with a modified Keller's reagent, so that the grain structure of

the various weld zones could be observed. The key stages of the experiment are demonstrated in Figure 2.4. An optical microscope was used to perform the microstructural analysis. An auto Vickers micro-hardness tester was then used to measure the hardness across the mid-thickness of the joint's cross-section in a direction normal to the weld line. The HV0.5 test method was applied with an indent time of 10 seconds.

2.4 RESULTS AND DISCUSSION

2.4.1 Weld Width Analysis and Penetration Depth

Three transverse tensile tests were achieved for each base material (BM) and welded joint

and the average values of the ultimate tensile strength (UTS) had been then calculated. Fig. 2.5 presents the average UTS value for each specimen in addition to that of the base alloy (AA6061). The maximum error recorded was less than 5% and the minimum values were observed near the starting point of welding. The UTS of the AA7075 base alloy was not drawn in this figure, because all specimens failed at the heat affected zone (HAZ) of the AA6061 alloy. Moreover, all of the welded plates exhibited good tensile strength ranging from 220.9 MPa for the (C3) specimen, where the rotation and welding speeds were 1200 rpm and 350 mm/min respectively, to the apex of 252.1 MPa when the rotation speed fixed at 1100 rpm and the welding speed at 300 mm/min for the (B2) specimen.

The highest value of the UTS represents an efficiency of about 82% with respect to the UTS of the AA6061 alloy. This efficiency is higher than the acceptable limit due to the standards of the American Welding Society (AWS) for FSW [40]. The joint efficiency was calculated with respect to the weaker alloy. For instance, it has been reported in all previous work on dissimilar FSW of alloys and materials, that the

maximum tensile strength of the weldment is always less than the weaker material [33]. Due to this, the challenge of joining dissimilar alloys and metals lies in the differences in their chemical and mechanical properties. The differences and gap are relatively high between the selected 7xxx and 2xxx series, as seen in previously in Tables 2.1 and 2.2. For that reason, it is hard to achieve very high strength of the welded joints for these two aluminum alloys [34]. However, the calculated efficiency is relatively high compared to the previous published data [40-44].

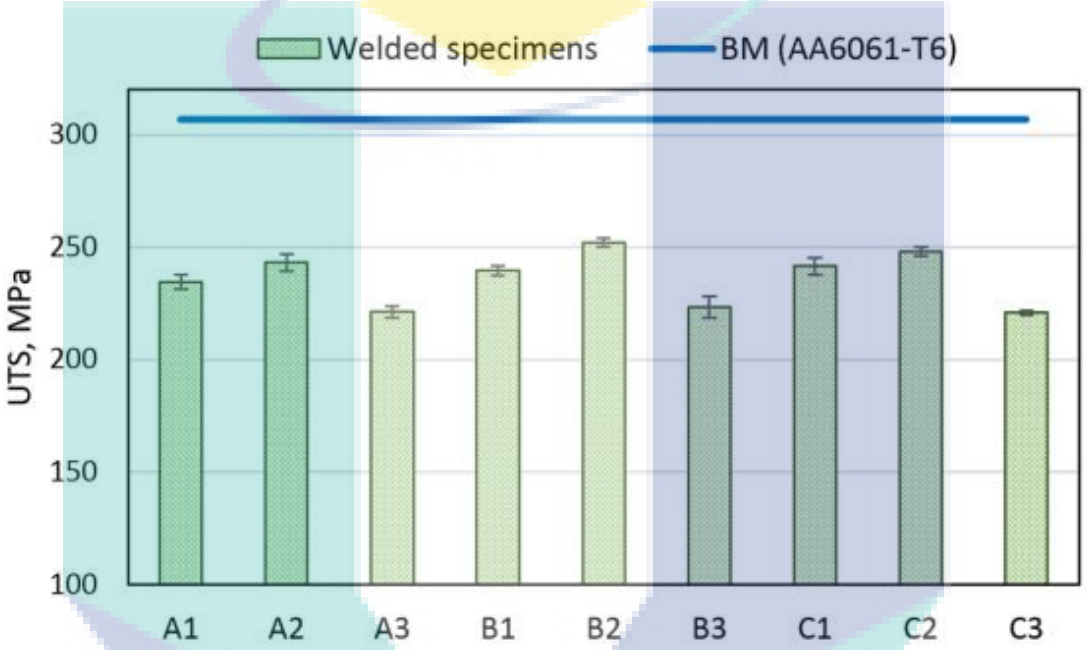

Fig. 2.5. Ultimate tensile strength of the welded joints.

On a centerline normal to the welding direction across the nugget, Fig. 2.6 shows the Vickers micro-hardness profiles of specimens B2 and C3, which exhibited the highest and lowest tensile strength, respectively. Compared to the base materials, it is clear from the two line graphs that the Vickers hardness number (VHN) fluctuated with a slight gradient in the nugget region and a noticeable drop in the HAZ of both alloys. The biggest drop was at the HAZ of the AA6061 alloy in the AS, where the hardness fell to the lowest values of 71 for specimen B2 and 66 for specimen C3 at about 5 mm away from the weld centerline. This decline clarifies the reason behind the location of failure in the tensiletests, as seen in the sample specimen surrounded by the red ellipse. Other than that, it has been reported that the change in material properties at the HAZ resulted from the sufficient heating during the welding process [4].

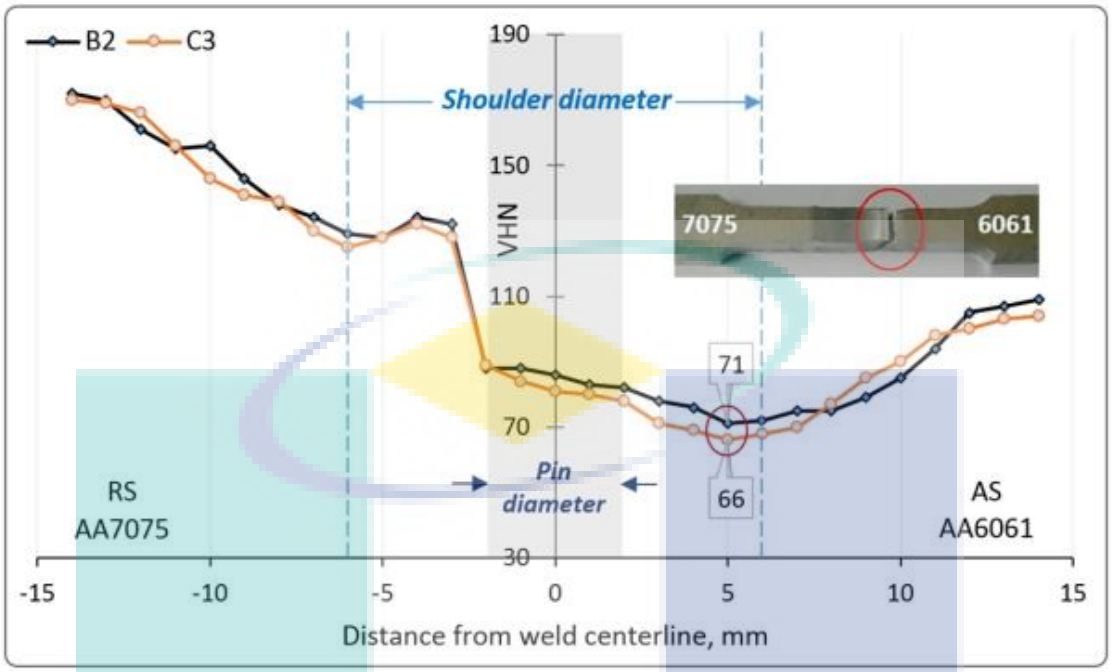

Fig. 2.6. Weld line produced on sample surface (CW) with different focal length.

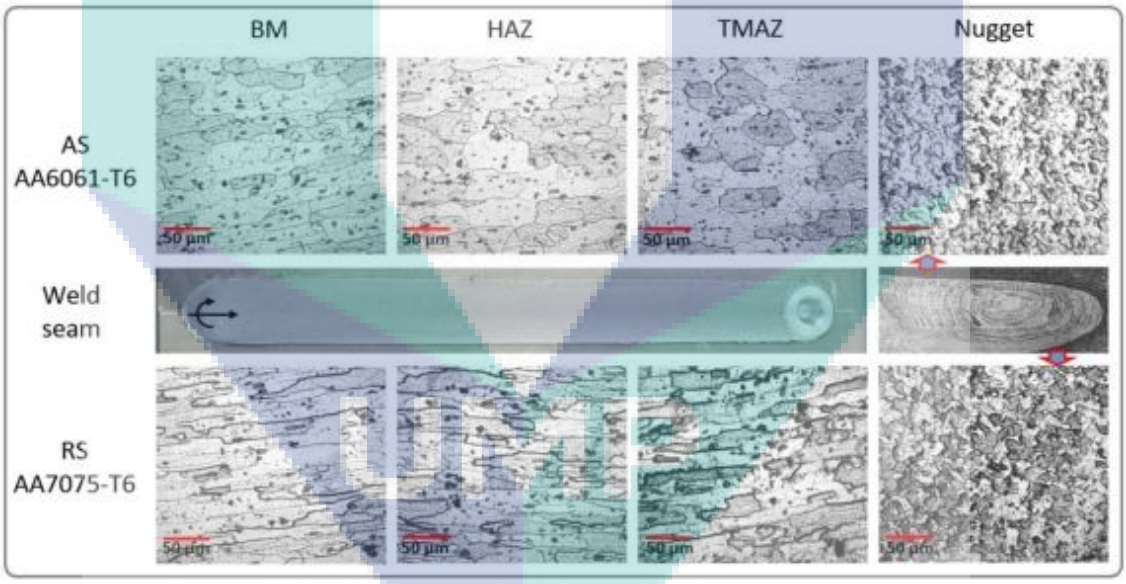

Fig. 2.7. Macro and microstructure with the weld seam of the (B2) specimen.

On the other side, the maximum tensile residual stresses commonly concentrated in the thermo-mechanical, affecting zone (TMAZ) and/or HAZ [49]. However, the use of aluminum, which has a high thermal diffusivity, as a backing plate and cover bar over the steel anvil and below the steel pressure bar contributes an increase in the cooling rate and hence reduces the alteration in the mechanical properties [50]. Similarly, the side L-shaped plates also assisted, as an additional heat sink, to extract more amount of

heat and control the temperature distribution. The average nugget hardness was lower compared to the base materials with a slight decrease in the AA6061-nugget related to the AA7075-nugget side. The best weldment with smooth surface finish, gap and defects free and good materials mixing were produced by the (B2) conditions, as shown in Fig. 2.7.

2.5 CONCLUSION

Results of the present work show that the present simplified design can effectively be used to achieve sound welds with smooth surface finish, gap and defects free and without

geometric imperfections. All of the test coupons of AA7075 and AA6061 aluminum alloys used to examine the validity of the clamping system exhibited relatively high tensile strength. The UTS of joints ranged from 220.9 MPa when the rotation and welding

speeds were 1200 rpm and 350 mm/min, respectively to the maximum value of 252.1 MPa when the rotation speed fixed at 1100 rpm and the welding speed at 300 mm/min. With this reason, the maximum value of the UTS represents an efficiency of about 82% with respect to the UTS of the AA6061 alloy. This efficiency is higher than the acceptable

limit due to the standards of the American Welding Society (AWS). Thus, the best test shows a minimum Vickers hardness number of about 71 at the HAZ of the AA6061 alloy,

where the failure in the tensile test occurred. For future research directions, it is recommended to improve the present test-rig for further investigations. While it is specially designed for butt-joint FSW research, it can be used as a clamping/backing system for lap-joint configuration.

2.6 REFERENCE

[1]. Parida B, Vishwakarma SD, Pal S. Design and development of fixture and force measuring system for friction stir welding process using strain gauges. Journal of Mechanical Science and Technology. 2015;29:739-49.

[2]. Upadhyay P, Reynolds AP. Effects of forge axis force and backing plate thermal diffusivity on FSW of AA6056. Materials Science and Engineering: A. 2012;558:394-402.

[3]. Imam M, Racherla V, Biswas K. Effect of backing plate material in friction stir butt and lap welding of 6063-T4 aluminium alloy. International Journal of Advanced Manufacturing Technology. 2015;77(9):2181-95.

[4]. Colligan KJ. The friction stir welding process: an overview. In: Lohwasser D, Chen Z, editors. Friction Stir Welding: Woodhead Publishing; 2010. p. 15-41.

[5]. Zappia T, Smith C, Colligan K, Ostersehlte H, Kallee SW. 4 - Friction stir welding equipment. In: Lohwasser D, Chen Z, editors. Friction Stir Welding: Woodhead Publishing; 2010. p. 73-117.
[6]. Sathari NAA, Shah LH, Razali AR. Investigation of Single-Pass/Double-Pass Techniques on Friction Stir Welding of Aluminium. Journal of Mechanical Engineering and Sciences. 2014;7:1053-61.
[7]. Abd Razak NA, Ng SS. Investigation of Effects of MIG Welding on Corrosion Behaviour of AISI 1010 Carbon Steel. Journal of Mechanical Engineering and Sciences. 2014;7:1168-78.
[8]. Mishra RS, Mahoney MW. Friction stir welding and processing: ASM International; 2007.
[9]. Smith CB, Hinrichs JF, Crusan WA, Leverett J. FSW Stirs Up Welding Process Competition. Forming and Fabricating. 2003:25–31.
[10]. Zain-Ul-Abdein M, Nélias D, Jullien JF, Deloison D. Thermo-mechanical analysis of laser beam welding of thin plate with complex boundary conditions. International Journal of Material Forming. 2008;1:1063-6.
[11]. Liu C, Zhang JX. Numerical simulation of transient welding angular distortion with external restraints. Science and Technology of Welding and Joining. 2009;14:26-31.
[12]. Liu QS, Mahdavian SM, Aswin D, Ding S. Experimental study of temperature and clamping force during Nd:YAG laser butt welding. Optics & Laser Technology. 2009;41:794-9.
[13]. Zain-ul-abdein M, Nélias D, Jullien J-F, Deloison D. Experimental investigation and finite element simulation of laser beam welding induced residual stresses and distortions in thin sheets of AA 6056-T4. Materials Science and Engineering: A. 2010;527:3025-39.
[14]. Sathari NAA, Razali AR, Ishak M, Shah LH. Mechanical Strength of Dissimilar Aa7075 and Aa6061 Aluminum Alloys Using Friction Stir Welding. International Journal of Automotive and Mechanical Engineering. 2015;11:2713-21.
[15]. Ishak M, Noordin NFM, Razali ASK, Shah LHA, Romlay FRM. Effect of filler on weld metal structure of AA6061 aluminum alloy by tungsten inert gas welding. International Journal of Automotive and Mechanical Engineering. 2015;11:2438- 46.
[16]. Ahmad R, Asmael MBA. Effect of aging time on microstructure and mechanical properties of AA6061 friction stir welding joints. International Journal of Automotive and Mechanical Engineering. 2015;11:2364-72.
[17]. Christner B, Sylva G. Friction stir welding development for aerospace applications. ICAWT. Columbus, OH, USA.1996, p. 359-68.
[18]. Leonard A, Lockyer S. Flaws in friction stir welds. 4th International Symposium on Friction Stir Welding: Park City, Utah, USA; 2003.
[19]. Richter-Trummer V, Suzano E, Beltrão M, Roos A, dos Santos JF, de Castro PMST. Influence of the FSW clamping force on the final distortion and residual stress field. Materials Science and Engineering: A. 2012;538:81-8.
[20]. Fratini L, Micari F, Buffa G, Ruisi VF. A new fixture for FSW processes of titanium alloys. CIRP Annals - Manufacturing Technology. 2010;59:271-4.
[21]. Upadhyay P, Reynolds A. Effect of Backing Plate Thermal Property on Friction Stir Welding of 25-mm-Thick AA6061. Metallurgical and Materials Transactions A. 2014;45:2091-100.
[22]. Khodir SA, Shibayanagi T, Naka M. Control of hardness distribution in friction stir welded AA2024-T3 aluminum alloy. Materials Transactions. 2006;47:1560- 7.
[23]. Hatifi MM, Firdaus MH, Razlan AY. Modal Analysis of Dissimilar Plate Metal Joining with Different Thicknesses using MIG Welding. International Journal of Automotive and Mechanical Engineering. 2014;9:1723-33.
[24]. Hariri A, Azreen P N, Abdull N, Leman AM, Yusof MZM. Determination of customer requirement for welding fumes index development in automotive industries by using quality function deployment approach. International Journal of Automotive and Mechanical Engineering. 2014;9:1609-19.
[25]. Chaki S, Ghosal S. A GA–ANN hybrid model for prediction and optimization of CO2 laser-mig hybrid welding process. International Journal of Automotive and Mechanical Engineering. 2015;11:2458-70.

[26]. Murphy A, Ekmekyapar T, Quinn D, Özakça M, Poston K, Moore G, et al. The influence of assembly friction stir weld location on wing panel static strength. Thin-Walled Structures. 2014;76:56-64.
[27]. Mishra RS, De PS, Kumar N. FSW of aluminum alloys. Friction stir welding and processing: Springer; 2014. p. 109-48.
[28]. Charde N. Effects of electrode deformation of resistance spot welding on 304 austenitic stainless steel weld geometry. Journal of Mechanical Engineering and Sciences. 2012;3:261-70.
[29]. Dursun T, Soutis C. Recent developments in advanced aircraft aluminium alloys. Materials & Design. 2014;56:862-71.
[30]. Bayazid SM, Farhangi H, Asgharzadeh H, Radan L, Ghahramani A, Mirhaji A. Effect of cyclic solution treatment on microstructure and mechanical properties of friction stir welded 7075 Al alloy. Materials Science and Engineering: A. 2016;649:293-300.
[31]. Abd Razak NA, Ng SS. Investigation of effects of MIG welding on corrosion behaviour of AISI 1010 carbon steel. Journal of Mechanical Engineering and Sciences. 2014;7:1168-78.
[32]. Shah L, Akhtar Z, Ishak M. Investigation of aluminum-stainless steel dissimilar weld quality using different filler metals. International Journal of Automotive and Mechanical Engineering. 2013;8:1121-31
[33]. Kumar N, Mishra RS, Yuan W. Friction Stir welding of dissimilar alloys and materials: A Volume in the Friction Stir Welding and Processing Book Series: Butterworth-Heinemann; 2015.
[34]. Çam G, Mistikoglu S. Recent developments in friction stir welding of Al-alloys. Journal of Materials Engineering and Performance. 2014;23:1936-53.
[35]. NAA S, AR R. Investigation of single-pass double-pass techniques on friction stir welding of aluminium. Journal of Mechanical Engineering and Sciences. 2014;7:1053-61.
[36]. Fu MJ, Li XH, Han XQ, Xu HY. Research on work hardening type superplastic deformation behavior of FSW titanium alloy. Materials Science Forum, 2016; 838-839; 506-11.
[37]. El-Batahgy A-M, Miura T, Ueji R, Fujii H. Investigation into feasibility of FSW process for welding 1600MPa quenched and tempered steel. Materials Science and Engineering: A. 2016;651:904-13.
[38]. Gao Y, Nakata K, Nagatsuka K, Matsuyama T, Shibata Y, Amano M. Microstructures and mechanical properties of friction stir welded brass/steel dissimilar lap joints at various welding speeds. Materials and Design. 2016;90:1018-25.
[39]. Murr LE. A Review of FSW Research on dissimilar metal and alloy systems. Journal of Materials Engineering and Performance. 2010;19:1071-89.
[40]. Guo JF, Chen HC, Sun CN, Bi G, Sun Z, Wei J. Friction stir welding of dissimilar materials between AA6061 and AA7075 Al alloys effects of process parameters. Materials & Design. 2014;56:185-92.
[41]. İpekoğlu G, Çam G. Effects of initial temper condition and postweld heat treatment on the properties of dissimilar friction-stir-welded joints between AA7075 and AA6061 aluminum alloys. Metallurgical and Materials Transactions A. 2014;45:3074-87.
[42]. Cole EG, Fehrenbacher A, Duffie NA, Zinn MR, Pfefferkorn FE, Ferrier NJ. Weld temperature effects during friction stir welding of dissimilar aluminum alloys 6061-t6 and 7075-t6. International Journal of Advanced Manufacturing Technology. 2013;71:64352.
[43]. Shah LH, Zainal Ariffin NF, Razali AR. Parameter optimization of AA6061- AA7075 dissimilar friction stir welding using the Taguchi method. Applied Mechanics and Materials. 2014;695:20-3.
[44]. Ishak M, Shah LH, Aisha ISR, Hafizi W, Islam MR. Study of resistance spot welding between AISI 301 stainless steel and AISI 1020 carbon steel dissimilar alloys. Journal of Mechanical Engineering and Sciences. 2014;6:793-806.
[45]. Metals ASf, Davis JR. ASM handbook. 2. Properties and selection: nonferrous alloys and special-purpose materials: ASM international; 2009.
[46]. Rai R, De A, Bhadeshia HKDH, DebRoy T. Review: friction stir welding tools. Science and Technology of Welding and Joining. 2011;16:325-42.
[47]. Thomas W, Norris I, Staines D, Watts E. Friction stir welding-process developments and variant techniques. The SME Summit. 2005;1:1-21.

[48]. Peel M, Steuwer A, Preuss M, Withers PJ. Microstructure, mechanical properties and residual stresses as a function of welding speed in aluminium AA5083 friction stir welds. Acta Materialia. 2003;51:4791-801.
[49]. Williams SW, Steuwer A. 8 - Residual stresses in friction stir welding. In: Lohwasser D, Chen Z, editors. Friction Stir Welding: Woodhead Publishing; 2010. p. 215-44.
[50]. Zettler R. 3 - Material deformation and joint formation in friction stir welding. In: Lohwasser D, Chen Z, editors. Friction Stir Welding: Woodhead Publishing; 2010. p. 42-72.
[51]. Cavaliere P, Nobile R, Panella FW, Squillace A. Mechanical and microstructural behaviour of 2024–7075 aluminium alloy sheets joined by friction stir welding. International Journal of Machine Tools and Manufacture. 2006;46:588-94.
[52]. Cavaliere P, Cerri E, Squillace A. Mechanical response of 2024-7075 aluminium alloys joined by Friction Stir Welding. Journal of Materials Science. 2005;40:3669-76.
[53]. Firouzdor V, Kou S. Formation of liquid and intermetallics in Al-to-Mg friction stir welding. Metallurgical and Materials Transactions A. 2010;41:3238-51.

CHAPTER 3

TECHNICAL PAPER #2

Title:- Influence of machine variables and tool profile on the tensile strength of dissimilar AA7075-AA6061 friction stir welded.

(International Jounral of Advance Manufacturing Technology (2017) 90:2605–2615
DOI: 10.1007/s00170-016-9583-3 – ISI Indexed)

3.1 ABSTRACT

Friction stir welding (FSW) of dissimilar alloys and materials is becoming progressively essential as it permits to take the benefits of both materials. Tensile strength is a measure of the weld quality, which mainly depends on machine variables and tool design. In this paper, FSW of dissimilar AA7075-AA6061 aluminium alloys was studied with respect to the welding speeds (rotational and axial), tool tilt angle andtool geometry by the response surface methodology (RSM) with central composite design (CCD). A reduced secondorder polynomial equation was successfully developed and validated to adequately fit the observed results of the ultimate tensile strength (UTS). Respectable fitness and well agreement between the experimental and calculated values with an elevated regression coefficient and low deviation were detected for this model within the range of the operating variables. Five tools with concave shoulders and different probe profiles (cylindrical and tapered, smooth and threaded, flattedand non-flatted) and a self-designed backing plate and clamping system were fabricated for this study. It was found that the welding tool with a threaded truncated cone pin andsingle flat results in a sound weld with higher tensile strength, wide nugget area and smooth surface finish.

3.2 INTRODUCTION

Friction stir welding (FSW), the solid-state technique, provides the opportunity of joining hard-to-weld and dissimilar alloys or materials [1]. Widespread benefits resulting from the pplication of this green technology in aerospace, shipbuilding, automotive, railway and other industries are due to its advantages over conventional

fusion welding methods [2]. Since 1991, when this novel technique was invented by The Welding Institute (TWI) in the UK [3], researchers started to understand the effect of the process on joint properties. The process parameters, such as tool design, machine and other variables, have been investigated in numerous research studies to determine the outcome of this technique. High-quality joints have been obtained between dissimilar alloys or metals [4, 5]. However, much remains to be learned about the process, and opportunities for advance research studies and improvements are still promising.

An important consideration in the plan of a successful FSW process is the issue of the welding tool, which is the main source of the heat required for material softening and mixing. Tool design is the most influential aspect of the process developmental to achieve sound welds with good mechanical properties. It mainly focuses on the shoulder and pin geometry and the added features which influence the material flow. Selection of tool material, geometry and features (flats, flutes, steps and threads) depends on the welding configuration (butt or lap), material and thickness of the workpiece and the type of welding (similar or dissimilar). Tool design has been comprehensively reviewed in a considerable amount of research articles and review papers [6–10]. Many of the advances made in FSW have been enabled by the development of new welding tools with different profiles and added features. However, there is no accepted optimum tool design in use nowadays [11], since a particular tool may produce different responses when the same set of input parameters is used on different alloys or with different plate thicknesses [12].

Ultimate strength is a measure of the joint quality, which is mainly dependent on machine variables and tool design. In addition, it was demonstrated that joint strength in FSW is also dependent on the manufacturing precision of the backing plate and clamping system [13–18]. It is hence thought necessary to use proper design of backing plate and fixtures as a preparatory step before the welding process. Measurement of the ultimate strength of the welded joints requires extensive use of experimentation with varying levels of influencing factors. Design of experiment and statistical methods can significantly increase the efficiency and minimize the number of these experiments [19]. It was demonstrated that joint formulation in the FSW of dissimilar alloys or materials is a complex route,especially for those with large contrast in mechanical, thermal and chemical properties, such as the AA7075-T6 and AA6061-T6 aluminium alloys [20].

These heat-treatable and hard-to-weld materials are widely used in the automotive, aircraft, aerospace, marine and transportation industries [21–24]. The AA7075 aluminium alloy is a relatively high-strength material, which can be used for highly stressed structural parts. The widely available AA6061 has a good workability, high resistance to corrosion and excellent welding characteristics. The effectiveness of similar friction stir welding of these two alloys has been demonstrated in multiple research studies. On the other hand, dissimilar friction stir welding of AA7075 to AA6061 has been investigated in a few studies [25–27]. Mathematical modelling and statistical analysis were not taken into account in these studies.

Accordingly, this work aims to develop an empirical model for predicting the tensile strength of dissimilar AA7075- AA6061 friction stir welds. The influence of machine parameters (welding speeds and tilt angle) and tool profile on the ultimate tensile strength (UTS) were presented by the response surface methodology (RSM) with the central composite design (CCD). Tests have been achieved using a special self-designed backing plate and clamping system

3.3 MATERIAL AND METHOD

3.3.1 Experimental Procedure

A special self-designed clamping system and fixtures, which had previously been fabricated [28], was used to perform the FSW experiments. As seen in Fig. 3.1, the vertical clamping forces in this test rig were applied by means of pressure bars, bolts and nuts to ensure uniform pressure and temperature distribution throughout the welded plates [29]. The lateral restraints consist of two L-shaped aluminium plates and two end-screwed bolts. This construction enables an increase in the heat sink [13] and allows to apply uniform side pressure on the specimens [18]. Composite backing plates and pressure bars of aluminium and stainless steel were used to perform stronger joints [17, 15, 14, 13]. The width of the backing plates is slightly less than the total width of the workpieces in order to apply the lateral pressure directly on the specimens. The horizontal plane containing the two sheets is free of bolts and their holes. This is to avoid any change in the heat sink during the process. Specimens of dissimilar aluminium alloys AA7075-T6 and AA6061-T6 were cut from 3-mm-thick rolled sheets with dimensions of 125 × 50 mm. The edges of specimens were ground by a precision

surface grinding machine (Okamoto GRIND-X ACC65DX) and cleaned with acetone to prevent aluminium oxide and other volumetric defects in the weld zone [11].

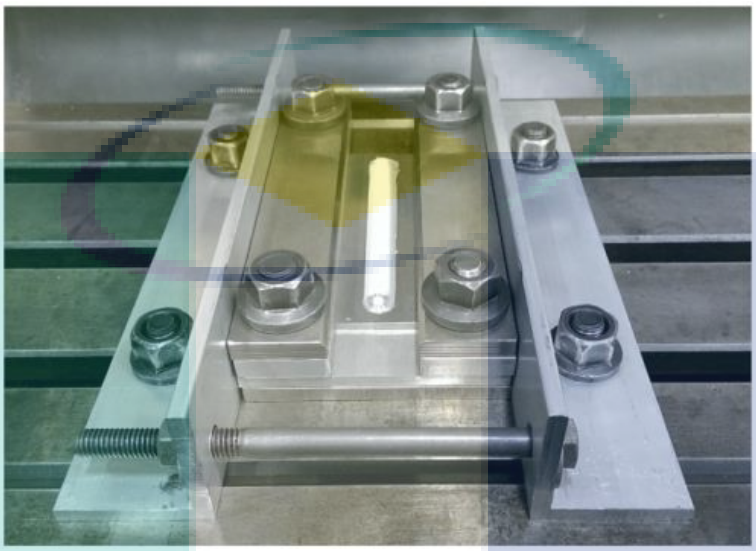

Fig. 3.1. Photo of the specially designed backing plates and clamping system

The chemical composition of the two alloys is listed in Table 3.1. Specimens were butt-joined along the rolling direction using a Vertical Milling Machine (VMM 3917). Since the strength of the workpiece can be slightly increased when softer alloy is placed on the advancing side (AS) of the welding tool [30, 26, 31-35], the AA6061 aluminium alloy was fixed on the AS. The rotating tool pin was slowly plunged into the seam axially until the tool shoulder came into intimate contact with the surfaces of the workpieces and a sufficient dwell time was allowed. The frictional and deformational heat required to locally soften the materials around the pin is generated during this plunge and dwell sequence. The penetration depth of the tool shoulder into the plates was about 0.2 mm, and the axial position of the tool pin was held constant between the two alloys while it traversed along the welding line at a constant speed.

Table 3.1. Chemical compositions (wt.%) of aluminium alloys

Alloy	**Si**	**Fe**	**Cu**	**Mn**	**Mg**	**Cr**	**Zn**	**Ti**	**Al**
AA7075-T6	0.07	0.27	1.6	0.03	2.5	0.19	5.7	0.02	Bal.
AA6061-T3	0.067	0.32	0.23	0.014	1.06	0.21	0.01	0.02	Bal.

For the age-hardenable alloys, the mechanical properties of the aswelded joints are considerably decreased due to the partial dissolution and coarsening of the hardening particles [36, 37]. To recover the hardness and strength of the welds, the metallographic and transverse tensile specimens were prepared after about 1 month of natural ageing [38] according to the American Society for Testing of Materials (ASTM E8-11) standard, whose geometry, positions and dimensions are shown in Fig. 3.2. Tests were then conducted at room temperature with a speed of 1 mm/min using a universal testing machine (INSTRON 3369). Average value of the ultimate tensile strength from three tensile specimens was noted down for each joint. Standard metallographic technique was followed to prepare the metallographic specimens. Manual and automatic grinding machines with 240, 320, 400, 600 and 800 grit silicon carbide papers were used to remove the saw marks and levels and clean the specimens' surfaces. After the finest grinding step, the specimens were polished with free 6-, 3- and 1-μm abrasives on cloths to remove the artefacts of grinding. Finally, the specimens were etched with a modified Keller's reagent so that the grain structure of the weld zone could be observed. An optical microscope was used to perform the microstructural analysis.

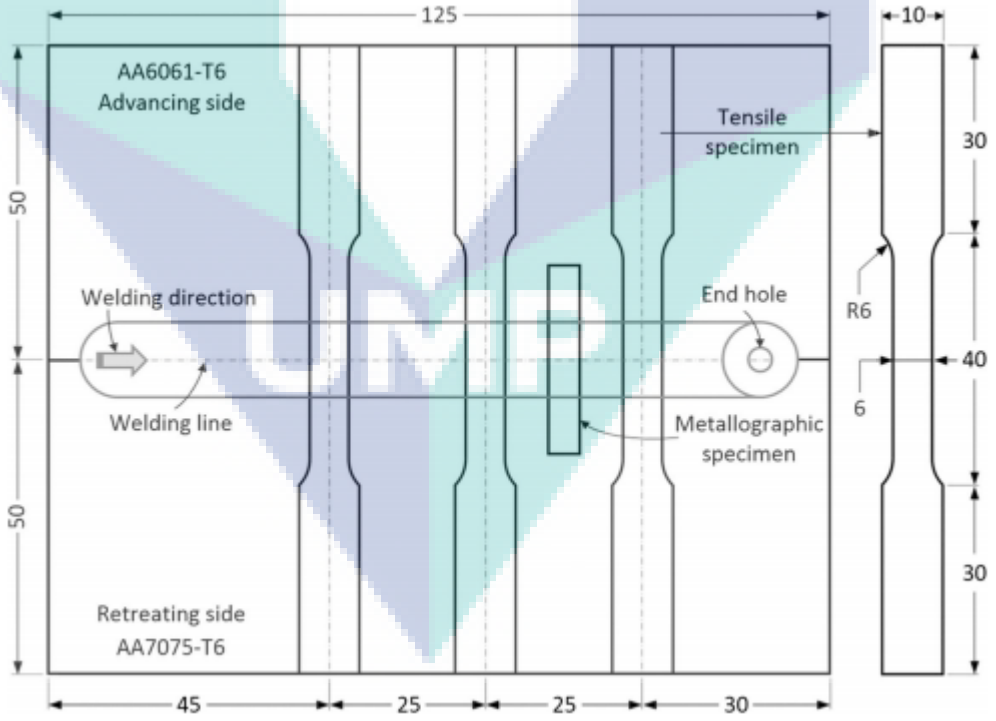

Fig. 3.2. Geometry, positions and dimensions of the tensile specimens in millimetres according to the ASTM E8-11 standard.

3.3.2 Experimental design and statistical analysis

Tool design and welding speeds are the most influential aspects of the FSW process development to achieve efficient and sound welds [6, 38, 2, 7–9, 4, 10]. Tool tilt angle is another variable affecting the tensile strength of the joint [39]. To perform the welding joints of this work, five tools with concave shoulders have been fabricated from AISI H13 steel. The most common shoulder design is the concave shoulder, which produces quality friction stir welds [40, 4, 3, 41]. This design requires 6° to 10° of concavity and 2° to 4° of tool tilt angle [38]. Accordingly, each tool has a shoulder of 12-mm diameter with an 8° of concavity. The flat bottom probe has a length of 2.7- and 4.2-mm base diameter.

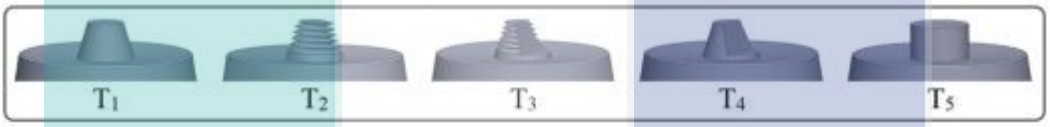

Fig. 3.3. The five tools used to perform the weldments in 3-D view.

As shown in Fig. 3.3, cylindrical pin was used in tool T5, while the core of the probe was tapered with 10° in the other tools. Left-hand threads were added to the tapered pins of tools T2 and T3, and a further tapered flat was added to the truncated cone pins of T3 and T4. In view of the previous research studies and based on results of the preliminary experiments, five levels of tool rotation and traverse speeds were selected. The working range of parameters was examined by varying one factor while keeping the others constant [42, 43].

Table 3.2. Welding parameters and tool dimensions for FSW.

Coded Level	**Values**			
	Tool (*T*)	Rotation Speed (ω), rpm	Transverse Speed (*v*), mm/min	Tilt Angle (θ), deg.
-2	T_1	900	200	2.0
-1	T_2	1000	250	2.5
0	T_3	1100	300	3.0
+1	T_4	1200	350	3.5
+2	T_5	1300	400	4.0

The tool tilt angle was varied between 2° and 4° due to the concavity of the tool shoulder. Surface finish and mechanical properties were observed for appropriate arrangement of the selected variables, which were coded according to the following form and reported in Table 3.2;

$$x_i = \frac{Xi - Xi}{\Delta Xi} \quad (3.1)$$

where xi and Xi are the coded and actual values of the factor, respectively; X i represents the average of the high and low actual values of the i factor; and ΔXi is the step change value. With this form, the upper and lower levels of each factor were coded as +2 and -2, respectively. The response surface methodology, which focuses on studying a mathematical relationship between parameters and the response of the studied system, was applied to optimize the tensile strength of the welded joints. Central composite design, the most important and common experimental design used in this methodology, was performed to investigate the significance of the effects of the four independent variables at five levels. The experiments were carried out randomly with a complete design matrix of 31 experimental points, as shown in Table 3.3 which also presents the tensile strength of the base materials (BM). This matrix consists of 16 factorial points (2k), 8 axial points (2 k) and 7 central points, where k is the number of independent variables. Second-order polynomial regression model is developed to fit the experimental data and expressed by using the following response surface equation [44]:

$$Y = \beta_o + \sum_{i=1}^{k} \beta_i X_i + \sum_{i=1}^{k} \beta_{ii} X_i^2 + \sum_{i=1}^{k-1} \sum_{j=2}^{k} \beta_{ij} X_i X_j \quad (3.2)$$

In this general form, Y is the predicted response which is a function of the independent variables (X) in coded representation. The regression coefficients βo, βi, βii and βij are the intercept constant, linear effect, squared effect and interactive effect terms, respectively. For the selected factors (T, ω, υ and θ), k = 4 and the ultimate tensile strength could then be expressed as follows:

$$UTS = \beta_o + \beta_1(T) + \beta_2(\omega) + \beta_3(\upsilon) + \beta_4(\theta) + \beta_{11}(T^2) + \beta_{22}(\omega^2) + \beta_{33}(\upsilon^2) + \beta_{44}(\theta^2) + \beta_{12}(T\omega) + \beta_{13}(T\upsilon) + \beta_{14}(T\theta) + \beta_{23}(\omega\upsilon) + \beta_{14}(\omega\theta) + \beta_{34}(\upsilon\theta) \quad (3.3)$$

The statistical significance of the regressive model and its coefficients were analysed using analysis of variance (ANOVA). The accuracy and general ability of the preferred polynomial model were evaluated by the coefficient of determination (R2)

with a 95 % confidence level. Therefore, P value of less than 0.05 was considered to be statistically significant. Design of experiments and statistical analysis were carried out by means of the Minitab software [45].

3.4 RESULTS AND DISCUSSION

The experimental procedures were followed to assess the ultimate tensile strength of the base materials and the welded joints according to the complete central composite design matrix. The proper clamping/backing system and the careful joint preparation enabled to obtain stable results with lower deviation, as seen in Table 3.3.

Table 3.3. The CCD matrix of the response surface methodology.

Run No.	The actual levels of parameters				Ultimate tensile strength, UTS (MPa)				
	T	ω	υ	θ	Test 1	Test 2	Test 3	Mean	SD
Factorial points									
1	T_2	1000	250	2.5	222.23	225.46	226.44	224.7	2.20
2	T_4	1000	250	2.5	213.87	218.27	219.13	217.1	2.82
3	T_2	1200	250	2.5	226.02	228.36	227.01	227.1	1.18
4	T_4	1200	250	2.5	219.82	221.73	225.83	222.5	3.07
5	T_2	1000	350	2.5	217.06	219.30	218.45	218.3	1.13
6	T_4	1000	350	2.5	210.76	215.48	212.82	213.0	2.37
7	T_2	1200	350	2.5	216.83	219.02	223.31	219.7	3.30
8	T_4	1200	350	2.5	212.10	214.35	214.29	213.6	1.28
9	T_2	1000	250	3.5	219.74	223.07	222.62	221.8	1.81
10	T_4	1000	250	3.5	216.18	215.89	217.31	216.3	0.75
11	T_2	1200	250	3.5	223.41	227.75	226.60	225.9	2.25
12	T_4	1200	250	3.5	216.67	220.20	220.79	219.2	2.23
13	T_2	1000	350	3.5	212.03	217.54	220.71	216.8	4.40
14	T_4	1000	350	3.5	207.24	206.71	208.94	207.6	1.17
15	T_2	1200	350	3.5	215.90	217.11	216.10	216.4	0.65
16	T_4	1200	350	3.5	212.36	210.01	208.59	210.3	1.90
Axial points									
17	T_1	1100	300	3.0	199.08	201.62	202.84	201.2	1.92
18	T_5	1100	300	3.0	188.54	193.21	194.61	192.1	3.19
19	T_3	900	300	3.0	229.81	227.94	227.39	228.4	1.27
20	T_3	1300	300	3.0	229.70	234.01	236.01	233.2	3.23
21	T_3	1100	200	3.0	232.07	231.84	234.70	232.9	1.59
22	T_3	1100	400	3.0	213.91	219.11	221.19	218.1	3.75
23	T_3	1100	300	2.0	239.46	240.30	239.67	239.8	0.44
24	T_3	1100	300	4.0	229.02	234.63	233.34	232.3	2.94
Central points									

25	T_3	1100	300	3.0	248.03	252.55	251.19	250.6	2.32
26	T_3	1100	300	3.0	250.48	251.20	248.05	249.9	1.65
27	T_3	1100	300	3.0	252.91	254.76	253.61	253.8	0.93
28	T_3	1100	300	3.0	248.82	253.57	255.83	252.7	3.58
29	T_3	1100	300	3.0	247.73	254.81	251.90	251.5	3.56
30	T_3	1100	300	3.0	251.50	253.28	255.18	253.3	1.84
31	T_3	1100	300	3.0	250.47	253.73	254.08	252.8	1.99
Base materials									
AA7075-T6 aluminum alloy					572.01	570.44	571.16	571.2	0.80
AA6061-T6 aluminium alloy					306.20	307.91	306.44	306.9	0.93

Coefficients of the model were evaluated as a result of analysing the response surface design. By removing the insignificant terms (P > 0.05) and taking the significant coefficients (linear and quadratic effect terms) into account, a developed model for the ultimate tensile strength of AA7075-AA6061 aluminium alloy friction stir weldment was constructed as follows:

$$UTS = 252.086 - 2.8875(T) + 1.19583(\omega) - 3.6875(\upsilon) - 1.52917(\theta) - 14.5433(T^2) - 6.0058(\omega^2) - 7.3308(\upsilon^2) - 4.6933(\theta^2)$$

(**Error! No text of specified style in document.**)

Least-squares fit and parameter estimates of the developed response surface model are shown in Table 3.4. All of the presented coefficients showed higher significance with very small P values and corresponding bigger amount of t ratios. Elevated regression coefficient (R2 = 0.9851) was recorded, which indicated that the developed model had a very high correlation and only about 0.902 % of the total variations would not be clarified by it. Simultaneously, the adjusted regression coefficient (R2 = 0.9796) gave another confirmation to the adequate fit of this reduced response surface model. Furthermore, adequacy of the empirical model for predicting the ultimate strength as a function of tool profile, rotation speed, feed rate and tilt angle is also clear from the ANOVA output shown in Table 3.5.

Table 3.4. Regression coefficients of the developed model

Term	Coefficient	Standard error	*t*-ratio	*P*-value
Constant	252.086	0.8996	280.212	0.000
T	−2.887	0.4859	−5.943	0.000
ω	1.196	0.4859	2.461	0.022
υ	−3.688	0.4859	−7.590	0.000
θ	−1.529	0.4859	−3.147	0.005
T^2	−14.543	0.4451	−32.674	0.000
ω^2	−6.006	0.4451	−13.493	0.000

v^2	−7.331	0.4451	−16.470	0.000
θ^2	−4.693	0.4451	−10.544	0.000

R^2 = 98.51%; Adjusted R^2 = 97.96%; Standard error = 2.38019

Consequently, the developed model was used to evaluate the ultimate tensile strength corresponding to the mean observed values shown in the complete CCD matrix (Table 3.3). The results show a respectable fitness of the mathematical model with the experimental data within the range of the operating variables, as is obvious by the scatter plot shown in Fig. 3.4.

Table 3.5. ANOVA of UTS for the developed model

Source	**DF**	**Sum of squares**	**Mean squares**	**Adj. Mean squares**	***F*−value**	***P*−value**
Model	8	8225.83	8225.83	1028.23	181.50	0.000
Linear	4	616.89	616.89	154.22	27.22	0.000
Square	4	7608.94	7608.94	1902.24	335.77	0.000
Residual error	22	124.64	124.64	5.67		
Lack-of-fit	16	112.01	112.01	7.00	3.33	0.072
Pure error	6	12.63	12.63	2.10		
Total	30	8350.47				

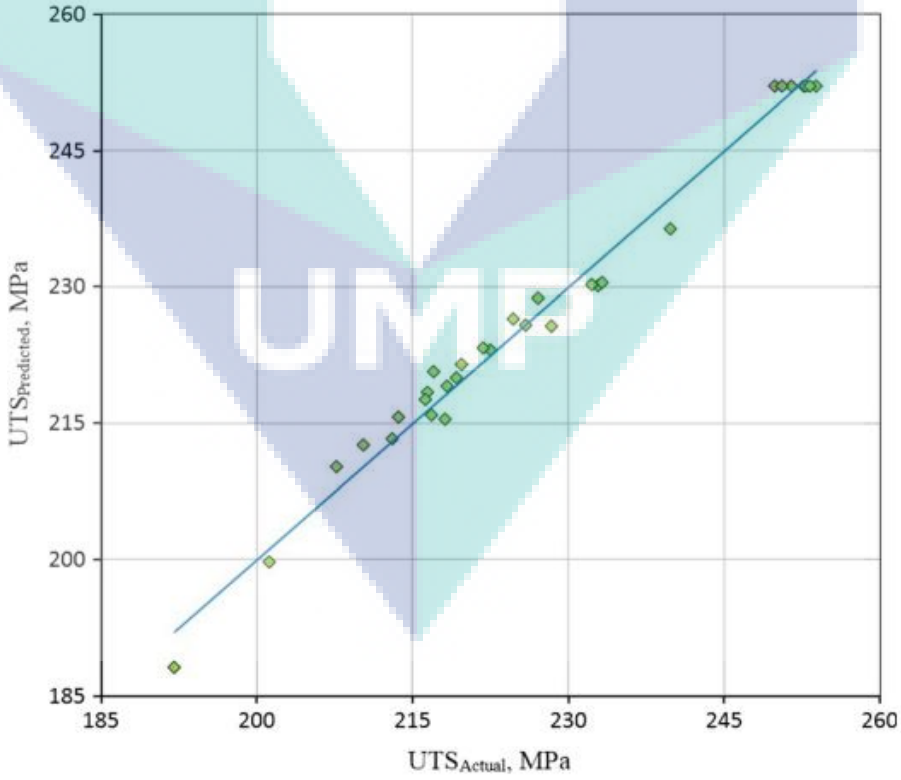

Fig. 3.4. Scatter plot of the observed and predicted results of UTS.

To validate the accuracy of the developed model, extra workpieces were friction stir welded with selected levels of variables (other than those used in the design matrix). Tools (T2 and T4) were tested at the central levels of the welding speeds and tilt angle to make a comparison between the five tools used in this study. Ultimate tensile strength of these joints was measured after the same natural ageing period and listed in Table 3.6. The developed model was used to predict the corresponding values. The verification tests showed well agreement between the observed and calculated values with low deviation (error within ±10 %).

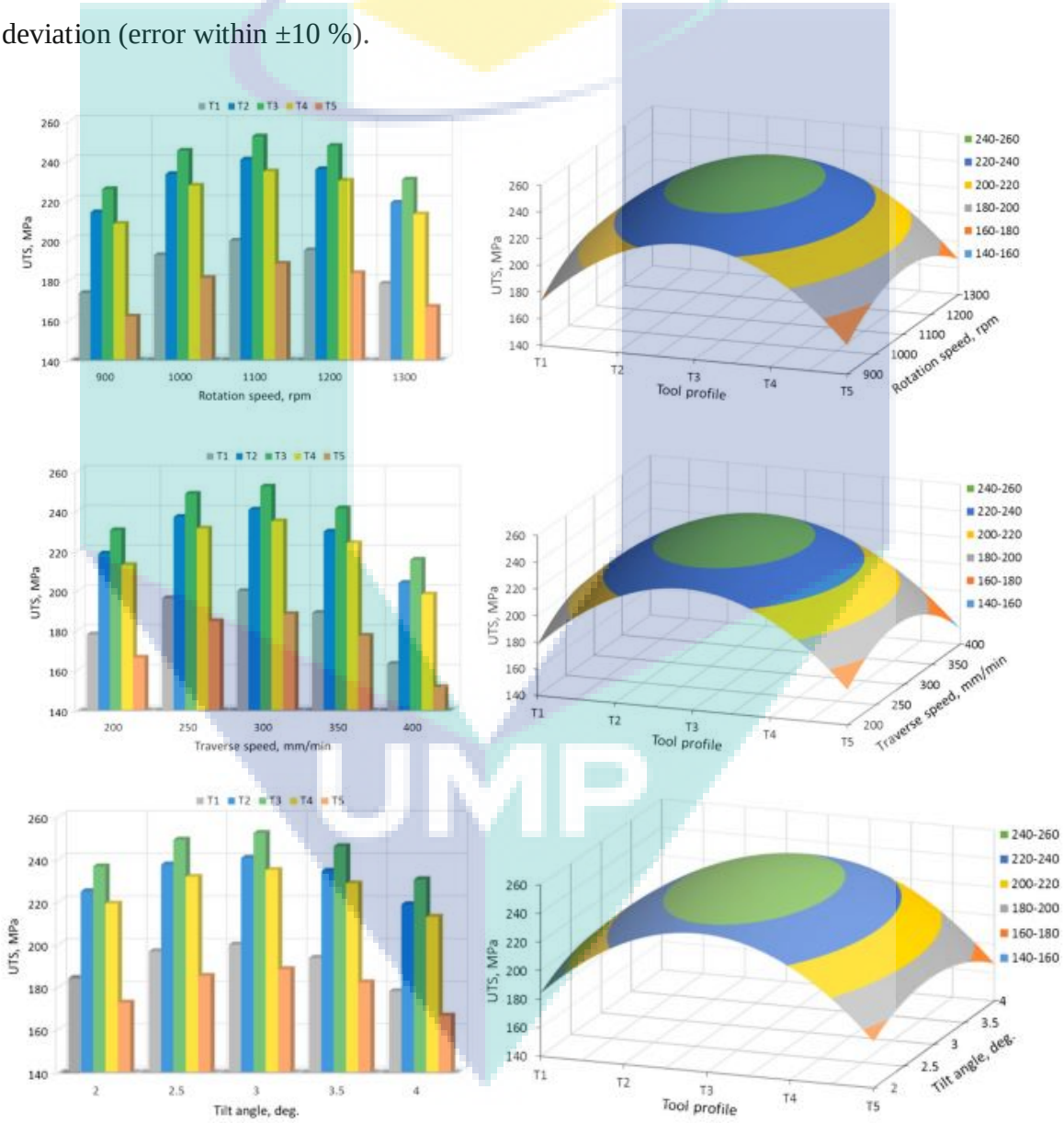

Fig. 3.5. Response 3-D contour plots and clustered column showing the relation between the independent variables and the ultimate strength. In each plot, the two other factors were fixed at their intermediate levels.

Relation between the ultimate strength and the independent variables was represented graphically by the developed response surface model in the three dimensional (3-D) contour plots and clustered column (Fig. 3.5). Response surface methodology efficiently enables to detect the effect of the selected variables on joint strength and to identify their optimal values that lead to gain the maximum response. In all plots, the predicted results of UTS were presented with two incessant variables, whereas the two other factors were fixed at their intermediate levels. The optimal values of the independent variables could be detected from these graphs. It is clear that the ultimate strength of the dissimilar joint is significantly affected by the rotation speed, feed rate and tilt angle regardless of the geometry of the welding tool. On the other side, tool pin profile played an important role in the response of these variables. To show which parameter plays a more influential role on the joint tensile strength, a brief sensitivity analysis on the developed model was attained. The sensitivity coefficient of each variable on the tensile strength was calculated by partially deriving Eq. 3.4 with respect to the affected parameters, as in the following equations:

$$\partial UTS/\partial T = -2.8875 - 29.0866T \quad (3.5)$$

$$\partial UTS/\partial \omega = 1.19583 - 12.0116\omega \quad (3.6)$$

$$\partial UTS/\partial v = -3.6875 - 14.6616v \quad (3.7)$$

$$\partial UTS/\partial \theta = -1.52917 - 9.3866\theta \quad (3.8)$$

The results of the analysis, which are presented in Fig. 3.6, show that the tensile strength is more sensitive to the design of tool followed by traverse speed, rotation rate and tilt angle. Consequently, the five welding tools that are described previously and viewed in Fig. 3.3 were examined at the central levels of the other three variables. Stress–strain curves and the macrographs of the weld nuggets with the ultimate strength for the joints produced by these tools are shown in Figs. 3.7 and 3.8, respectively.

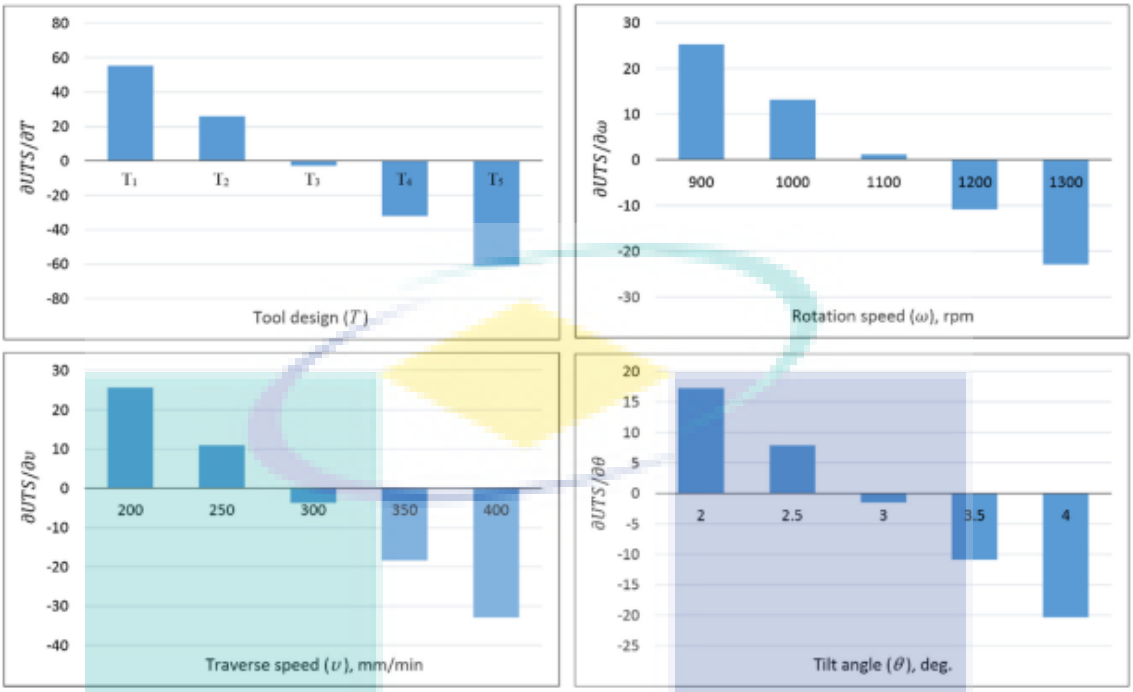

Fig. 3.6. Results of the sensitivity analysis.

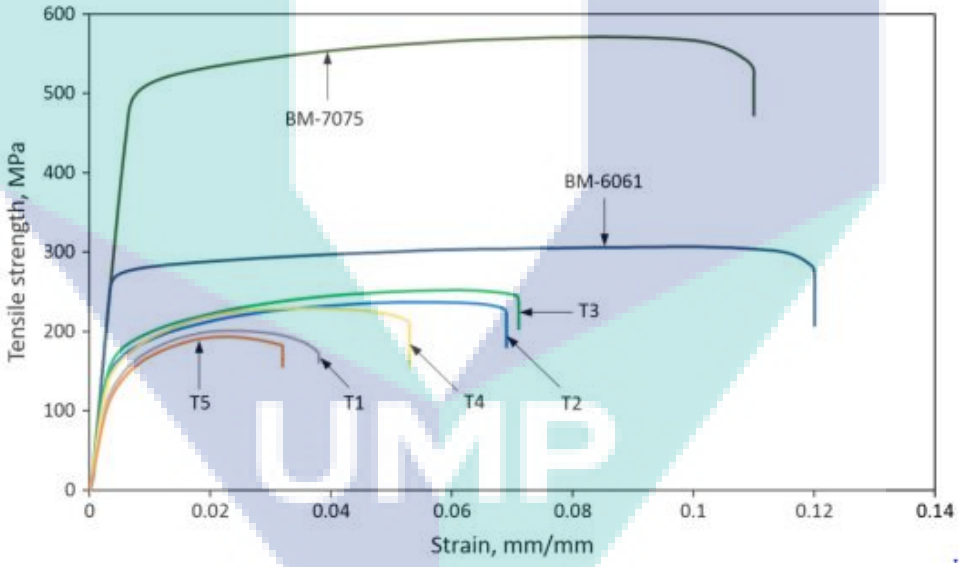

Fig. 3.7. Stress–strain curves of the base materials and the welded joints using the five tools at the central levels of the other three variables.

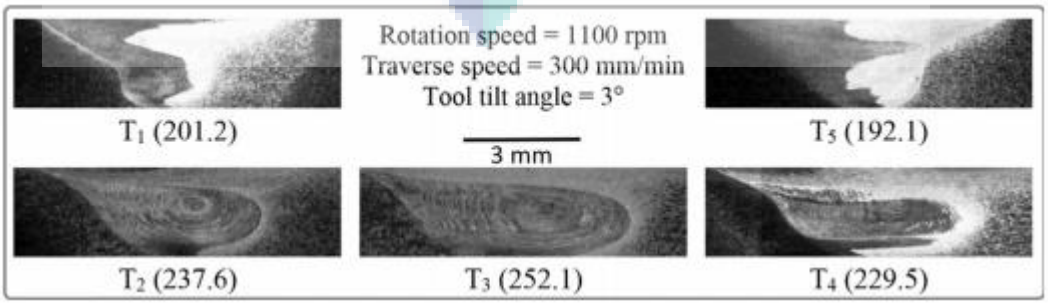

Fig. 3.8. Macrographs of the weld nuggets and the ultimate tensile strength (UTS, MPa) for the five tools. The AA6061 is placed on the left-hand side (AS) of each photo

Lower tensile strength, elongation at fracture and poor material mixing resulted from the first and last tools (T1 and T5), which consist of smooth tapered and cylindrical probes, respectively. However, the tensile strength was slightly higher with the tapered tool pin. Similar observations have been reported by other researchers [46–50]. By the fourth tool (T4), ultimate strength started to relatively increase and the weld nugget became wider. This is due to the flat that has been added to the core of the probe which improved the local deformation and material flow [51, 52]. Nevertheless, the additional feature used with the smooth or non-threaded probe design did not significantly improve the joint strength and material mixing. Consequently, left-hand threads were added to the tapered pin of tool (T2) to promote more effective material mixing. Threads were fabricated in a direction opposite to that of the tool rotation, in order to transport material from the shoulder down to the bottom of the pin to improve the vertical material flow [53, 54]. With this tool, a noticeable growth in joint strength and an improved mixing of the two alloys at the welding zone were observed.

The best outcomes were gained by stirring with tool (T3), which was similar to the previous one but with an additional tapered flat. By this tool, the two aluminium alloys were successfully friction stir welded with a smooth surface finish, bigger nugget area, maximum elongation and high tensile strength (about 31 % higher than T5). It is worth noting that the weld zone was free of internal voids for all joints, especially for those produced by the first and last tools. This is due to the proper and active design of the clamping system and backing plates, which has been explained previously. The complexity of the thermo-mechanical FSW process, especially in the case of dissimilar alloys, makes the traditional ways of investigation unable to show the interaction between the affecting arameters.

The machine variables, tool design and clamping/backing system control the temperature generation and dissipation throughout the joining route [55, 56]. This in turn affects material flow and tensile properties of the welded coupons. Temperature in the workpiece must be high enough to adequately soften material for the pin to stir but low enough to avoid access to the melting points [57]. Too cold and too hot welding result in non-bonding and excessive material flow, respectively, and hence degradation of the mechanical properties of the joint [58, 59]. The response surface and column

graphs show that the apex tensile strength could be achieved by applying 1100 rpm of rotation speed and 300 mm/min feed rate together with tool (T3), which tilted by 3° away from the vertical axes to the stirring direction. By these conditions, the joint efficiency reached about 82 % with respect to the UTS of the aluminium 6061-T6. Strength of the friction stir weldment started to decrease out of these conditions of the selected variables for all tool profiles.

3.5 CONCLUSION

In the present work, statistical analysis and central composite design of the response surface methodology were used successfully to investigate the influence of tool profile and machine variables (rotation speed, feed rate and tilt angle) on the tensile strength of dissimilar AA7075-AA6061 aluminium alloys joined by friction stir welding. Five different tools and special clamping/backing system were designed and fabricated to prepare the welded coupons. Results of this study lead to the following conclusions:

1. The reduced response surface model developed in this work seemed to be an active tool for the prediction of the joint strength as a function of the four selected variables. A respectable fitness of this model with the experimental data within the range of the operating variables was indicated with an elevated regression coefficient (R^2 = 0.9851). Well agreement between the observed and calculated values with low deviation (error within ±10 %) was also recorded through the validation tests.

2. Joint strength in FSW could be improved when tool design is studied in conjunction with welding speeds and tilt angle, taking into account the clamping/backing system. The RSM methodology with CCD enabled to reduce the umber of experiments and the proper clamping design resulted in stable joints with defect-free welds.

3. Tool design is the most influential factor affecting the tensile strength and material mixing throughout the joining route. Tool with tapered probe and additional features (threads and flat) results in sound weld with smooth surface finish, good material mixing and high tensile strength. On the other side, tools with smooth

cylindrical or even tapered pin result in poor material mixing and hence lower joint strength.

4. FSW of AA7075-AA6061 aluminium alloys with 1100 rpm tool rotation speed, 300 mm/min traverse speed and 3° of tool tilt angle results in a stronger joint. In these conditions, the AA6061 was located on the AS and welding seam was parallel to the rolling direction of both alloys. Ultimate strength reached the maximum value at bout 252 MPa, which represents an efficiency of 82 % with respect to the UTS of the AA6061-based material.

3.6 REFERENCE

[1]. Murr LE (2010) A review of FSW research on dissimilar metal and alloy systems. J Mater Eng Perform 19(8):1071–1089. doi:10.1007 s11665-010-9598-0

[2]. Nandan R, Debroy T, Bhadeshia H (2008) Recent advances in friction-stir welding—process, weldment structure and properties. Prog Mater Sci 53(6):980–1023. doi:10.1016/j.pmatsci.2008.05.001

[3]. Thomas WM, Nicholas ED, Needham JC, Murch MG, Templesmith P, Dawes CJ (1991) Friction stir butt welding. International Patent Application No. PCT/GB92 Patent Application No. 91259788

[4]. Kumar N, Mishra RS, Yuan W (2015) Friction stir welding of dissimilar alloys and materials: a volume in the friction stir welding and processing book series. Butterworth-Heinemann.

[5]. Islam MR, Ishak M, Shah LH, Idris SRA, Meriç C (2016) Dissimilar welding of A7075-T651 and AZ31B alloys by gas metal arc plug welding method. Int J Adv Manuf Technol: 1–11. doi: 10.1007/s00170-016-8993-6

[6]. Mishra RS, Ma ZY (2005) Friction stir welding and processing. Materials Science and Engineering: R: Reports 50(1–2):1–78. doi:10.1016/j.mser.2005.07.001

[7]. Çam G (2011) Friction stir welded structural materials: beyond Alalloys. Int Mater Rev 56(1):1–48.doi:10.1179/095066010X12777205875750

[8]. Rai R, De A, Bhadeshia HKDH, DebRoy T (2011) Review: friction stir welding tools. Sci Technol Weld Join 16(4):325–342. doi:10.1179/1362171811y.0000000023

[9]. Zhang YN, Cao X, Larose S, Wanjara P (2012) Review of tools for friction stir welding and processing. Can Metall Q 51(3):250–261. doi:10.1179/1879139512y.0000000015

[10]. Thomas WM, Johnson KI, Wiesner CS (2003) Friction stir welding—recent developments in tool and process technologies. Adv Eng Mater 5(7):485–490

[11]. Colligan KJ (2010) 2—the friction stir welding process: an overview. In: Lohwasser D, Chen Z (eds) Friction stir welding. Woodhead Publishing, pp 15–41. doi:10.1533/9781845697716.1.15

[12]. Blignault C, Hattingh DG, James MN (2011) Optimizing friction stir welding via statistical design of tool geometry and process parameters. J Mater Eng Perform. doi:10.1007/s11665-011-9984-2

[13]. Upadhyay P, Reynolds A (2014) Effect of backing plate thermal property on friction stir welding of 25-mm-thick AA6061. Metall and Mat Trans A 45(4):2091–2100. doi:10.1007/s11661-013-2121-0

[14]. Imam M, Racherla V, Biswas K (2014) Effect of backing plate material in friction stir butt and lap welding of 6063-T4 aluminium alloy. Int J Adv Manuf Technol. doi:10.1007/s00170-014-6617-6

[15]. Upadhyay P, Reynolds AP (2012) Effects of forge axis force and backing plate thermal diffusivity on FSW of AA6056. Mater Sci Eng A 558(0):394–402. doi:10.1016/j.msea.2012.08.018

[16]. Fratini L, Micari F, Buffa G, Ruisi VF (2010) A new fixture for FSW processes of titanium alloys. CIRP Annals-Manufacturing Technology 59(1):271–274. doi:10.1016/j.cirp.2010.03.003.

[17]. Khodir SA, Shibayanagi T, Naka M (2006) Control of hardness distribution in friction stir welded AA2024-T3 aluminum alloy. Mater Trans 47(6):1560–1567

[18]. Richter-Trummer V, Suzano E, Beltrão M, Roos A, dos Santos JF, de Castro PMST (2012) Influence of the FSW clamping force on the final distortion and residual stress field. Mater Sci Eng A 538(0):81–88. doi:10.1016/j.msea.2012.01.016

[19]. Montgomery DC (2013) Design and analysis of experiments, 8th Edition. John Wiley & Sons Singapore Pte. Ltd.

[20]. Luijendijk T (2000) Welding of dissimilar aluminium alloys. J Mater Process Technol 103(1):29–35. doi:10.1016/S0924-0136(00)00415-5

[21]. Dursun T, Soutis C (2014) Recent developments in advanced aircraft aluminium alloys. Mater Des 56:862–871. doi:10.1016/j.matdes.2013.12.002

[22]. Salih OS, Ou H, Sun W, McCartney DG (2015) A review of friction stir welding of aluminium matrix composites. Mater Des 86:61–71. doi:10.1016/j.matdes.2015.07.071

[23]. Murphy A, Ekmekyapar T, Quinn D, Özakça M, Poston K, MooreG, Niblock J (2014) The influence of assembly friction stir weldlocation on wing panel static strength. Thin-Walled Struct 76(0):56–64.doi:10.1016/j.tws.2013.11.004

[24]. Mishra RS, De PS, Kumar N (2014) FSW of aluminum alloys. In: Friction stir welding and processing. Springer, pp 109–148

[25]. İpekoğlu G, Çam G (2014) Effects of initial temper condition and postweld heat treatment on the properties of dissimilar friction-stirwelded joints between AA7075 and AA6061 aluminum alloys. Metall and Mat Trans A 45(7):3074–3087. doi:10.1007/s11661-014-2248-7

[26]. Guo JF, Chen HC, Sun CN, Bi G, Sun Z, Wei J (2014) Friction stir welding of dissimilar materials between AA6061 and AA7075 Al alloys effects of process parameters. Mater Des 56:185–192. doi:10.1016/j.matdes.2013.10.082

[27]. Cole EG, Fehrenbacher A, Duffie NA, Zinn MR, Pfefferkorn FE, Ferrier NJ (2013) Weld temperature effects during friction stir welding of dissimilar aluminum alloys 6061-t6 and 7075-t6. Int J Adv Manuf Technol 71(1–4):643–652. doi:10.1007/s00170-013- 5485-9

[28]. Hasan MM, Ishak M, Rejab MRM (2015) A simplified design of clamping system and fixtures for friction stir welding of aluminium alloys. Journal of Mechanical Engineering and Sciences 9:1628–1639. doi:10.15282/jmes.9.2015.10.0158

[29]. Zappia T, Smith C, Colligan K, Ostersehlte H, Kallee SW (2010) 4—friction stir welding equipment. In: Lohwasser D, Chen Z (eds) Friction stir welding. Woodhead Publishing, pp 73–117. doi:10.1533/9781845697716.1.74

[30]. Al-Badour F, Merah N, Shuaib A, Bazoune A (2014) Thermomechanical finite element model of friction stir welding of dissimilar alloys. Int J Adv Manuf Technol 72(5–8):607–617. doi:10.1007
/s00170-014-5680-3

[31]. Park S-K, Hong S-T, Park J-H, Park K-Y, Kwon Y-J, Son H-J (2010) Effect of material locations on properties of friction stir welding joints of dissimilar aluminium alloys. Science and Technology of Welding & Joining 15(4):331–336

[32]. Hong S, Kwon Y, Son H (2008) The mechanical properties of friction stir welding (FSW) joints of dissimilar aluminum alloys. In: Proc. 1st Int. Symp. on Hybrid materials and processing

[33]. Jamshidi Aval H, Serajzadeh S, Kokabi AH (2011) Evolution of microstructures and mechanical properties in similar and dissimilar friction stir welding of AA5086 and AA6061. Mater Sci Eng A 528(28):8071–8083. doi:10.1016/j.msea.2011.07.056

[34]. Khodir SA, Shibayanagi T (2007) Microstructure and mechanical properties of friction stir welded dissimilar aluminum joints of AA2024-T3 and AA7075-T6. Mater Trans 48(7):1928–1937.
doi:10.2320/matertrans.MRA2007042

[35]. Lee W, Yeon Y, Jung S (2003) The mechanical properties related to the dominant microstructure in the weld zone of dissimilar formed Al alloy joints by friction stir welding. J Mater Sci 38(20):4183–4191

[36]. Koohbor B, Ohadi D, Serajzadeh S, Akhgar J (2010) Effect of rolling speed on the occurrence of strain aging during and after warm rolling of a low-carbon steel. J Mater Sci 45(13):3405–3412

[37]. Aval HJ, Serajzadeh S (2014) A study on natural aging behavior and mechanical properties of friction stir-welded AA6061-T6 plates. Int J Adv Manuf Technol 71(5–8):933–941

[38]. Mishra RS, Mahoney MW (2007) Friction stir welding and processing. ASM International
[39]. Mehta KP, Badheka VJ (2014) Effects of tilt angle on the properties of dissimilar friction stir welding copper to aluminum. Mater Manuf Process 31(3):255–263. doi:10.1080/10426914.2014.994754
[40]. Trimble D, O'Donnell GE, Monaghan J (2015) Characterisation of tool shape and rotational speed for increased speed during friction stir welding of AA2024-T3. J Manuf Process 17(0):141–150.
doi:10.1016/j.jmapro.2014.08.007
[41]. Sutton MA, Reynolds AP, Yan J, Yang B, Yuan N (2006) Microstructure and mixed mode I/II fracture of AA2524-T351 base material and friction stir welds. Eng Fract Mech 73(4):391–407
[42]. Heidarzadeh A, Saeid T (2013) Prediction of mechanical properties in friction stir welds of pure copper. Mater Des 52:1077–1087
[43]. Karthikeyan R, Balasubramanian V (2013) Statistical optimization and sensitivity analysis of friction stir spot welding process parameters for joining AA 7075 aluminum alloy. Exp Tech 37(2):6–15
[44]. Mason RL, Gunst RF, Hess JL (2003) Statistical design and analysis of experiments: with applications to engineering and science, vol 474. John Wiley & Sons
[45]. Mathews PG (2010) Design of experiments with MINITAB. ASQ Quality Press
[46]. Zettler R, Lomolino S, Dos Santos J, Donath T, Beckmann F, Lippman T, Lohwasser D A Study on material flow in FSW of AA 2024-T351 and AA 6056-T4 alloys. In: 5th International FSW Symposium-Metz, France, 2004, pp 14–16
[47]. Elangovan K, Balasubramanian V (2007) Influences of pin profile and rotational speed of the tool on the formation of friction stir processing zone in AA2219 aluminium alloy. Mater Sci Eng A
459(1–2):7–18. doi:10.1016/j.msea.2006.12.124
[48]. Elangovan K, Balasubramanian V (2008) Influences of tool pin profile and welding speed on the formation of friction stir processing zone in AA2219 aluminium alloy. J Mater Process Technol 200(1–3):163–175. doi:10.1016/j.jmatprotec.2007.09.019
[49]. Elangovan K, Balasubramanian V, Valliappan M (2008) Influences of tool pin profile and axial force on the formation of friction stir processing zone in AA6061 aluminium alloy. Int J Adv Manuf Technol 38(3–4):285–295. doi:10.1007/s00170-007-1100-2
[50]. Padmanaban G, Balasubramanian V (2009) Selection of FSW tool pin profile, shoulder diameter and material for joining AZ31B magnesium alloy—an experimental approach. Mater Des 30(7):2647–2656. doi:10.1016/j.matdes.2008.10.021
[51]. Thomas W, Nicholas E, Needham JC, Murch M, Templesmith P, Dawes C (1991) Friction stir welding. International patent application no PCT/GB92102203 and Great Britain patent application (9125978.8)
[52]. Thomas W, Norris I, Staines D, Watts E (2005) Friction stir welding—process developments and variant techniques. The SME Summit 1:1–21
[53]. Thomas W, Dolby R (2003) Friction stir welding developments. Proceedings of the sixth international trends in welding research:203–211
[54]. Peel M, Steuwer A, Preuss M, Withers PJ (2003) Microstructure, mechanical properties and residual stresses as a function of welding speed in aluminium AA5083 friction stir welds. Acta Mater 51(16):4791–4801. doi:10.1016/S1359-6454(03)00319-7
[55]. Colligan KJ, Mishra RS (2008) A conceptual model for the process variables related to heat generation in friction stir welding of aluminum. Scr Mater 58(5):327–331. doi:10.1016/j.scriptamat.2007.10.015
[56]. Yan J, Sutton MA, Reynolds AP (2005) Process–structure–property relationships for nugget and heat affected zone regions of AA2524–T351 friction stir welds. Science and Technology of Welding & Joining 10(6):725–736
[57]. Tang W, Guo X, McClure J, Murr L, Nunes A (1998) Heat input and temperature distribution in friction stir welding. J Mater Process Manuf Sci 7:163–172
[58]. Zettler R, Vugrin T, Schmücker M (2010) 9—effects and defects of friction stir welds. In: Lohwasser D, Chen Z (eds) Friction stir welding. Woodhead Publishing, pp 245–276. doi:10.1533/
9781845697716.2.245

[59]. Zettler R (2010) 3—material deformation and joint formation in friction stir welding. In: Lohwasser D, Chen Z (eds) Friction stir welding. Woodhead Publishing, pp 42–72. doi:10.1533/9781845697716.1.42

CHAPTER 4

TECHNICAL PAPER #3

Title:- Effect of backing material and clamping system on the tensile strength of dissimilar AA7075-AA2024 friction stir welds

(*The International Journal of Advanced Manufacturing Technology*, *91*(9-12), 3991-4007. doi: http://dx.doi.org/10.1007/s00170-017-0033-7-ISI)

4.1 ABSTRACT

Friction stir welding of dissimilar aluminum alloys has become an important application in the modern industries. Joint strength is a major consideration in this advanced technology. This paper presents an attempt made to improve the weld tensile strength by

controlling the temperature distribution during the joining process. High-strength AA7075-T651 and AA2024-T351 aluminum alloys were friction stir welded using different backing and clamping materials. The tool rotation rate was preliminarily investigated to estimate the optimal spindle speed. Next, three composite backing plates and clamping systems were tested in conjunction with varying levels of traverse speeds and materials position. The transient temperatures were experimentally measured at different distances from the welding line. Asymmetric temperature distributions were observed with maximum records on the advancing side of the weld. Moreover, the influence of backing and cover materials on the joint strength was found to be varied with the applied level of the welding traverse speed. Based on these results, an idea to use asymmetric system of backing and cover materials was inspired. This system assisted to improve the temperature distribution and resulted in a sound weld with higher tensile strength. The detailed results of this work were discussed and the main outputs were outlined in the conclusions

4.2 INTRODUCTION

Friction stir welding (FSW) is a solid-phase continuous hot shear welding process. The fundamentals of this green joining method are plunging and stirring a non-consumable rotating tool with a specially designed shoulder and probe or pin int the abutting materials to be welded [1, 2]. The workpieces are joined together through heating, material movement, and forging dominated by the tool geometry in addition to the welding parameters. Heating is created both by the friction between the rotating tool (pin at the initial plunge stage and mainly shoulder during the run) and the workpiece and by severe plastic deformation of the workpieces. Materials around the probe are softened due to localized heating and move from front to back during tool rotation and stirring. Consequently, the hole in the tool wake is filled and the welding joint is produced. The shoulder restricts the plasticized materials from flowing outand applies forging pressure to consolidate the materials right behind the moving pin.

Reducing the heat input during the FSW process by decreasing the tool rotation rate and/or increasing the workpiece travel speed is one of the methods used for increasing the joint strength [3]. Since the temperature must be kept high enough to soften the materials around the welding pin tool to stir, this method requires inspection of the optimal welding speeds which are varied according to the joint configuration

(butt or lap) and material types and dimensions [4]. For this reason, there is a limited range of tool rotation rate and travel speeds that could be controlled. Cooling of the welding tool and backing plate should offer another way of reducing the elevated temperature. Water or gas cooling and welding under water can be effectively used for joining high-temperature materials, such as steel and titanium [5]. For aluminum alloys, ambient air is found to be enough for cooling the welding tool and anvil, and the coolant-cooling is not required for such low- temperature materials [6]. The use of a proper and effective tool design with additional shoulder and pin features is an active way to improve materials flow and mixing with minimum energy input throughout the plunging and stirring sequences [7, 8]. One of the methods used to decrease the process temperature in the FSWof dissimilar alloys or materials is the tool offset [9]. Controlling the position of the pin tool between the abutting edges of the plates to be joined could be achieved by a suitable placement of the workpieces on the advancing side (AS) and retreating side (RS) of the welding seam [10]. It has been reported that the temperatures are higher on the AS when similar alloys or materials are welded [11–13]. This asymmetry in temperature distribution may be increased in case of dissimilar FSW and leads to lower the quality of the joint [14]. On the other side, thermal boundary conditions present at the workpieces are also affecting the temperature distribution and joint strength for a given set of welding parameters. The rates of heat flux through the top, sides, and bottom of the workpieces mostly depend on the thermal diffusivity of the backing plate and fixtures [15].

In the published literature, effect of thermal properties of the backing/clamping system has not received as much attention as tool design, welding speeds, and other process parameters. In the work of Khodir and his group of researchers [16], three types of backing and cover materials (steel, copper, and steel-copper) were used to control the hardness distribution during the butt FSW of 3-mm-thick AA2024 aluminum alloy. The authors mentioned that the cover block was used to extract more amount of frictional heat throughout the joining process. The higher joint strength has been recorded when the combined steelcopper backing/cover system was used. The hardness of the nugget and heat-affected zone (HAZ) increased when the maximum temperature was higher and lower, respectively. Upadhyay and Reynolds [17] reported that the peak process temperature can be controlled by changing the backing plate without any variation in

the spindle and travel speeds. Ceramic, titanium, steel, and aluminum backing plates were used to join 4.2-mm-thick AA6056 aluminum alloy in butt configuration. In another work [18], the same backing materials were used to weld 25.4-mm-thick plate of AA6061 aluminum alloy. Joints were also produced by the use of composite aluminum-steel-aluminum backing plate. This backing system resulted in stronger joints with respect to the hardness and tensile tests. Butt and lap joining of 3- and 6-mm-thick AA6063 aluminum alloy were made by Imam and his co-authors [19] using mild steel, stainless steel, and asbestos backing plate materials. It was concluded that the lowest thermal diffusivity asbestos backing plate resulted in defect-free welds in both butt and lap arrangements. Similar aluminum alloys were joined in these previous studies using limited range of welding speeds. It is hence thought necessary to understand the influence of backing and clamping materials on the joint strength in conjunction with varying levels of the welding speeds during the dissimilar FSW. In this case, materials position on the advancing and retreating sides of the weld is another factor that has to be taken into account [20].

Dissimilar welding is becoming progressively essential as it permits combining the best properties of the joined materials [21,22]. A wide range of ferrous and nonferrous materials such as steel, titanium, aluminum, magnesium, and some of plastics can be effectively joined by the efficient FSW technique [23, 24]. The high-strength 7xxx and 2xxx aluminum alloys are hard to weld by the traditional fusion welding techniques since they are highly affected by the elevated temperatures [25, 26]. The friction stir welding facilitates joining of such these types of materials without exceeding the melting point. Dissimilar welding of AA7075-T6 and AA2024-T3 aluminum alloys by the FSW in butt configuration was studied by several researchers. Cavaliere et al. [27, 28] investigated the mechanical and microstructural response of the dissimilar joints. Sheets of 2.5 mm thick were friction stir welded using 700 rpm of tool rotation rate and 160 mm/min of traverse speed. In these two works, AA7075 was fixed on the AS of the weld. Khodir and Shibayanagi [29,30] reported that defect-free joints with maximum tensile strength could be obtained by applying 1200 rpm of rotation speed with 100 mm/min of feed rate to join 3-mm-thick sheets. Aluminum 7075 was placed on the RS of the welding tool in these studies. Fatigue properties of a weld made from 4-mmthick AA7075 and AA2024 plates were inspected by Cavaliere and Panella [9] under different tool positions. In this work, AA2024 was located on the AS, and

1600 rpm rotation rate with 120 mm/min traverse speeds were selected. Mechanical properties and material flow of 3-mm-thick welded sheets were evaluated in the work of da Silva and his group of researchers [31]. It has been shown that 254 mm/min of traverse speed resulted in a higher joint strength when the tool rotation rate was fixed at 1000 rpm and the AA7075 alloy was placed on the AS. Low feed rate of 12 mm/min with 1200 rpm of rotation speed was used by Saravanan et al. [32] to produce the weldments. The thickness of the abutted plates was 5 mm and the AA2024 alloy was kept on the AS during the weld. According to these literature findings, optimal welding speeds could not be assigned due to the fluctuation in the previously applied parameters.

In view of that, the present work aims to investigate the friction stir (butt) welding of dissimilar AA7075-T651 and AA2024-T351 aluminum alloys via planned backing/ clamping systems in conjunction with varying levels of welding speeds and materials position. The advanced aircraft AA2024 aluminum alloy in the T351 temper condition has lower tensile and yield strengths and more pronounced plasticity than the AA2024-T3 alloy and deform more homogeneously than the AA7075-T651 alloy [33-38]. Friction stir welding of the aluminum 2024-T351 results in average static properties of about 85% of the base material and very high fatigue strength [39]. Dissimilar joining of this developed alloy to the higher strength aluminum 7075-T651 by the FSW could enhance the mechanical properties of the joint

4.3 EXPERIMENTAL PROCEDURES

4.3.1 Design of the backing/clamping system

According to Upadhyay and Reynolds [18], composite backing plate was fabricated from AA6061-T6 aluminum (Al) bars and AISI 304 stainless steel (SS) strip (Fig. 4.1a). These materials have relatively high and low thermal conductivities at elevated temperatures. Thermal conductivity of the Al alloy increases from 167 W/m K at 25 °C to 230 W/m K at 450 °C [40], while it remains below 19 W/m K up to 450 °C for the stainless steel [41].

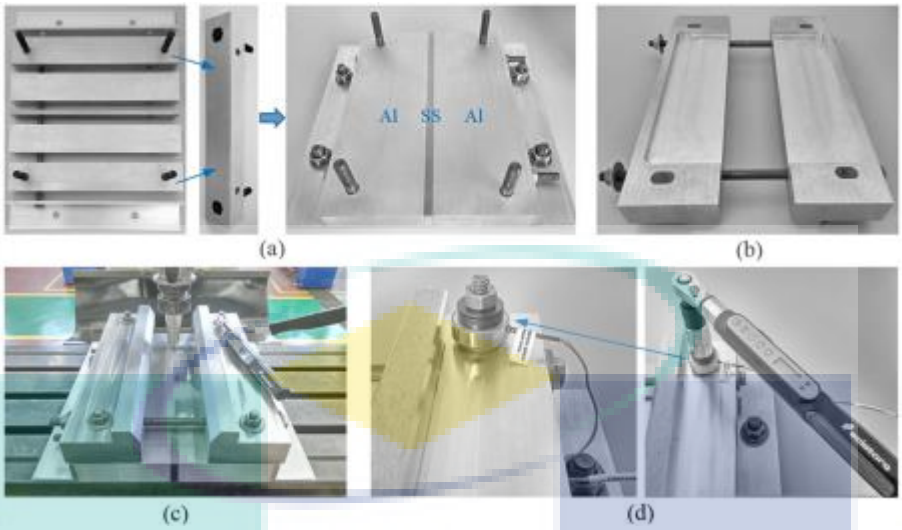

Fig. 4.1 The backing and clamping parts. a The composite backing plate, b the pressure bars, c the assembled backing/clamping system with the workpieces, and d the load cell and torque wrench

Two lateral restraints of L-shaped aluminum plates were used to assemble the backing plates, increase the heat sink, and fix the system to the machine table. The vertical clamping forces were applied by means of bolts and nuts using aluminum pressure bars to ensure uniform pressure and temperature distribution throughout the welded plates (Fig. 4.1b). All parts were ground by a precision grinding machine (Okamoto GRIND-X ACC65DX) to produce smooth surfaces with accurate dimensions. To avoid any change in the heat sink during the welding process, the horizontal plane containing the workpieces was free of bolts and their holes (Fig. 4.1c). As per the results presented in the works of Christner and Sylva [42] and Leonard and Lockyer [43], the formation of a gap between specimens up to 33%–36% of the plate thickness does not affect the joint strength and could be tolerated without the existence of weld flaws. However, Richter-Trummer et al. [44] observed that a lesser distortion and more consistent distribution of the residual stresses through the weld thickness can be achieved by applying higher clamping forces. It has been demonstrated that the possibility of defects could also be minimized by preventing any creation of gaps between the abutting edges of the welding plates. In addition, it is important that the workpieces should not be spread or lifted during the process; therefore, the welding fixtures must be designed with features enable to achieve this objective [45].

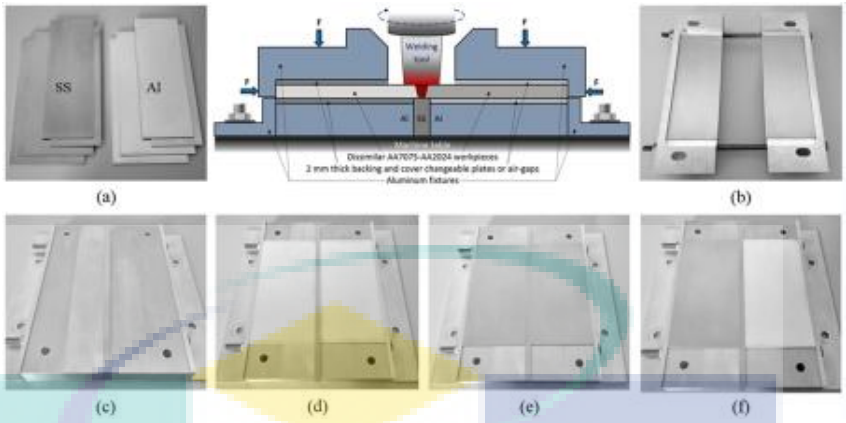

Fig. 4.2. Modification of the backing/clamping system with a schematic representation. **a** The backing and cover changeable sheets, **b** the pressure bars with cover sheets, **c** the modified backing plate, **d** Al-SS-Al composite backing plate, **e** SS backing system, and asymmetric system. **f** clamping force, SS stainless steel, Al aluminum

Fig. 4.3. Locations of the drilled holes in the composite backing plate and pressure bars used to insert the thermocouple wires to the workpieces. A1–A4 thermocouple wires on AS, R1– R4 thermocouple wires on RS, AS advancing side, RS retreating side

Consequently, the workpieces were subjected to constant moderate vertical and lateral clamping forces. These forces were controlled by means of a mini-torque wrench, which was previously calibrated by a thru-hole load washer (LCMWD) from Omega (Fig. 4.1d). For that reason, the bottom surfaces of the pressure bars were machined to apply a uniform side pressure on the specimens using two long bolts. To use different backing and cover materials, the backing/clamping system was modified as shown in the schematic representation of Fig. 4.2. Backing and covering changeable sheets were cut from 2-mm-thick AA6061-T6 and AISI 304 plates, respectively (Fig. 4.2a). The Al pressure and backing bars were machined and ground to a depth of 2 mm to insert the prepared sheets (Figs. 4.2b, c). This design systems as shown in Fig. 4.2d–f, or fixing the workpieces on the steel strip without inserting the thin sheets. Three thru-holes of 3 mm diameter were drilled on each side of the SS strip at the transverse centerline of the

composite backing plate to insert the thermocouple wires to the welding coupons, as seen in Fig. 4.3. The centers of these holes were located at 10, 20, and 30 mm from the longitudinal centerline of the SS strip (welding centerline). For the same purpose, another two holes were made on the bottom side edges of the pressure bars.

4.3.2 Materials and Method

The welding coupons were cut from 6-mm-thick rolled plates of AA7075-T651 and AA2024-T351 aluminum alloys. The edges of specimens were ground by the precision surface grinding machine to the final dimensions of 200 × 103 mm and cleaned with acetone before welding. The chemical compositions and physical properties of the base materials are listed in Tables 4.1 and 4.2 respectively. Three small holes of 1 mm diameter were drilled from the bottom surface of each workpiece to a depth of 3 mm [46, 47] to imbed high-quality GG-K-36 thermocouple wires from Omega.

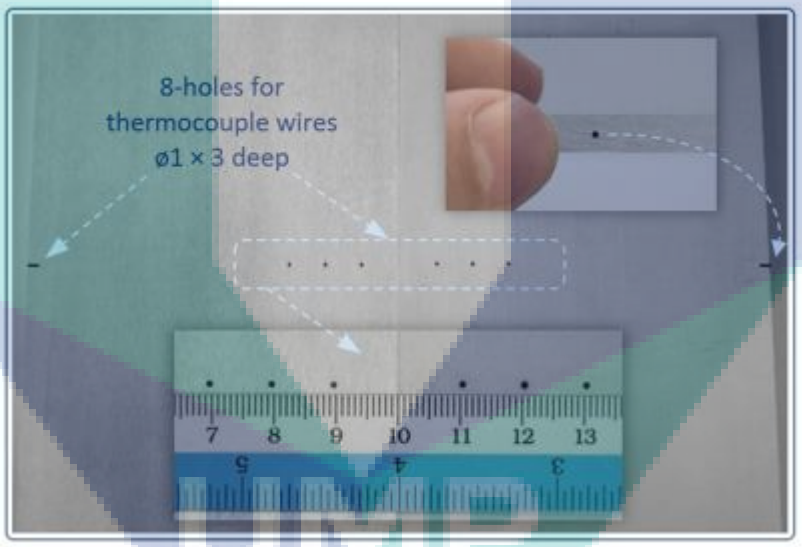

Fig. 4.4. Locations of the holes drilled at the side and bottom surfaces of the workpieces to embed the thermocouple wires

The holes shown in Fig. 4.4 were created at a suitable distance from the weld start point (on the transverse centerline of the workpiece) to ensure thermal stability [48]. These holes does not affect the temperature field during the joining process [49] and were located at 10.5, 20.5, and 30.5 mm from the weld centerline on each side. Another hole was drilled at the center of each side-edge of the workpieces. The diameter and depth of these two holes were also 1 and 3 mm, respectively. The thermocouple wires were secured inside the holes using high temperature and thermal conductivity epoxy adhesive (Omega-Bond).

Table 4.1. Chemical composition (wt.%) of the base materials

Alloy	Si	Fe	Cu	Mn	Mg	Cr	Zn	Ti	Al
AA7075-T651	0.04	0.12	1.3	0.02	2.4	0.19	5.8	0.07	Bal.
AA6061-T351	0.06	0.15	4.37	0.5	1.47	0.01	0.02	0.06	Bal.

Table 4.2. Mechanical Properties of the base materials

Alloy	Yield Strength (Mpa)	Tensile Strength (Mpa)	Vickers Hardness	Elongation
AA7075-T6	514	568	170	11.75
AA6061-T3	330	449	142	17.34

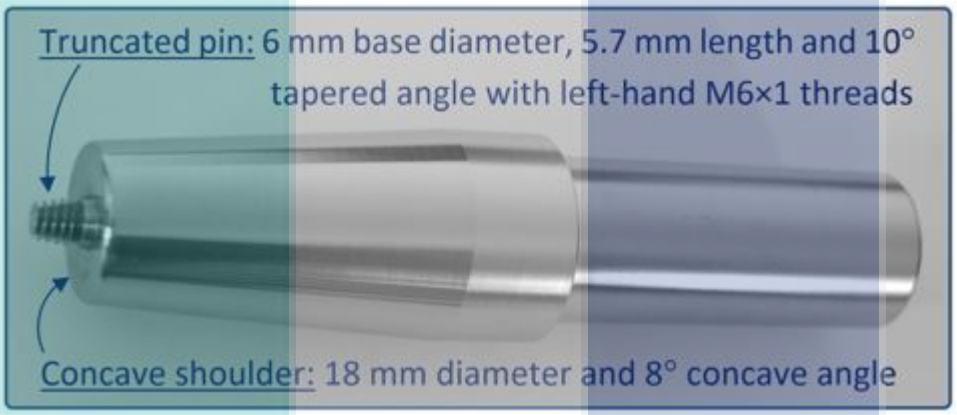

Fig. 4.5. Geometry and dimensions of the welding tool

The wires were connected to an 8-channel data logger to inspect the transient temperatures during the welding process using DASYLab software at an interval of 0.5 s. The workpieces were joined in butt configuration along the rolling direction of the base materials. The tool used was fabricated from H13 steel with a concave shoulder and truncated probe, whose dimensions and geometry are shown in Fig. 4.5. The welded plates were left 2 months for natural aging [50, 51], then metallographic and tensile specimens were cut by a wire cutting machine as per the ASTM E8/E8M-11 standard, whose geometry, positions, and dimensions are shown in Fig. 4.6.

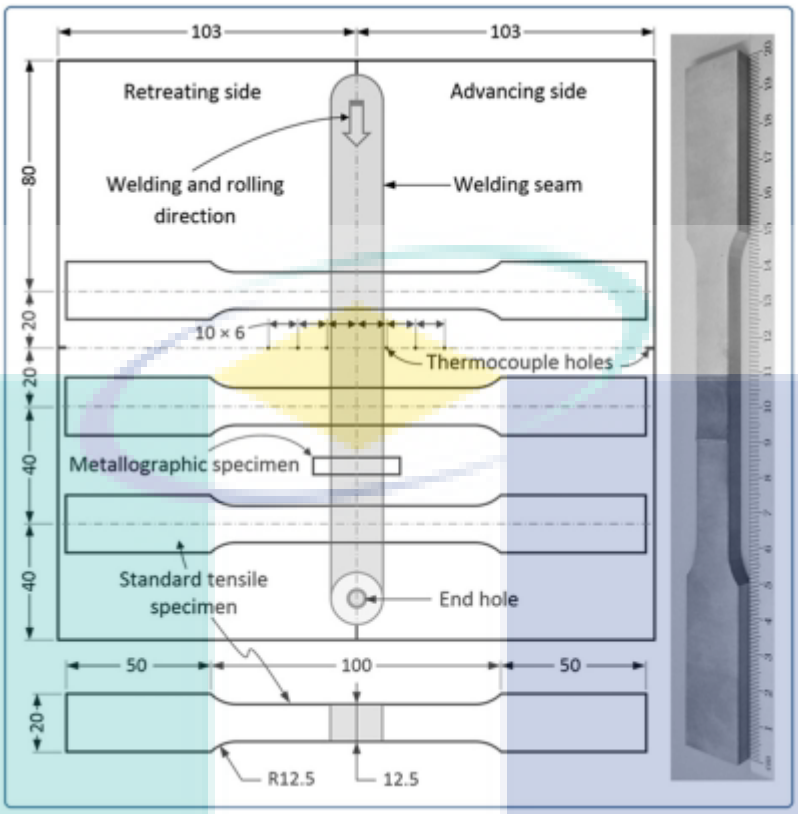

Fig. 4.6. Geometry, positions, and dimensions in millimeters of the tensile and metallographic specimens with the thermocouple holes

The tensile tests were conducted at room temperature with a speed of 1 mm/min using a universal testing machine (Instron 3369). Standard procedures were followed to prepare the metallographic specimens which were then ground, polished, and etched with a modified Keller's reagent to reveal the grain structure of the different weld zones. The macro- and microstructural evaluations were performed under an optical microscope. The average grain intercept (AGI) method was used to measure the grain size by drawing a set of randomly positioned line segments on the micrograph, counting the number of times each line segment intersects a grain boundary and finding the ratio of intercepts to line length [52]. The mean AGI value calculated from the microstructure was then considered as the average grain size. A Vickers microhardness tester (Tukon 1202) was used to measure the hardness across the weld centerline, in a direction normal to the weld seam. The HV0.5 test method was applied with an indent time of 10 s.

4.4 RESULTS AND DISCUSSION

4.4.1 Tool Rotation Speed

Based on the background information outlined in the introduction, five spindle speeds from 600 to 1800 rpm were examined at a fixed feed rate of 100 mm/min, 3° of tilting angle, and equal penetration of the tool shoulder inside the workpieces. During this preliminary investigation, the location of materials on the advancing and retreating sides of the weld was considered. The backing/clamping system shown in Fig. 4.1 was used in this stage of the study. Visual inspection was firstly adopted to examine the surface finish of the resulting welds. Fig. 4.7 shows the surface finish of the welding seam according to the tool rotation rate and placement of the aluminum alloys on the advancing and retreating sides of the weld. Regardless of the relative materials position, surface defects were significantly grown when the spindle speed was increased. This can be attributed to the increase of heat generated during the welding process, which is proportional to the tool rotation rate [53, 54]. Too hot welding condition results in an excessive material flow and leads to material expulsion. The excessive flash and surface galling or scaling shown at 1500 and 1800 rpm are clear results of this materials overflow. The most excessive flash was formed at the AA7075 side when the AA2024 was placed on the AS. On the other hand, better surface finish was observed at 900 rpm when the AA7075 was located on the AS. This gives an indication that the relative position of the base materials is also affects the heat generation and material flow in dissimilar FSW. This conclusion coincides with the results obtained by Al-Badour et al. [55] and Mironov et al. [56]. They reported that the amount of heat generated during the welding process is sensitive to the material location and spindle speed. However, detailed discussion on the temperature distribution is beyond the scope of this part of the study.

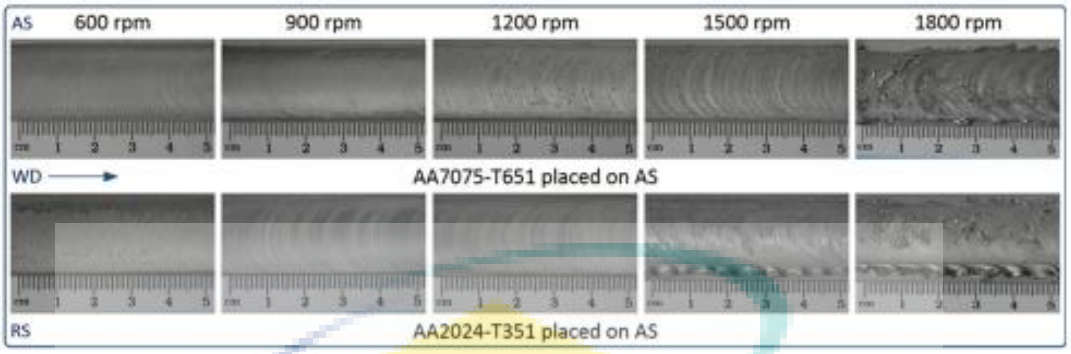

Fig.4.7. Surface finish of the resulting welds at different tool rotation speeds and materials position. WD welding direction, AS advancing side, RS retreating side

Weld macrographs related to the tool rotation rate and materials location are presented in Fig. 4.8. The metallographic specimens were prepared along the weld cross section, and the right-hand side of each photo represents the advancing side of the welding tool. The high strain rate due to the tool rotation and translation resulted in a severe deformation and dynamic recrystallization of the grains at the mixing stir zone. It is well established that vertical and circular plastic flows of the coupled materials occur during the FSW process [57]. The left-hand threads of the pin tool push the material down away from the shoulder in conjunction with the circular motion of the tool. The heat generated and materials movement lead the grains of the base alloys to enter into each other and form the weld nugget [58].

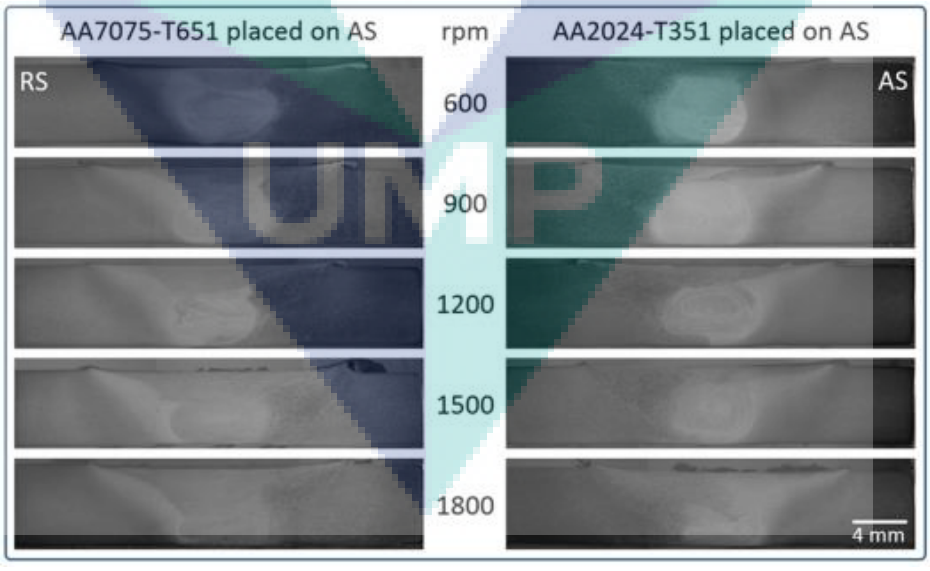

Fig. 4.8. Macrographs of the weld at different tool rotation speeds. AS advancing side, RS retreating side

As seen in Fig. 4.9, the materials flow and mixing were improved and the nugget became more uniform when the tool was rotated with 900 rpm. The penetration of the

softened materials into each other seemed to be incomplete when the AA7075 was placed on the AS, and discontinued onion rings were seen at the advancing and retreating sides of the weld. Much more uniform mixing and concentric rings were observed when the AA2024 was fixed at the advancing side. This behavior agrees with the results of Khodir and Shibayanagi [29] and Guo et al. [14]. They reported that improved material mixing and thinner ring layers could be attained when the softer alloy is placed on the AS. As seen in Fig. 4.10, the weld nugget has collapsed when the rotation speed was raised to 1800 rpm. This can be attributed to the excessive material flow and high power input [53]. This in turn resulted in a relatively bigger grain size and nonuniform material mixing.

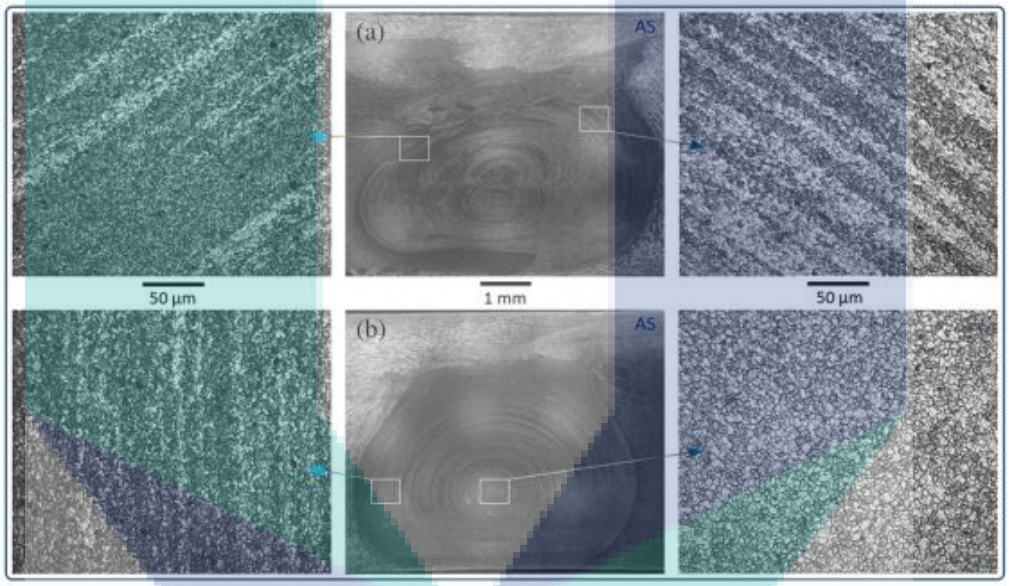

Fig. 4.9. Micrographs of the nugget at 900 rpm. a AA7075-T651 placed on AS and b AA2024-T351 placed on AS. AS advancing side, RS retreating side

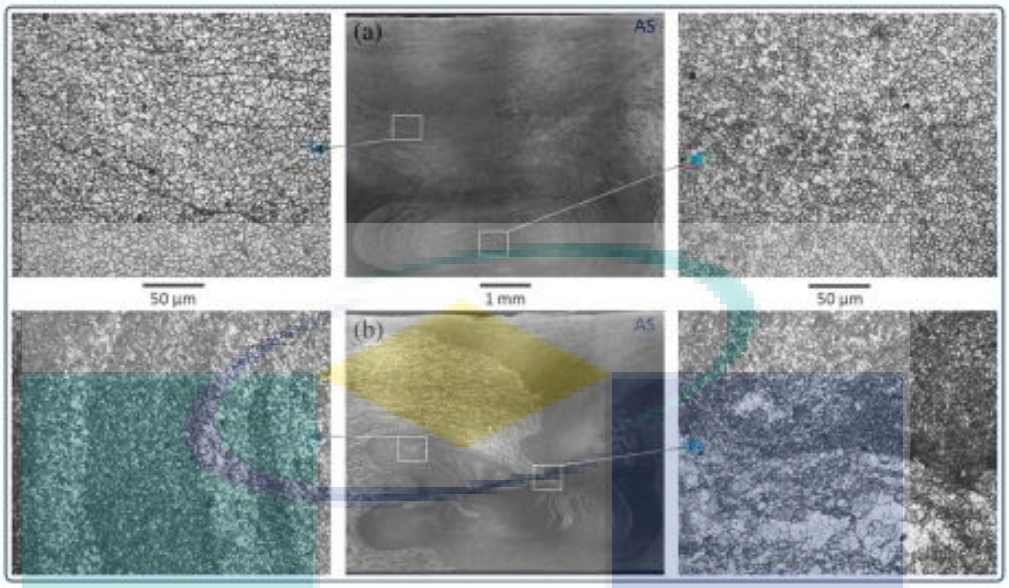

Fig. 4.10 Micrographs of the nugget at 1800 rpm. a AA7075-T651 placed on AS and b AA2024-T351 placed on AS. AS advancing side

Long microcracks were created when the AA7075 was placed on the AS. On the other side, inhomogeneous grains were appeared when the AA2024 was located on the AS. These non-equiaxed grains were formed in the stir zone due to the relatively high circular material flow. It was noticed that the average grain size increased from 4.3 µm at 600 rpm to about 8.2 µm at 1800 rpm when the AA7075 was located on the AS. Similarly, the average grain size increased from 4.7 µm at 600 rpm to 7.8 µm at 1800 rpm when the AA2024 was located on the AS. This growth in grain size could be attributed to the increase of weld temperature at higher rotation rate [17, 56].

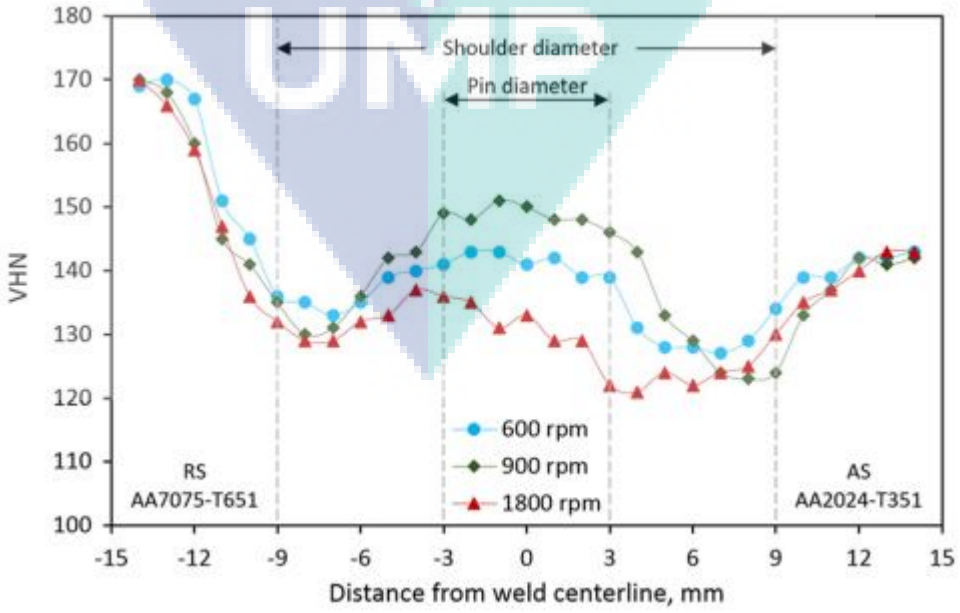

Fig. 4.11. Distribution of the Vickers microhardness number (VHN) at different tool rotation rates

Distributions of the Vickers hardness number (VHN) along the transverse nugget centerline are drawn in Fig. 4.11 for three different joints. The three samples were selected to compare the results at the highest, lowest, and best rotation rates when the AA2024 was fixed on the AS. In general, the weld joint exhibited a noticeable microhardness decrease compared to the base materials. This hardness drop was also observed in the previous studies that carried out on similar and dissimilar FSW of aluminum alloys [4, 24]. In comparison between the higher and lower tool rotation rates, the lowest hardness level in the nugget was observed at 1800 rpm. Hardness level of the weld nugget was higher at 600 rpm, in which the grain size was smaller. These results indicate that the nugget hardness is affected by the tool rotation rate and inversely proportion to the grain size. Several researchers reported that the microhardness decreases with increasing grain size [5, 19]. However, the maximum hardness level in the weld nugget was obtained at 900 rpm. At this rate of spindle speed, more effective material mixing was produced by the welding tool. The weld hardness at the mixing stir zone increased with the increase of tool rotation speed until it reached the maximum level and decreased again when the spindle speed was further raised. Accordingly, material mixing plays an important role in the resulting level of nugget hardness. Along the whole welding joint, the minimum VHN was recorded on the AA2024 side in the heat-affected zone (HAZ) and thermo-mechanical affected zone (TMAZ). The fracture locations of the tensile test specimens were observed at these weakest regions for the defectfree welds, as shown clearly in Fig. 4.12.

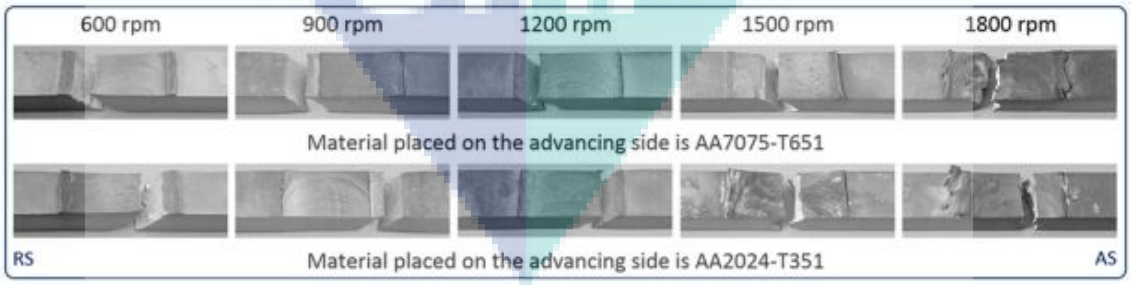

Fig. 4.12. Fracture locations of the tensile test specimens at different tool rotation rates. AS advancing side, RS retreating side

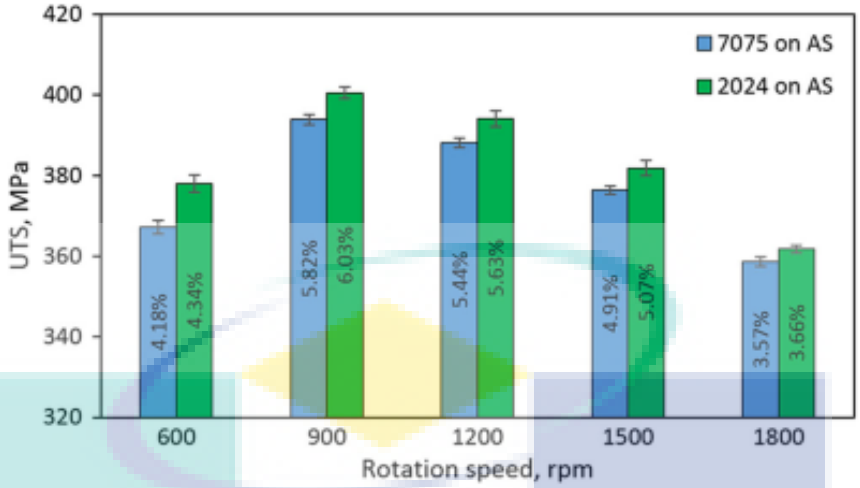

Fig. 4.13. The weld ultimate tensile strength (UTS) and percentage elongation at different spindle speeds and materials position. Error bars correspond to standard deviation of three tests for each case. AS advancing side

Due to the microcracks and insufficient material mixing resulted at 1800 rpm, the fracture was initiated from the weld nugget. Detailed discussion of the fracture location will be explained later. The ultimate tensile strength (UTS) of the weld and the corresponding elongation at fracture are presented in Fig. 4.13 related to the applied spindle speeds. It was noted that the joint strength improved at 900 rpm regardless of the relative materials position. The maximum joint strength and tensile elongation of about 400 MPa and 6%, respectively, were observed when the AA2024 was fixed on the AS, where the most uniform nugget with the best hardness level was produced. Since the joint efficiency for a dissimilar welding could be calculated based on the softer material [59], this value of UTS represents an efficiency of about 89% with respect to the strength of the AA2024 alloy. The lowest UTS value of about 359 MPa, which represents an efficiency of about 80%, was recorded at 1800 rpm when the AA7075 was placed on the AS. In this case, the lowest tensile elongation of about 3.5% was recorded. This means that the tensile elongation is proportional to the joint strength. It is also obvious that the difference in tensile strength (ΔUTS) related to the materials location decreased with the increase of tool rotation rate, as seen in Fig. 4.14. This behavior implies that the effect of materials position on the joint strength reduced at high rotation rates and vice versa.

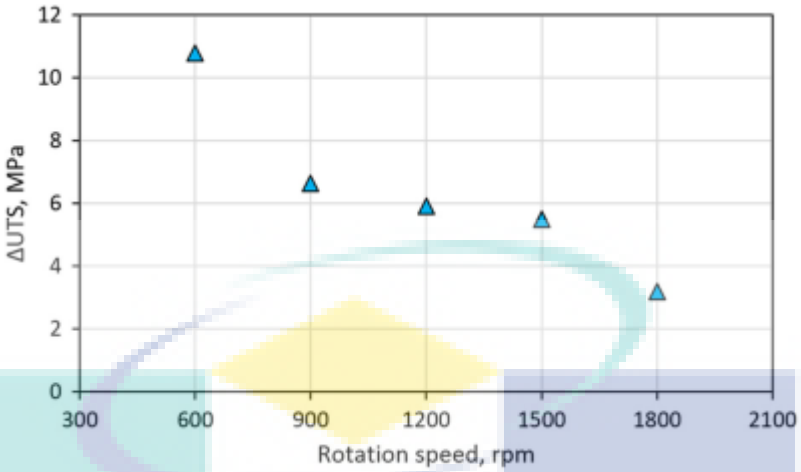

Fig. 4.14. Difference in the weld ultimate tensile strength (UTS) related to the materials position under various spindle speeds

4.4.2 Backing/clamping systems

Three composite backing and clamping systems were considered to investigate the influence of backing and covering materials on the weld tensile strength. The first system consists of Al-SS-Al composite backing plate, as seen previously in (Fig. 4.2d). System 2 was prepared by inserting the SS sheets instead of the Al ones, as shown in (Fig. 4.2e). The same arrangements were followed to cover the workpieces (Fig. 4.2b). In the third backing/clamping system, the welding coupons were supported on the SS strip without inserting any sheet inside the air gaps of the backing and pressure bars. The optimal tool rotation rate was applied at this stage of the study with the same tool design and tilting angle. First, the three systems were examined at 100 mm/min of traverse speed. The visual monitoring of the weld showed a slight surface galling when the workpieces were only clamped on the steel strip (system 3), as seen in (Fig. 4.15a). The tensile test specimens fractured at the HAZ of the AA2024 alloy for all backing/clamping systems, as shown in (Fig. 4.15b).

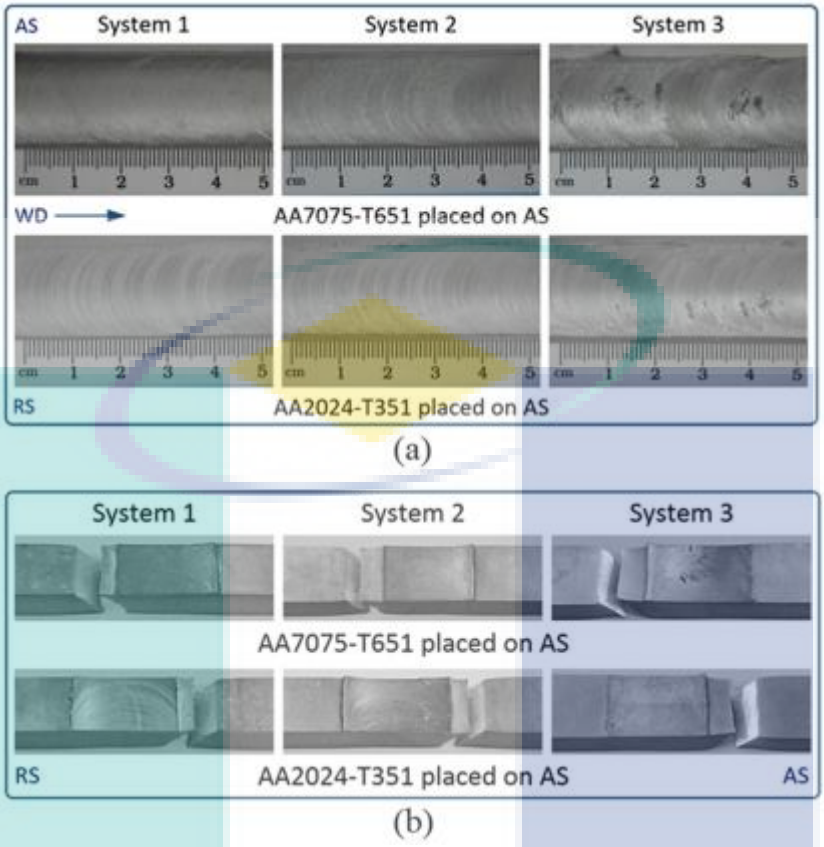

Fig. 4.15. **a** Surface finish of the resulting welds and **b** fracture locations of the tensile test specimens related to the backing/clamping systems at 900 rpm and 100 mm/min. WD welding direction, AS advancing side, RS retreating side

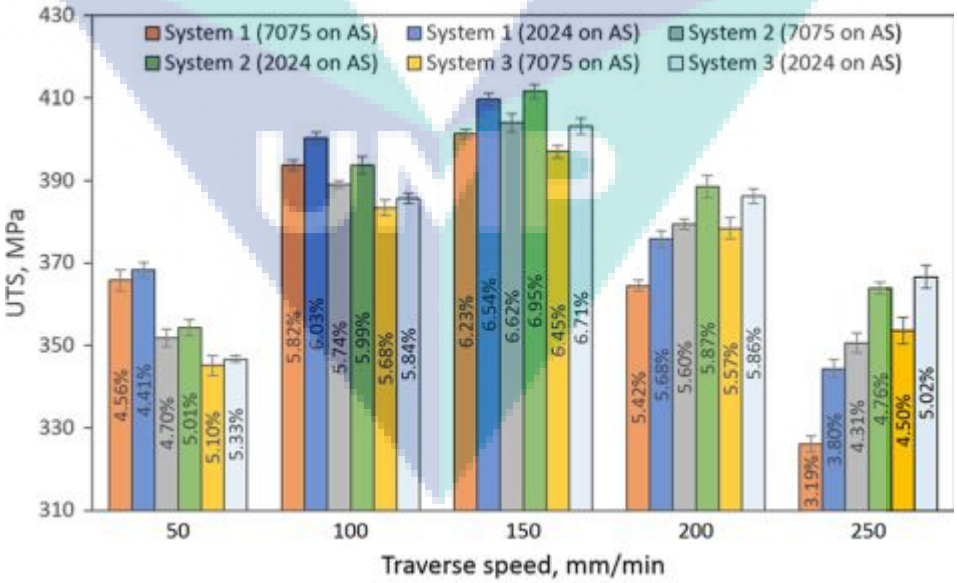

Fig. 4.16. The weld ultimate tensile strength (UTS) and percentage elongation at different traverse speeds and materials position. Error bars correspond to standard deviation of three tests for each case. AS advancing side

Regardless of the materials placement on the advancing and retreating sides, the use of system 1 resulted in the maximum joint strength followed by system 2 and system 3, as shown in Fig. 4.16, which represents the effect of backing/clamping systems on the weld tensile strength and elongation at various traverse speeds. The observed results showed that the tensile elongation is proportional to the joint strength and the highest value was also resulted from using system 1. When the traverse speed was reduced to 50 mm/min, the weld strength decreased with the same effect of the backing/clamping systems. This drop in joint strength could be attributed to the increase of the heat input, since the FSW process temperature increases with the decrease of the traverse speed [46].

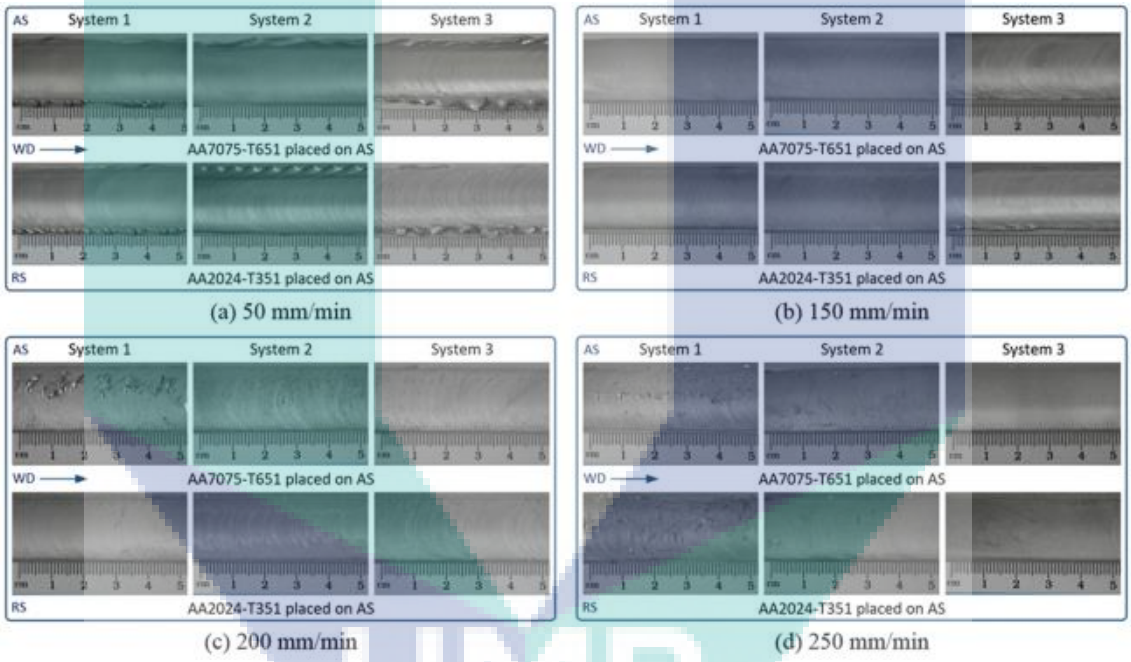

Fig. 4.17. Surface finish of the resulting welds related to the backing/clamping systems at 900 rpm and different traverse speeds. WD welding direction, AS advancing side, RS retreating side

As a result, significant amounts of flash were generated at this low level of traverse speed, as shown in (Fig. 4.17a). The flash formation reduces the amount of material at the mixing stir generated under system 3 and system 1, respectively. This difference of weld flash or the equivalent amount of material lost made the tensile elongation non-proportional to the joint strength. In addition, the various regions produced in the FSW make the elongation inappropriate measure of the weld ductility [18]. As shown in (Fig. 4.18a), the fracture occurred at the TMAZ and HAZ of the

AA2024 alloy. Joint strength was improved when the traverse speed was raised to 150 mm/min.

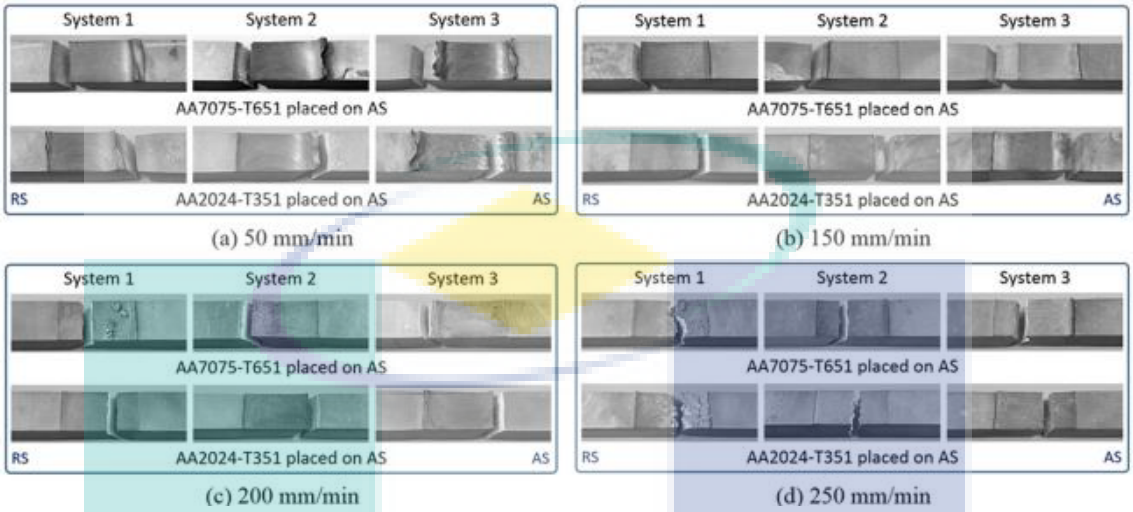

Fig. 4.18. The fracture locations related to the backing/clamping systems at 90 rpm and various traverse speeds. AS advancing side, RS retreating side

The maximum UTS value of about 411.6 MPa, which represents an efficiency of 91.6%, was recorded when the AA2024 was placed on the AS using system 2. The weld efficiency slightly decreased when system 1 and system 3 were used. The surface finish of the resulting welds seemed free of defects, as shown in (Fig. 4.17b). The tensile test specimens failed at the TMAZ of the AA2024 alloy for system 1 and at the HAZ of the same material for system 2 and system 3, as presented in (Fig. 4.18b). Increasing the traverse speed beyond this level resulted in a degradation of the joint strength with an inverse effect of the backing/clamping systems. The maximum reduction in UTS was recorded for the welds produced using system 1. Some surface defects started to appear on the weld surface as shown in (Fig. 4.17c, d), and the fracture locations moved toward the weld nugget as seen in (Fig. 4.18c, d). This implies that the generated temperature was not enough to properly soften the materials around the pin tool. In the FSW, fracture of the tensile test specimens normally arises from the weakest region. The HAZ of the softer alloy represents the weakest region of the sound dissimilar friction stir welds regardless of the relative materials location [60–62]. The microhardness dropped in this region due to the elevated temperature and mechanical extension of the grains. If the failure takes place at the stir zone, this means that there is an over or poor material mixing resulted from high rotation or traverse speeds. It is worth noting herein that the influence of materials position on the tensile strength has grown with the increase of traverse speed. This behavior is similar to that appeared when the effect of tool rotation

rate on the weld strength was investigated. The difference in joint strength related to the materials placement hence increases when the generated temperature decreases. This could be clarified by the fact that higher process energy is required when the harder material is placed on the AS in dissimilar FSW [10, 24]. Variation of the effect of backing/clamping materials on joint strength could be attributed to the difference in thermal conductivity of these materials and the amount of heat generated during the welding process. At lower traverse speed, the aluminum backing and cover material used in system 1, which has a relatively high thermal conductivity, worked as an adequate heat sink to extract some of the welding heat.

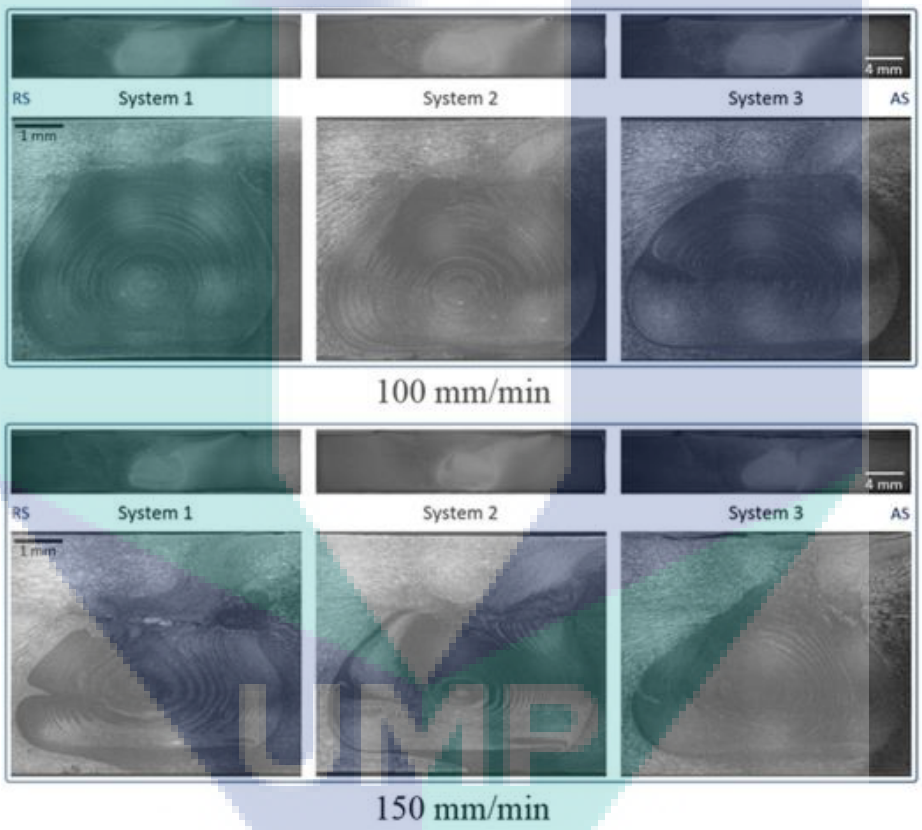

Fig. 4.19. Macro- and micrographs of the nugget related to the backing/clamping systems at 900 rpm and various traverse speeds. AA2024-T351 placed on AS. AS advancing side, RS retreating side

This heat dissipation minimized the overheating effect which resulted from the low-speed or hot welding. On the other side, the insulation of the workpieces at higher traverse speeds by the air gaps in system 3 reduced the drop in joint strength which resulted from the high-speed or cold welding. It is true then to say that the generation and dissipation of the FSW process heat could be controlled by using a proper design of backing/clamping system in conjunction with appropriate selection of the welding

speeds and other process parameters. Macro- and micrographs of the weld nugget for the three backing/clamping systems at 100 and 150 mm/min are presented in Fig. 4.19. Aluminum 2024 was placed on the AS of the welding tool. Obviously, the effect of backing and clamping systems on material mixing depends on the applied traverse speed. Producing defect-free weld with efficient material mixing is essential to attain strong joint. In addition, controlling the temperature distribution during the welding process could further improve the joint strength through enhancing the weld hardness [16]. The transient temperatures along the transverse centerline of the workpieces at 150 mm/min are presented in Fig. 4.20 for the three backing/clamping systems.

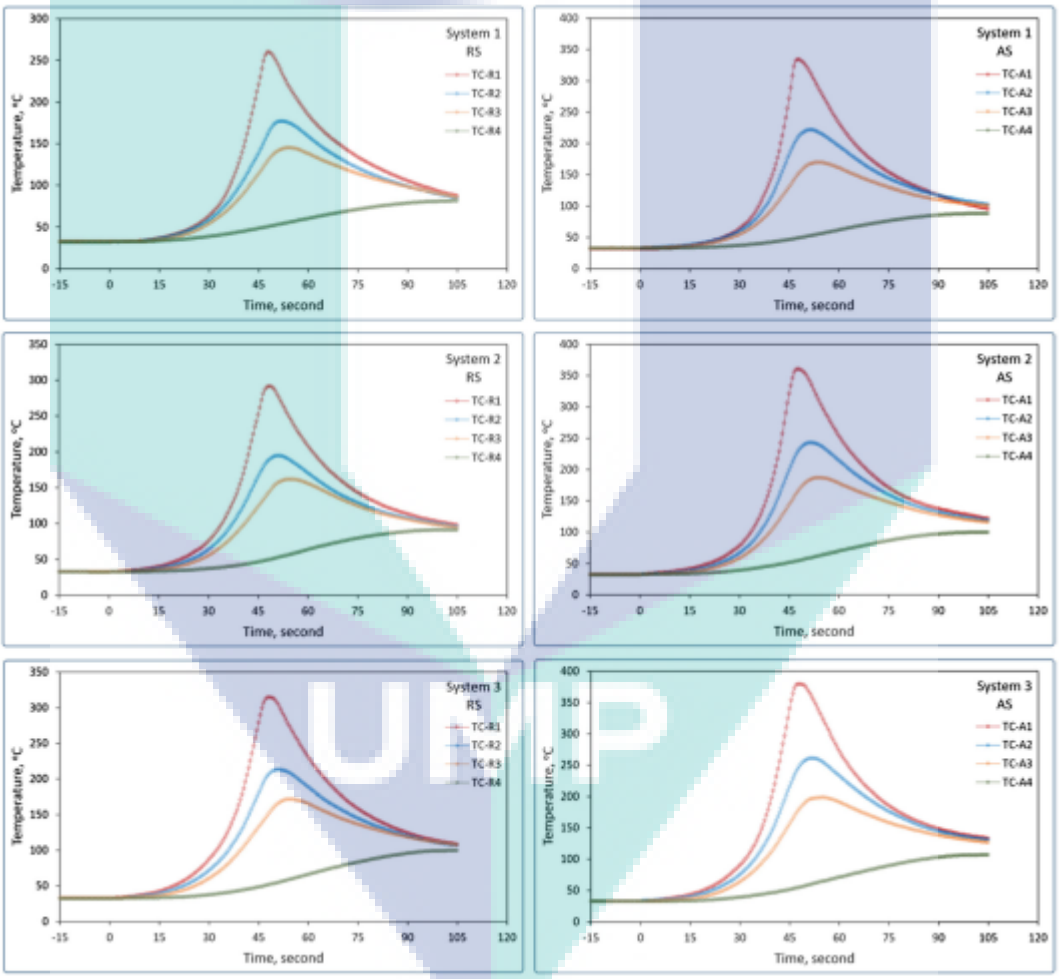

Fig. 4.20. Temperature distributions at 900 rpm and 150 mm/min related to the materials position and backing/clamping systems. AA2024-T351 placed on AS. AS advancing side, RS retreating side, TC thermocouple

The typical temperature-time data were recorded when the AA2024 was placed on the AS. In comparison between the three backing/clamping systems, the graphs show that the amount of heat transferred toward the backing and covering materials increased

throughout the use of system 1. This extraction of the welding heat reduced the peak temperature compared to system 3. For all systems, the temperature decreased as the distance from the welding seam increased. Furthermore, the temperatures were higher on the advancing side compared to those measured on the retreating side. The peak temperature was recorded by TC-A1 close to the welding seam, where the fracture occurred in the tensile tests of the stronger joints. According to these results, an idea was inspired to use asymmetric backing/clamping system (system 4). A composite backing plate consists of SS-SS-Al materials was used in this system, as seen in Fig. 4.2f. Aluminum 2024 was placed on the advancing side above the Al sheet and covered by the same material, while the steel sheets were used under and above the AA7075 alloy on the retreating side. This arrangement was used to extract more amount of welding heat from the advancing side and keep the temperature high enough in the stir zone. This may assist to reduce the temperature asymmetry between the advancing and retreating sides of the weld and enhance the joint strength.

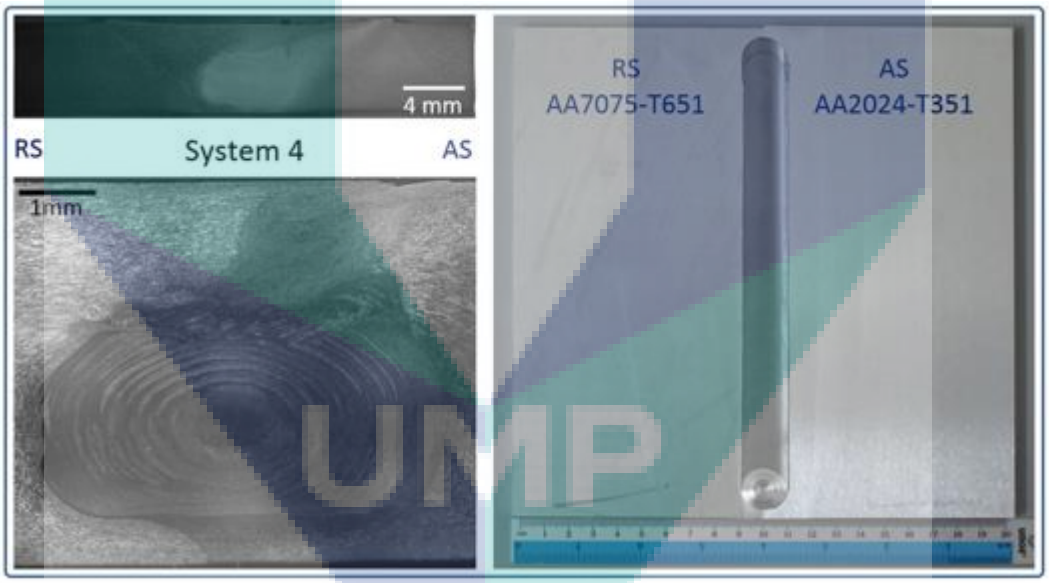

Fig. 4.21. Macro- and micrographs of the nugget and a photo of the welding joint resulting from using the asymmetric backing/clamping system (system 4) at 900 rpm and 150 mm/min. AS advancing side, RS retreating side

Fig. 4.21 shows the weld macrograph and nugget microstructure with a photo of the welding joint obtained through using this asymmetric system. The surface finish of the resulting weld appeared excellent and the materials were more properly mixed with uniform microstructure in the stir zone. The temperature distributions through the advancing and retreating sides are presented in Fig. 4.22. The temperatures on the AS were slightly higher than those of system 1, whereas the temperatures on the RS were

slightly lower than those of system 2. The recorded peak temperatures for this system and the other three primary systems are drawn in Fig. 4.23.

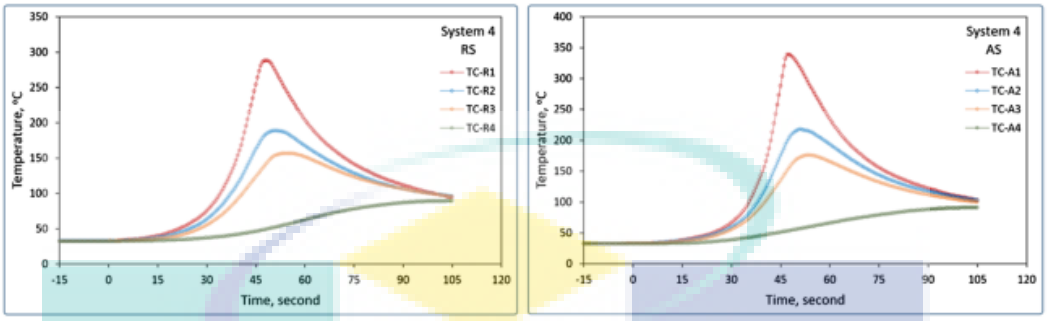

Fig. 4.22. Temperature distributions at 900 rpm and 150 mm/min resulting from using the asymmetric backing/clamping system (system 4). AA2024-T351 placed on AS. AS advancing side, RS retreating side, TC thermocouple

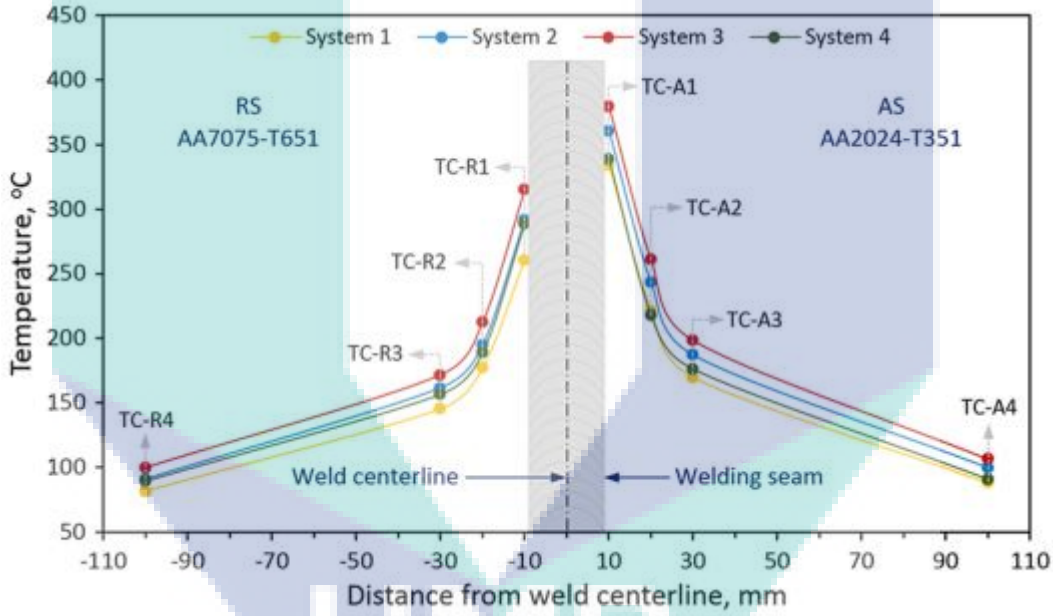

Fig. 4.23. Peak temperatures from the eight thermocouples at 900 rpm and 150 mm/min related to the backing/clamping systems. AS advancing side, RS retreating side, TC thermocouple

It is clear that the difference in peak temperatures between the advancing and retreating sides of the weld was reduced compared to the other backing/clamping systems. This contributed to improve the mixing of materials and enhance the hardness distribution of the weld, which presented in Fig. 4.24. The microhardness level was slightly higher than that of system 1 and the HAZ minimum hardness was improved in the advancing side. As a result, the ultimate strength and tensile elongation of the weld has considerably increased, as seen the stress-strain curves presented in Fig. 4.25. The graphs indicate that the highest joint strength of about 426 MPa were obtained through

using system 4. This value represents an efficiency of 94.8% with respect to the strength of the softer base material. At this case, the maximum tensile elongation of about 7.1% was observed.

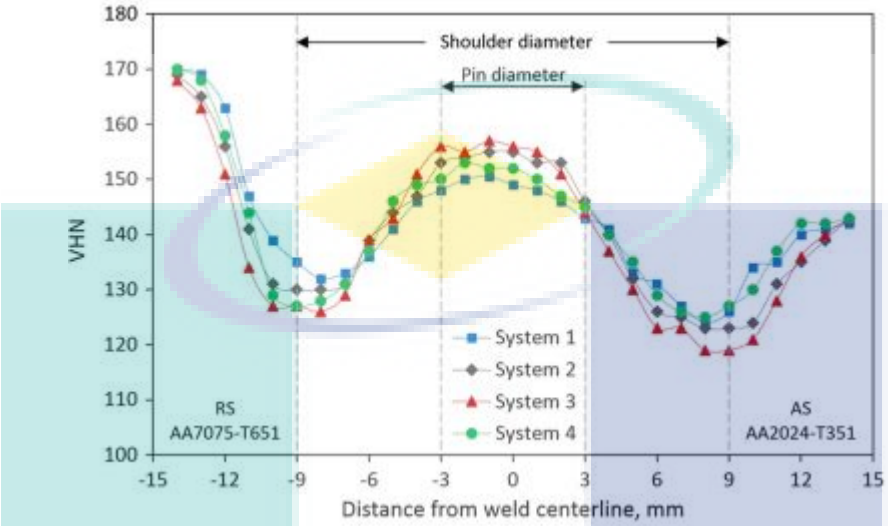

Fig. 4.24. Distribution of the Vickers microhardness number (VHN) at 900 rpm and 150 mm/min related to the backing/clamping systems. AS advancing side, RS retreating side

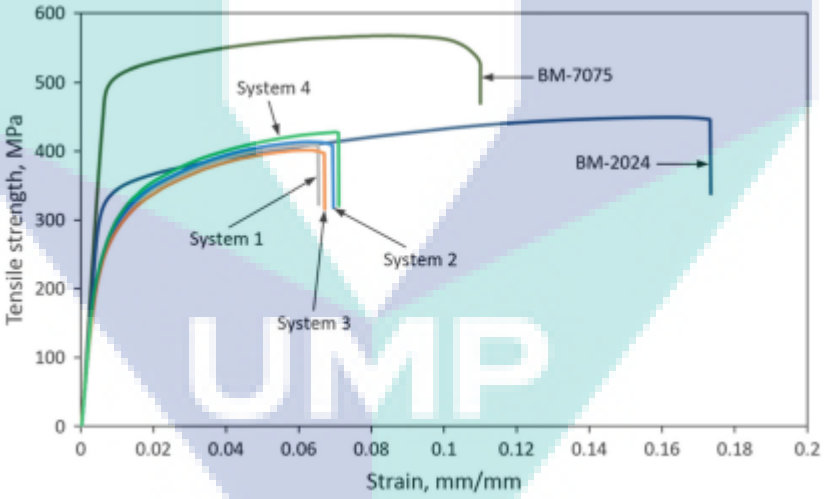

Fig. 4.25. Stress-strain curves of the base materials (BM) and welding joints related to the backing/clamping systems at 900 rpm and 150 mm/min. AA2024-T351 placed on the advancing side

4.5 CONCLUSIONS AND FUTURE RECOMMENDATION

In this work, a trial was made to improve the joint strength by controlling the temperature distribution during the FSW of dissimilar AA7075-T651 and AA2024-T351 aluminum alloys. The tool rotation rate, traverse speed, and materials position

were studied in conjunction with specially designed backing and clamping systems. According to the obtained results, the following conclusions could be outlined:

1. The maximum joint strength was recorded at 900 rpm when the tool rotation speed was preliminarily investigated at 100 mm/min of traverse speed and 3° of tilting angle. Raising this rotation rate resulted in a stretching of the nugget grains due to the fast cycling of materials mixing and elevation of the welding temperature, which in turn led to decrease the hardness at the HAZ and hence, affected the weld ultimate strength.

2. The welding temperature must be kept high enough in the mixing stir zone and reduced at the heat affected zone to improve the joint strength. Consequently, the use of material with high thermal conductivity in the modified backing/clamping system at hot welding (welding at low traverse speed) was favorable. At this case, the system worked as an adequate heat sink to dissipate some of the
4004 Int J Adv Manuf Technol (2017) 91:3991–4007 welding heat and minimize the drop of the joint strength due to the overheating effect. On the other side, the
welding traverse speed could be raised by minimizing the dissipated heat through insulating the workpieces or inserting low thermal conductive material in the composite backing/clamping system.

3. The effect of materials position has increased with decreasing tool rotation rate and increasing traverse speed. In other words, the weld strength decreased when the harder material was placed on the AS. This drop of strength has enlarged at cold welding (welding at low rotation rate or raised traverse speed) due to the higher power required to drive the welding tool when the harder material is fixed on the advancing side.

4. Temperature distribution is different between the advancing and retreating sides of the weld. The temperatures were higher on the advancing side compared to those measured on the retreating side. The peak temperature was observed close to the welding seam where the fracture occurred during the tensile testing of the stronger joints. Accordingly, the asymmetric backing/clamping system was used to extract more amount of the welding heat from the advancing side and keep the

temperature high enough in the mixing stir zone. As a result, the temperature asymmetry between the welding sides was reduced and the joint microhardness was enhanced. The produced weld has exhibited a considerable increase in the tensile strength and elongation of about 426 MPa and 7.1, respectively. The obtained joint strength represents an efficiency of 94.8% with respect to the softer base material.

4.6 REFERENCE

[1]. Thomas W, Dolby R (2003) Friction stir welding developments. Proceedings of the sixth international trends in welding research: 203–211

[2]. Ma ZY, Mishra RS, Mahoney MW (2002) Superplastic deformation behaviour of friction stir processed 7075Al alloy. Acta Mater 50(17):4419–4430. doi:10.1016/S1359-6454(02)00278-1

[3]. Threadgill P, Leonard A, Shercliff H, Withers P (2009) Friction stir welding of aluminium alloys. Int Mater Rev 54(2):49–93

[4]. Salih OS, Ou H, Sun W, McCartney DG (2015) A review of friction stir welding of aluminium matrix composites. Mater Des 86:61–71. doi:10.1016/j.matdes.2015.07.071

[5]. Fratini L, Micari F, Buffa G, Ruisi VF (2010) A new fixture for FSW processes of titanium alloys. CIRPAnn Manuf Technol 59(1): 271–274. doi:10.1016/j.cirp.2010.03.003

[6]. Mishra RS, Mahoney MW (2007) Friction stir welding and processing. ASM International

[7]. Rai R, De A, Bhadeshia HKDH, DebRoy T (2011) Review: friction stir welding tools. Sci Technol Weld Join 16(4):325–342. doi:10.1179/1362171811y.0000000023

[8]. Hasan MM, Ishak M, Rejab MRM (2016) Influence of machine variables and tool profile on the tensile strength of dissimilar AA7075-AA6061 friction stir welds. Int J Adv Manuf Technol:1–11. doi:10.1007/s00170-016-9583-3

[9]. Cavaliere P, Panella F (2008) Effect of tool position on the fatigue properties of dissimilar 2024-7075 sheets joined by friction stir welding. J Mater Process Technol 206(1–3):249–255. doi:10.1016/j.jmatprotec.2007.12.036

[10]. Cole EG, Fehrenbacher A, Duffie NA, Zinn MR, Pfefferkorn FE, Ferrier NJ (2013) Weld temperature effects during friction stir welding of dissimilar aluminum alloys 6061-t6 and 7075-t6. Int J Adv Manuf Technol 71(1–4):643–652. doi:10.1007/s00170-013-5485-9

[11]. Casavola C, Cazzato A, Moramarco V, Pappalettere C (2015) Temperature field in FSW process: experimental measurement and numerical simulation. In: Sottos N, Rowlands R, Dannemann K (eds) Experimental and applied mechanics, Volume 6. Conference Proceedings of the Society for Experimental Mechanics Series. Springer International, pp 177–186. doi:10.1007/978-3-319-06989-0_24

[12]. Abbasi M, Bagheri B, Keivani R (2015) Thermal analysis of friction stir welding process and investigation into affective parameters using simulation. J Mech Sci Technol 29(2):861–866

[13]. Nandan R, Debroy T, Bhadeshia H (2008) Recent advances in friction-stir welding–process, weldment structure and properties. Prog Mater Sci 53(6):980–1023. doi:10.1016/j.pmatsci.2008.05.001

[14]. Guo JF, Chen HC, Sun CN, Bi G, Sun Z, Wei J (2014) Friction stir welding of dissimilar materials between AA6061 and AA7075 Al alloys effects of process parameters. Mater Des 56:185–192. doi:10.1016/j.matdes.2013.10.082

[15]. Zappia T, Smith C, Colligan K, Ostersehlte H, Kallee SW (2010) 4–Friction stir welding equipment. In: Lohwasser D, Chen Z (eds) Friction stir welding. Woodhead, pp 73–117. doi:10.1533/9781845697716.1.74

[16]. Khodir SA, Shibayanagi T, Naka M (2006) Control of hardness distribution in friction stir welded AA2024-T3 aluminum alloy. Mater Trans 47(6):1560–1567

[17]. Upadhyay P, Reynolds AP (2012) Effects of forge axis force and backing plate thermal diffusivity on FSW of AA6056. Mat Sci Eng A-Struct 558:394–402. doi:10.1016/j.msea.2012.08.018

[18]. Upadhyay P, Reynolds A (2014) Effect of backing plate thermal property on friction stir welding of 25-mm-thick AA6061. Metall Mater Trans A 45(4):2091–2100. doi:10.1007/s11661-013-2121-0
[19]. Imam M, Racherla V, Biswas K (2014) Effect of backing plate material in friction stir butt and lap welding of 6063-T4 aluminium alloy. Int J Adv Manuf Technol. doi:10.1007/s00170-014-6617-6
[20]. Aliha MRM, Shahheidari M, Bisadi M, Akbari M, Hossain S (2016) Mechanical and metallurgical properties of dissimilar AA6061-T6 and AA7277-T6 joint made by FSW technique. Int J Adv Manuf Technol 86(9–12):2551–2565. doi:10.1007/s00170-016-8341-x
[21]. Islam MR, Ishak M, Shah LH, Idris SRA, Meriç C (2016) Dissimilar welding of A7075-T651 and AZ31B alloys by gas metal arc plug welding method. Int J Adv Manuf Technol:1–11. doi:10.1007/s00170-016-8993-6
[22]. Bertoncello JCB, Manhabosco SM, Dick LFP (2015) Corrosion study of the friction stir lap joint of AA7050-T76511 on AA2024- T3 using the scanning vibrating electrode technique. CorrosSci 94:359–367. doi:10.1016/j.corsci.2015.02.029
[23]. Sadeghian N, Besharati Givi MK (2015) Experimental optimization of the mechanical properties of friction stir welded acrylonitrile Int J Adv Manuf Technol (2017) 91:3991–4007 4005 butadiene styrene sheets. Mater Des 67:145–153. doi:10.1016/j. matdes.2014.11.032
[24]. Kumar N, Mishra RS, Yuan W (2015) Friction stir welding of dissimilar alloys and materials: a volume in the friction stir welding and processing book series. Butterworth-Heinemann
[25]. Bayazid SM, Farhangi H, Asgharzadeh H, Radan L, Ghahramani A, Mirhaji A (2016) Effect of cyclic solution treatment on microstructure and mechanical properties of friction stir welded 7075 Al alloy. Mat Sci Eng A-Struct 649:293–300. doi:10.1016/j.msea.2015.10.010
[26]. Li Z, Yue Y, Ji S, Chai P, Zhou Z (2016) Joint features and mechanical properties of friction stir lap welded alclad 2024 aluminum alloy assisted by external stationary shoulder. Mater Des 90:238– 247. doi:10.1016/j.matdes.2015.10.056
[27]. Cavaliere P, Nobile R, Panella FW, Squillace A (2006) Mechanical and microstructural behaviour of 2024–7075 aluminium alloy sheets joined by friction stir welding. Int J Mach Tools Manuf 46(6):588–594. doi:10.1016/j.ijmachtools.2005.07.010
[28]. Cavaliere P, Cerri E, Squillace A (2005) Mechanical response of 2024-7075 aluminium alloys joined by friction stir welding. J Mater Sci 40(14):3669–3676. doi:10.1007/s10853-005-0474-5
[29]. Khodir SA, Shibayanagi T (2007) Microstructure and mechanical properties of friction stir welded dissimilar aluminum joints of AA2024-T3 and AA7075-T6. Mater Trans 48(7):1928–1937. doi:10.2320/matertrans.MRA2007042
[30]. Khodir SA, Shibayanagi T (2008) Friction stir welding of dissimilar AA2024 and AA7075 aluminum alloys. Mater Sci Eng B- Adv 148(1–3):82–87. doi:10.1016/j.mseb.2007.09.024
[31]. da Silva AAM, Arruti E, Janeiro G, Aldanondo E, Alvarez P, Echeverria A (2011) Material flow and mechanical behaviour of dissimilar AA2024-T3 and AA7075-T6 aluminium alloys friction stir welds. Mater Des 32(4):2021–2027. doi:10.1016/j.matdes.2010.11.059
[32]. Saravanan V, Rajakumar S, Banerjee N, Amuthakkannan R (2016) Effect of shoulder diameter to pin diameter ratio on microstructure and mechanical properties of dissimilar friction stir welded AA2024-T6 and AA7075-T6 aluminum alloy joints. Int J Adv Manuf Technol 87(9–12):3637–3645. doi:10.1007/s00170-016-8695-0
[33]. Radisavljevic I, Zivkovic A, Radovic N, Grabulov V (2013) Influence of FSW parameters on formation quality and mechanical properties of Al 2024-T351 butt welded joints. Trans Nonferrous Metals Soc China 23(12):3525–3539. doi:10.1016/s1003-6326(13)62897-6
[34]. Đurđević A, Živojinović D, Grbović A, Sedmak A, Rakin M, Dascau H, Kirin S (2015) Numerical simulation of fatigue crack propagation in friction stir welded joint made of Al 2024-T351 alloy. Eng Fail Anal 58 Part 2:477–484. doi:10.1016/j.engfailanal.2015.08.028
[35]. Li WY, Jiang RR, Huang CJ, Zhang ZH, Feng Y (2015) Effect of cold sprayed Al coating on mechanical property and corrosion behavior of friction stir welded AA2024-T351 joint. Mater Des (1980-2015) 65:757–761. doi:10.1016/j.matdes.2014.10.007
[36]. Veljić D, Međo B, Rakin M, Radosavljević Z, Bajić N (2015) Analysis of the tool plunge in friction stir welding-comparison of aluminium alloys 2024T3 and 2024T351. Therm Sci:59–59
[37]. Moghadam DG, Farhangdoost K, Nejad RM (2016) Microstructure and residual stress distributions under the influence of welding speed in friction stir welded 2024 aluminum alloy. Metall Mater Trans B:1–15
[38]. Jaffee R (2013) Fundamental aspects of structural alloy design. Springer Science & Business Media

[39]. Dursun T, Soutis C (2014) Recent developments in advanced aircraft aluminium alloys. Mater Des 56:862–871. doi:10.1016/j.matdes.2013.12.002
[40]. Maisonnette D, Suery M, Nelias D, Chaudet P, Epicier T (2011) Effects of heat treatments on the microstructure and mechanical properties of a 6061 aluminium alloy. Mat Sci Eng A-Struct 528(6):2718–2724
[41]. Deng D, Murakawa H (2006) Numerical simulation of temperature field and residual stress in multi-pass welds in stainless steel pipe and comparison with experimental measurements. Comput Mater Sci 37(3):269–277. doi:10.1016/j.commatsci.2005.07.007
[42]. Christner B (1996) Sylva G Friction stir welding development for aerospace applications. In: ICAWT, Columbus, pp 359–368
[43]. Leonard A, Lockyer S 2003 Flaws in friction stir welds. In: 4th International Symposium on Friction Stir Welding. Park City
[44]. Richter-Trummer V, Suzano E, Beltrão M, Roos A, dos Santos JF, de Castro PMST (2012) Influence of the FSW clamping force on the final distortion and residual stress field. Mat Sci Eng A-Struct 538:81–88. doi:10.1016/j.msea.2012.01.016
[45]. Colligan KJ (2010) 2–The friction stir welding process: an overview. In: Lohwasser D, Chen Z (eds) Friction stir welding. Woodhead, pp 15–41. doi:10.1533/9781845697716.1.15
[46]. Chao YJ, Qi X, Tang W (2003) Heat transfer in friction stir welding—experimental and numerical studies. J Manuf Sci Eng 125(1):138–145
[47]. Mahoney M, Rhodes C, Flintoff J, Bingel W, Spurling R (1998) Properties of friction-stir-welded 7075T651 aluminum. Metall Mater Trans A 29(7):1955–1964
[48]. Tang W, Guo X, McClure J, Murr L, Nunes A (1998) Heat input and temperature distribution in friction stir welding. J Mater Process Manuf Sci 7:163–172
[49]. McClure JC, Tang W, Murr L, Guo X, Feng Z, Gould JE (1998) A thermal model of friction stir welding. Trends Weld Res 1(999):6
[50]. Çam G, Mistikoglu S (2014) Recent developments in friction stir welding of Al-alloys. J Mater Eng Perform 23(6):1936–1953. doi:10.1007/s11665-014-0968-x
[51]. Aval HJ, Serajzadeh S (2014) A study on natural aging behavior and mechanical properties of friction stir-welded AA6061-T6 plates. Int J Adv Manuf Technol 71(5–8):933–941
[52]. Prakash DGL, Regener D (2008) Quantitative characterization of Mg17Al12 phase and grain size in HPDC AZ91 magnesium alloy. J Alloys Compd 461(1–2):139–146. doi:10.1016/j.jallcom.2007.07.017
[53]. Zettler R (2010) 3–Material deformation and joint formation in friction stir welding. In: Lohwasser D, Chen Z (eds) Friction stir welding. Woodhead, pp 42–72. doi:10.1533/9781845697716.1.42
[54]. Zettler R, Vugrin T, Schmucker M (2010) 9–Effects and defects of friction stir welds. In: Lohwasser D, Chen Z (eds) Friction stir welding. Woodhead, pp 245–276. doi:10.1533/9781845697716.2.245
[55]. Al-Badour F, Merah N, Shuaib A, Bazoune A (2014) Thermomechanical finite element model of friction stir welding of dissimilar alloys. Int J Adv Manuf Technol 72(5–8):607–617. doi:10.1007/s00170-014-5680-3
[56]. Mironov S, Inagaki K, Sato YS, Kokawa H (2015) Effect of welding temperature on microstructure of friction-stir welded aluminum alloy 1050. Metall Mater Trans A 46(2):783–790
[57]. Luo C, Li X, Song D, Zhou N, Li Y, Qi W (2016) Microstructure evolution and mechanical properties of friction stir welded dissimilar joints of Mg–Zn–Gd and Mg–Al–Zn alloys. Mat Sci Eng AStruct 664:103–113
[58]. Trimble D, O'Donnell GE, Monaghan J (2015) Characterisation of tool shape and rotational speed for increased speed during friction stir welding of AA2024-T3. J Manuf Process 17:141–150. doi:10.1016/j.jmapro.2014.08.007
[59]. Giraud L, Robe H, Claudin C, Desrayaud C, Bocher P, Feulvarch E (2016) Investigation into the dissimilar friction stir welding of AA7020-T651 and AA6060-T6. J Mater Process Technol 235: 220–230. doi:10.1016/j.jmatprotec.2016.04.020 4006 Int J Adv Manuf Technol (2017) 91:3991–4007
[60]. İpekoğlu G, Çam G (2014) Effects of initial temper condition and postweld heat treatment on the properties of dissimilar friction-stir-welded joints between AA7075 and AA6061 aluminum alloys. Metall Mater Trans A 45(7): 3074–3087. doi:10.1007/s11661-014-2248-7

[61]. Hasan MM, Ishak M, Rejab MRM (2015) A simplified design of clamping system and fixtures for friction stir welding of aluminium alloys. JMES 9:1628–1639. doi:10.15282 /jmes.9.2015.10.0158
[62]. Rodriguez RI, Jordon JB, Allison PG, Rushing T, Garcia L (2015) Microstructure and mechanical properties of dissimilar friction stir welding of 6061-to-7050 aluminum alloys. Mater Des 83:60–65. doi:10.1016/j.matdes.2015.05.07

CHAPTER 5

CONCLUSION AND RECOMENDATION

5.1 CONCLUSION

Joining dissimilar high-strength and lightweight AA7075-T6 and AA2024-T351 aluminum alloys by the FSW was investigated in this dissertation. Tool design, process parameters and thermal boundary condition were optimized to produce quality weld. The experiments were accomplished using specially designed backing/clamping systems. Several aspects were presented and discussed related to the broad scope to provide advanced knowledge in the field of study. Summary of the findings obtained from the work carried out in the present scientific research is presented in this chapter. In addition, the future recommendations that may be followed to extend the study of the friction stir welding of dissimilar materials are outlined.

5.2 SUMMARY OF FINDINGS

The following sections present the main concluding remarks that can be drawn as per the observed results of the current research work.

5.2.1 Tool Design

Five welding tools with concave shoulders and different probe profiles (cylindrical and tapered, smooth and threaded, flatted and non-flatted) were examined through the FSW of dissimilar 3-mm-thick AA7075-T6 and AA6061-T6 aluminum alloys under a range of machine variables planned by the central composite design. The obtained results showed that tool design is the most influential aspect in dissimilar friction stir welding. The welding tools with tapered probe and additional features (threads and flat) can be effectively used to produce sound welds with smooth surface finish, good material mixing and high tensile strength. On the other side, tools with smooth straight cylindrical or even tapered probes are not preferable, since they result in poor material mixing and hence lower joint strength.

Tool design was further investigated through analyzing the effect of flute radius of the probe on the material flow and joint strength of dissimilar 6-mm-thick AA7077-T651 and AA2024-T351 aluminum alloys. Different sizes of cutting tools were used to add a single flute or flat to the cone of the base truncated threaded pin tool. The observed results showed that the strongest welding joint can be produced by using featured pin tool with a flute of radius equal to the base radius of the probe.

5.2.2 Mathematical Modelling

The welding tool rotation and traverse speeds were optimized in this work for different joint thicknesses. These principal variables were optimized in conjunction with the tool design and tilt angle during the FSW of the thinner aluminum alloys 7075 and 6061. A reduced second order polynomial equation was successfully developed and validated to adequately fit the observed results of the weld ultimate tensile strength. This model seemed to be an active tool for the prediction of joint strength as a function of the selected variables. A respectable fitness of the developed model with the experimental data within the range of the operating variables was indicated with an elevated regression coefficient (R^2 = 0.9851). Well agreement between the observed and calculated values with low deviation (error within ±10 %) was also recorded through the validation tests. It was concluded that the weld strength increases with the increasing of process parameters until it reached the apex level and decrease again when these parameters are further raised. The stronger joint with maximum joint strength of about 252 MPa, which represents an efficiency of 82 % was reached at 1100 rpm of tool rotation speed, 300 mm/min of traverse speed and 3° of tool tilt angle.

The optimal welding speed were different when the joint thickness of the dissimilar AA7075-AA2024 friction stir welds was 6 mm. The maximum joint strength of about 400 MPa, which represents an efficiency of 89% was recorded at 900 rpm when the tool rotation speed was preliminarily investigated at 100 mm/min of traverse speed and 3° of tilting angle. Raising this rotation rate resulted in a stretching of the nugget grains due to the fast cycling of materials mixing and elevation of the welding temperature, which in turn led to decrease the hardness at the HAZ and hence, affected the weld ultimate strength. This means that the spindle speed should be reduced for the thicker welding joints. Same behavior was noticed regarding the tool traverse speed. The maximum weld efficiency of 91.6% was calculated at 150 mm/min, which is equal to half of the optimal traverse speed used to join the thinner plates.

5.2.3 Materials Direction and Position

Four different configurations related to the rolling direction of welding plates were examined in two groups related to the materials position on the advancing and retreating sides of the weld. The eight case studies were conducted through the FSW of the 3-mm-thick AA7075 and AA6061 aluminum alloys. It was noticed that stronger joint could be achieved by placing the softer alloy on the advancing side of the weld and stirring the tool in a direction parallel to the RD of the abutting plates. The weld strength can be further improved when the welding seam is produced in a direction parallel to the RD of the softer material and normal to that of the harder one. Through this welding configuration and materials location, the joint tensile strength reached the maximum value of 255.8 MPa, which represents an efficiency of about 84.3%. On the other side, the strength of joint was slightly decreased when the welding seam generated in a direction normal to the RD of both welding sheets, regardless of the relative materials position on the advancing and retreating sides. Minimum joint strength of about 221.3 was recorded when the RD of both sheets was normal to the welding line, and the softer material placed on the AS.

The influence of the fixed location of the welding base materials on the joint strength was also studied during the FSW of the 6-mm-thick aluminum 7075 and 2024. It was concluded that the effect of materials position has increased with decreasing tool rotation rate and increasing traverse speed. In other words, the weld strength decreased when the harder material was placed on the AS. This drop of strength has enlarged at

cold welding (welding at low rotation rate or raised traverse speed) due to the higher power required to drive the welding tool when the harder material is fixed on the advancing side.

5.2.4 Clamping Force

The optimal clamping pressure was detected through joining several pairs of AA7075 and AA2024 aluminum coupons secured on the machine table by equal vertical and lateral forces ranged from 1-6 kN using the developed backing/clamping system. It was exposed that 1 kN is not enough force to prevent the separation of the workpieces during the initial plunging stage of the welding process. Beyond this level of clamping force, the produced joints were free of the undesirable initial gap. The weld strength was reached the maximum value of 394 MPa when the clamping force was fixed at 3 kN. Further increase in the clamping force resulted in a gradient reduction in the weld tensile strength, which have reached the lowest value of about 381 MPa when the clamping force was fixed at 6 kN. Accordingly, the abutting plates should be subjected to moderate clamping pressure to produce efficient and stable weld.

5.2.5 Initial Heating Stage or Dwell Sequence

The ordinary plunge phase of the friction stir processing is the main cause of the early wear in the welding pin tool due to the high compressive stress and temperature endured by the probe. Omitting this plunge cycle assists to extend the lifetime of the pin tool, which is essential for producing stable weldments with minimum manufacturing cost. A pilot hole slightly smaller than the probe can be created at the weld start point to achieve this objective. An estimation of the appropriate stationary dwell time is then indispensable to generate the sufficient heat required to soften the abutting materials before the main welding phase. Consequently, the stationary delay time was examined and a new method of using two-stage welding was introduced in this work. The latter way was attained to minimize the shoulder wear that may result from the stationary dwell period. The test-coupons were prepared through dissimilar joining of the high-strength AA7075 and AA2024 aluminum alloys. It was noticed that surface-breaking voids generate during the shorter dwell sequences, while the defect-free weld is produced after 12 seconds of stationary delay time. Raising this period to 24 seconds reduces the joint strength due to the hardness drop at the HAZ of the softer alloy, which

indicates that the amount of the generated frictional heat is higher than the required level. The most stable weldment with the highest tensile strength and minimum deviation was achieved by using the two-stage welding method, which significantly reduced the longitudinal deformation of the pin tool compared to the ordinary plunging cycle. It is also able to minimize the shoulder wear that may result from the stationary dwell sequence.

5.2.6 Backing and Clamping Materials

An attempt was made to improve the joint strength by controlling the temperature distribution during the FSW of dissimilar AA7075-T6 and AA2024-T351 aluminum alloys. Three composite backing plates and clamping systems were tested in conjunction with varying levels of the tool traverse speeds and materials position. The developed backing/clamping system was modified to insert high and low thermal conductivity aluminum and stainless steel sheets below and above the workpieces. Moreover, the dissimilar base material was insulated in the third system by an air-gap to minimize the process heat lost. The transient temperatures were experimentally measured at different distances from the welding line. The welding temperature must be kept high enough in the mixing stir zone and reduced at the heat affected zone to improve the joint strength. Consequently, the use of material with high thermal conductivity in the modified backing/clamping system at hot welding (welding at low traverse speed) was favorable. At this case, the system worked as an adequate heat sink to dissipate some of the welding heat and minimize the drop of the joint strength caused by the overheating effect. On the other side, the welding traverse speed could be raised by minimizing the dissipated heat through insulating the workpieces or inserting low thermal conductivity material in the composite backing/clamping system.

High-temperature difference was noticed between the advancing and retreating sides of the weld. The temperatures were higher on the advancing side compared to those measured on the retreating side. The peak temperature was observed close to the welding seam where the fracture occurred during the tensile testing of the stronger joints. Accordingly, a novel asymmetric backing/clamping system was used to extract more amount of the welding heat from the advancing side and keep the temperature high enough in the mixing stir zone. This was attained by inserting high-thermal conductivity material below and above the workpiece in the AS and low-thermal

conductivity material below and above the workpiece in the RS. Accordingly, the temperature asymmetry between the welding sides was reduced and the joint micro-hardness was enhanced. The produced weld has exhibited a considerable increase in the tensile strength of 426 MPa, which represents a superior joint efficiency of about 95%.

5.3 RECOMMENDATION

Future research will continue to advance the knowledge of dissimilar FSW, extending the understanding of the complex physical interactions which motivate a process that developed first as a technology. Areas of much interest recently are tool design and thermal management, which is being attempted with both thermal boundary condition modification and closed-loop temperature control. With the objective of producing high efficient dissimilar welds, these important topics were considered in the current dissertation. However, the research should be extended to cover the following headlines, which are recommended for future work:

i. Higher thickness aluminum plates can be welded by employing double sided FSW. One can try to use tools made of different materials to improve the quality of the joints.

ii. Using new tool designs which have frustum shapes, surface coating of the probe and surface heat treatment techniques could be viable solutions to improve both tool life and joint efficiency.

iii. Inspecting the FSW of dissimilar aluminum alloys in lap and T-joint configurations through introducing asymmetric backing and clamping system.

iv. Studying the influence of backing materials and clamping system on the FSW of dissimilar materials from different families, such as aluminum and steel.

i. Investigation of the forces generated during the FSW of different alloys at different process parameters might be very beneficial.

CHAPTER 6

RESEARCH OUTPUT

6.1 List of Published Papers

1. Hasan, M. M., Ishak, M., & Rejab, M. (2017). Effect of backing material and clamping system on the tensile strength of dissimilar AA7075-AA2024 friction stir welds. *The International Journal of Advanced Manufacturing Technology*, *91*(9-12), 3991-4007. doi: http://dx.doi.org/10.1007/s00170-017-0033-7 ISI (IF = 2.209)
2. Hasan, M. M., Ishak, M., & Rejab, M. R. M. (2016). Influence of machine variables and tool profile on the tensile strength of dissimilar AA7075-AA6061 friction stir welds. *The International Journal of Advanced Manufacturing Technology*, *90*(9), 2605-2615. doi: http://dx.doi.org/10.1007/s00170-016-9583-3 ISI (IF = 2.209)
3. Hasan, M. M., Ishak, M., & Rejab, M. R. M. (2015). A simplified design of clamping system and fixtures for friction stir welding of aluminum alloys. *Journal of Mechanical Engineering and Sciences*, *9*, 1628-1639. doi: http://dx.doi.org/10.15282/jmes.9.2015.10.0158 (Scopus Index)
4. Hasan, M. M., Ishak, M., & Rejab, M. R. M. (2017). Effect of pin tool design on the material flow of dissimilar AA7075-AA6061 friction stir welds. *IOP Conf. Series: Materials Science and Engineering*, *257* (2017) 012022. doi: http://dx.doi.org/10.1088/1757-899X/257/1/012022. (Scopus Index)
5. Hasan, M. M., Ishak, M., & Rejab, M. R. M. (2017). Effect of tool rotation rate on the tensile strength of friction stir weldments of AA7075-T651 and AA2024-T351 aluminum alloys. *Journal of Mechanical Engineering and Sciences*. (Scopus Index). Revised

6. Hasan, M. M., Ishak, M., & Rejab, M. R. M. (2017). Effect of pin tool flute radius on the material flow and microstructure of dissimilar AA7075-AA2024 friction stir welds. *International Journal of Mechanical Sciences.* ISI (IF = 2.884). Under review
7. Hasan, M. M., Ishak, M., & Rejab, M. R. M. (2017). A methodology for reducing the longitudinal wear of the pin tool in friction stir welding of dissimilar aluminum alloys. *Journal of Material Processing Technology*. ISI (IF = 2.236). Under review
8. Hasan, M. M., Ishak, M., & Rejab, M. R. M. (2017). Effect of material direction and location on the friction stir welding of dissimilar aluminum alloys. *Journal of Materials Science and Technology*. ISI (IF = 1.909). Under review

6.2 List of Conferences

1. 3nd International Conference on Mechanical Engineering Research (ICMER2015)/ Kuantan, Pahang, Malaysia. 18-19 August 2015.

2. 2nd International Conference on Automotive Innovation and Green Energy Vehicle (AiGEV2016)/ Malaysia Automotive Institute (MAI), Cyberjaya, Selangor, Malaysia. 2-3 August 2016.

3. 4nd International Conference on Mechanical Engineering Research (ICMER2017)/ Kuantan, Pahang, Malaysia. 1-2 August 2017.

6.3 List of Awards

1. *Best presenter award* in the 2nd International Conference on Automotive Innovation and Green Energy Vehicle (AiGEV2016)/ Malaysia Automotive Institute (MAI), Cyberjaya, Selangor, Malaysia. 2-3 August 2016.

2. *Best achievement award* for excellent achievement in Preparatory Intensive English (PIE) Programme, UMP, 2014.

3. *Bronze Medal* in the Citrex 2017 Exhibition. UMP, Gambang, Malaysia.

6.4 Patent

Clamping jig for dissimilar friction stir welding. *Patent Application No. PI2017700587*.

APPENDICES

OTHER RELATED PUBLISHED WORKS

1. A Simplified Design of Clamping System and Fixtures for Friction Stir Welding of Aluminium Alloy

(Journal of Mechanical Engineering and Sciences (JMES), 9 . pp. 1628-1639. ISSN 2289-4659- SCOPUS INDEXED)

Abstract: Sound friction stir welds could be attained by using an active design of backing/clamping system with a proper selection of the welding parameters. This work presented a simplified design of fixtures and backing plates to be used for friction stir welding of aluminum alloys. The test-rig was constructed to prevent dispersal or lifting of the specimens throughout the joining process and to ensure uniform distribution of temperature along the plates. The workpieces were subjected to uniform lateral and vertical pressures by means of bolts and nuts. Compound backing plates and pressure bars with additional side plates were included to increase the heat sink. Several coupons of dissimilar aluminum alloys AA7075 and AA6061 were joined to inspect the validity of this design. The tests showed promising results with defects - free welds, good strength and smooth surface finish without geometric imperfection and gap creation

between the welded specimens . Efficiency of the joint reached its maximum value of about 82% with respect to the ultimate strength of the AA6061 alloy at 1100 rpm rotation speed and 300 mm/min feed. These results encourage using and improving th e present design for future studies of friction stir welding

2. A Methodology for Reducing the Longitudinal Wear of the Pin Tool in Friction Stir Welding of High-Strength Aluminum Alloys

(*Journal of Material Processing Technology*. ISI (IF = 2.236). Under review)

Abstract: This work presents a methodology for welding without the initial plunge cycle to avoid the premature deformation in the pin tool. Dissimilar AA7075 and AA2024 high-strength aluminum alloys were joined using a steel tool with truncated threaded probe and specially-designed backing/clamping system. An initial pilot hole was drilled at the weld start point, and the dwell sequence was studied. Four stationary dwell periods between 3- and 24-seconds were examined and compared to a non-stationary dwell (NSD) of slow feed rate at the weld start. The revealed microstructure and measured ultimate strength of the welded joints were considered. Four transverse tensile specimens normal to the welding seam were tested to inspect the efficiency of each weldment. The results showed that the longitudinal wear of the pin tool could be significantly reduced by omitting the ordinary plunge phase and allowing moderate dwell time, in conjunction with utilizing an initial pilot hole. Uniform joints with minor deviation in weld strength were obtained through the NSD and by applying 12 seconds of stationary dwell time. On the other hand, poor material mixing with deep surface-

breaking voids or lack of fills were detected, and high non-conformity in joint strength were recorded at lower dwell periods.